2019

Exploring the Molecular Origin of Jet Fuel Thermal Oxidative Deposition Through Statistical Analysis of Mass Spectral Data and Pyrolysis Gas Chromatography/Mass Spectrometry of Deposits

Krege Matthew Christison
University of the Pacific, kmchristison@gmail.com

EXPLORING THE MOLECULAR ORIGIN OF JET FUEL THERMAL OXIDATIVE DEPOSITION THROUGH STATISTICAL ANALYSIS OF MASS SPECTRAL DATA AND PYROLYSIS GAS CHROMATOGRAPHY/MASS SPECTROMETRY OF DEPOSITS

By

Krege M. Christison

A Dissertation Submitted to the

Graduate School

In Partial Fulfillment of the

Requirements for the Degree of

DOCTOR OF PHILOSOPHY

Thomas J. Long School of Pharmacy and Health Sciences
Pharmaceutical and Chemical Sciences

University of the Pacific
Stockton, CA

2019

EXPLORING THE MOLECULAR ORIGIN OF JET FUEL THERMAL OXIDATIVE DEPOSITION THROUGH STATISTICAL ANALYSIS OF MASS SPECTRAL DATA AND PYROLYSIS GAS CHROMATOGRAPHY/MASS SPECTROMETRY OF DEPOSITS

By

Krege M. Christison

APPROVED BY:

Dissertation Advisor: Liang Xue, Ph.D.

Committee Member: O. David Sparkman, Ph.D.

Committee Member: Jianhua Ren, Ph.D.

Committee Member: Andreas Franz, Ph.D.

Committee Member: Douglas Cyr, Ph.D.

Department Co-Chair: Jianhua Ren, Ph.D.

Department Co-Chair: Jerry Tsai, Ph.D.

Dean of Graduate School: Thomas Naehr, Ph.D.

EXPLORING THE MOLECULAR ORIGIN OF JET FUEL THERMAL OXIDATIVE DEPOSITION THROUGH STATISTICAL ANALYSIS OF MASS SPECTRAL DATA AND PYROLYSIS GAS CHROMATOGRAPHY/MASS SPECTROMETRY OF DEPOSITS

By

Krege M. Christison

DEDICATION

This dissertation is dedicated to my mom, Sharon Lucille Edith Montagne Brown Christison, who always wanted the best for me. To my family; rocky, Lola, and Kai – you make all the hard work worth it. To my dad, Kenneth M. Christison, thank you for everything. And to Tommy Thompson who showed me a better way of life.

ACKNOWLEDGEMENTS

I have deep gratitude for the many people who have helped me in this journey. First, I would like to thank Prof. O. David Sparkman for his mentorship and teaching me to be a mass spectrometrist. Dr. Liang Xue has been a great mentor and I have been lucky to have him as my advisor. The other graduate students who have been a part of the Pacific Mass Spectrometry facility during my tenure; Patrick Batoon, Michael Pastor, and Michael Browne – thank you for all the support and discussions.

I am grateful to my many colleagues at Chevron. My supervisor Doug Cyr who has supported me in my goal of earning a Ph.D. Thomas Smagala who first hired me and introduced me to the world of jet fuel. Rob Lorenz, Theresa Gunawan, Suzanne Golisz, and Deirdra Evers-McGregor for the many discussions and advice on writing manuscripts and this dissertation. I would never have been able to get the work done without the help of Camden Cook, Keyang Sun, Jeanelle Smoot, and Andy Chen all of who contributed in some way to the laboratory work presented here.

Exploring the Molecular Origin of Jet Fuel Thermal Oxidative Deposition Through Statistical Analysis of Mass Spectral Data and Pyrolysis Gas Chromatography/Mass Spectrometry of Deposits

Abstract

By Krege M. Christison

University of the Pacific
2019

ASTM D3241 (Standard Test Method for Thermal Oxidation Stability of Aviation Turbine Fuels) measures the thermal oxidative stability of jet fuels under elevated temperature and pressure conditions. When jet fuels fail ASTM D3241, either at the refinery or in the distribution system, there can be supply disruptions and financial losses. Understanding the causes of poor thermal oxidative stability in jet fuels could help prevent or mitigate issues. In order to develop a deeper understanding of the molecular precursors that lead to ASTM D3241 failures, a number of analytical methodologies and data treatment techniques have been developed, applied, and reported here. Statistical analysis of LC/MS ESI data from jet fuels with varying thermal oxidative stabilities allows for the identification of molecules that are significant to ASTM D3241 failures. Differential statistical analysis of LC/MS ESI data from jet fuels before and after thermal oxidative stressing in a QCM reactor elucidates which significant molecules are being consumed during oxidation and which molecules are increasing in abundance. The analysis of thermal oxidative deposits that form during thermal oxidative stressing in the QCM reactor allows for the insight into the molecular components of the deposits. Attapulgus clay removes the polar molecules that lead to

thermal oxidative stability issues in the refinery. Extraction of Attapulgus clay that has been used in a refinery to filter jet fuel with a series of solvents removes the polar molecules into a series of fractions. The subsequent analysis of the fractions by comprehensive GCxGC/MS leads to the identification of the different homologous series of molecules that are removed by the clay.

The analyses developed and employed here are shown to be particularly useful for the analysis of trace polar nitrogen and oxygen containing molecules. Similar homologous series of molecules are identified across all of the different analyses. It is also clear from some of the analyses, along with previously reported data in the literature, that reactive sulfur-containing molecules are significant to poor thermal oxidative stability as measured by ASTM D3241 and to the formation of thermal oxidative deposits. There is still an opportunity to find methodologies to better characterize the sulfur species present and correlate them to the data that is reported here.

TABLE OF CONTENTS

LIST OF TABLES

Table

LIST OF FIGURES

Figure

LIST OF ABBREVIATIONS

ANOVA – Analysis of Variance

API-TOF – Atmospheric Pressure Ionization-Time-of-Flight

°C/min – Degrees Celsius per Minute

Da - Dalton

DCM – Dichloromethane (Methylene Chloride)

DCM/MeOH – 1 to 1 Dichloromethane to Methanol

EAS – Electrophilic Aromatic Substitution

EGA – Evolved Gas Analysis

EI – Electron Ionization

EIC – Extracted Ion Chromatogram

EIP – Extraction Isolated Precipitate

ESI – Electrospray Ionization

FID – Flame Ionization Detector

GC/MS – Gas Chromatography/Mass Spectrometry

GCxGC – Gas Chromatography by Gas Chromatography

GCxGC/MS – Gas Chromatography by Gas Chromatography/Mass Spectrometry

GCxGC-FID/MS – Gas Chromatography by Gas Chromatography-Flame Ionization Detection/Mass Spectrometry

GHz - Gigahertz

HEFA – Hydrotreated Esters and Fatty Acids

HPLC – High Performance Liquid Chromatography

Hz – Hertz

ICP/MS – Inductively Coupled Plasma/Mass Spectrometry

ITR – Interferometry Tube Rater

kPa - Kilopascal

LC/MS – Liquid Chromatography/Mass Spectrometry

m – Meter

m/m – Mass Divided by Mass

m/z – Mass to Charge Ratio

MeOH – Methanol

MFE – Molecular Feature Extraction

MHz - Megahertz

min – Minute

mL/min – Milliliter per Minute

mM – Millimolar

mm – Millimeter

mmHg – Millimeter of mercury

MPP – Mass Profiler Professional

N/A – Not Analyzed

PCA – Principal Component Analysis

PCDL – Personal Compound Database Library

PI – Photoionization

psi – Pounds per Square Inch

Py/FIMS – Pyrolysis/Field Ionization Mass Spectrometry

Py-GC/MS – Pyrolysis-Gas Chromatography/Mass Spectrometry

QC – Quality Control

QCM – Quartz Crystal Microbalance

RSSOT – Rapid Small-Scale Oxidation Test

RTICC – Reconstructed Total Ion Current Chromatogram

s - Second

SMORS – Soluble Macromolecular Oxidatively Reactive Species

SPE – Solid Phase Extraction

SPK – Synthetic Paraffinic Kerosene

TOD - Thermal Oxidative Deposition

TOF – Time-of-Flight

TOS - Thermal Oxidative Stressing

$\mu g/cm^2$ – Microgram per Centimeter Squared

UHPLC – Ultrahigh Performance Liquid Chromatography

µl - Microliter

µm - Micrometer

V - Volt

Vol - Volume

VTR – Visual Tube Rater

Chapter 1 : Introduction

Jet fuel is a petroleum derived product meeting the criteria of ASTM D1655 (Standard Specification for Aviation Turbine Fuels) in the United States[1] and the Defense Standard 91-91 (Def Stan 91-91) in most other countries.[2] The only notable difference between the two specifications is freeze point. Def Stan 91-91 specifies a lower freeze point than ASTM D1655, however for the purposes of this dissertation the two specifications are nearly identical.[3] The boiling range of commercial jet fuels is approximately 110-300°C, very close the boiling range of kerosene, and between the boiling range of gasoline and diesel fuel.[3] The molecular composition of jet fuel is primarily alkane, cycloalkane, and aromatic molecules with up to 3000 ppm (m/m) sulfur-containing molecules and trace levels (typically <1000 ppm (m/m)) of nitrogen and oxygen containing molecules.[3]

The thermal oxidative stability of a jet fuel as measured by ASTM D3241 (Standard Test Method for Thermal Oxidation Stability of Aviation Turbine Fuels) is an important property with specification limits outlined in the jet fuel specifications.[4] Jet fuel undergoes significant stress when in service in aircraft in the form of elevated temperature and pressure conditions.[5] It is used as a coolant throughout an aircraft which can lead to the formation of gums, varnishes, large soluble precursors to deposits and particulate matter that can deposit in numerous different places causing catastrophic failure to important aircraft systems.[3, 5-6] ASTM D3241 is also one of the more unpredictable test methods and fuel can fail without warning. Additionally, fuels that leave the refinery meets specificationification can be exposed to contaminants in

multi-purpose pipeline distribution systems that lead to the fuel becoming off-specification and failing ASTM D3241 at the destination.[7] These failures can have financial repercussions along with damage to the reputation of the fuel supplier.[3]

ASTM D3241 measures the tendency of a fuel to form deposits under high temperature and pressure conditions, which correlates to the fuel's thermal oxidative stability. A failure is characterized by either excessive deposit formation on an aluminum tube that is heated during the test or plugging of a filter in the test apparatus resulting in a pressure drop across the filter in the system. This is an attempt to mimic the type of conditions the fuel will experience while in-service in a shorter time frame. The cause of ASTM D3241 failures can be due to a number of factors.[5] It has been shown that the presence of a combination of trace polar molecules containing heteroatoms (oxygen, nitrogen, and sulfur) can be involved in generating deposits that lead to ASTM D3241 failures.[5, 8-13] However, the development of a simple correlation to predict ASTM D3241 failures has proved elusive. In addition to trace heteroatom-containing molecules, trace dissolved metal ions can lead to failures.[14] In the refinery, if there are trace heteroatom-containing molecules present in the final jet product, they are typically reduced in concentration or removed by filtering the jet fuel through Attapulgus clay prior to release.[3, 15] However, when the clay becomes deactivated, the molecules can pass through or be increased in concentration through desorption from the clay leading to poor ASTM D3241 results.[3, 5] Trace dissolved metal ions can be mitigated through the use of metal deactivator additive if necessary.[16] Metal deactivator can also improve ASTM D3241 when trace dissolved metal ions are not present through an unknown

mechanism, however it is postulated that the metal deactivator may bind to the aluminum tube inhibiting deposit accumulation.[17]

There have been numerous studies into the cause of poor thermal oxidative stability. A prevailing area of research is the study of the precursors in jet fuel that lead to deposits. This is difficult because of the trace levels of the polar compounds and the complex nature of petroleum derived fuels. Both liquid chromatography/mass spectrometry (LC/MS) and gas chromatography/mass spectrometry (GC/MS) have been utilized to characterize the polar molecules in jet fuel that show a correlation with thermal oxidative deposition (TOD) and have helped to elucidate the complex mechanisms that leads to ASTM D3241 failures.[8, 11, 18-19]

Balster, *et al.* extensively characterized the polar composition of 20 different jet fuels by separating the polar molecules with high performance liquid chromatography (HPLC) and solid phase extraction (SPE) then analyzing them by GC/MS.[8] They were able to show a correlation between total polar concentration extracted from the fuels and the propensity of the fuel to form deposits by the quartz crystal microbalance (QCM) technique. However, there were two outliers in the 20 samples that showed high polar content along with good thermal oxidative stability which were not easily explained. It is important to note that this study did not look at metals, hydroperoxides, trace sulfur species, or acid/base reactions which have been shown to affect thermal oxidative stability.[8] The QCM technique has a standard practice defined by ASTM D7739.[20] In general, a sample of fuel is heated in an enclosed vessel with a quartz crystal submerged in the fuel which measures the mass of deposits that form on it. This

is similar to the principle of ASTM D3241 however the analysis is run at lower temperatures (typically 140 °C) and over a longer period of time (15 hours).

A more recent study looked at the oxidation products formed after accelerated oxidation tests.[19] One of the tests was the QCM method described earlier. The other test was rapid small-scale oxidation testing (RSSOT, ASTM D7545). In this test, 5 mL of fuel is placed in a heated (140°C), enclosed vessel in an oxygen rich environment (700 kPa O_2) and the time for the pressure of the oxygen to drop 10% is measured. The two test methods measure different types of thermal oxidative stability and do not necessarily correlate with each other. In both cases the fuel is heated in the presence of oxygen. However, RSSOT measures oxygen consumption and QCM measures both oxygen consumption and TOD. The RSSOT samples were retained after oxidation and characterized to determine the composition of the oxidation products. The complexity of the sample necessitated the use of high resolution GCxGC/MS to characterize the molecules that had formed. Homologous series of aldehydes and 2-ketones were found, likely from the oxidation of alkane molecules. The study identified a molecule produced during oxidation that was common to all samples tested, 5-methyl-2-hexanol, that correlates positively with QCM deposit formation. They also discovered a molecule produced during oxidation, 1-pentanol, that correlates positively with the oxidation induction time of the RSSOT. Only 4 samples were analyzed in this study, so the correlations might not hold for a larger sample size. However, this study suggests that studying the oxidation products for jet fuel could provide insight into thermal oxidative stability.

The type of deposits that form from trace heteroatom compounds in middle distillate fuels were originally called soluble macromolecular oxidatively reactive species (SMORS) by Hardy and Wechter.[21] Their study looked at a solid material that could be extracted from diesel fuel which was called extraction induced precipitate (EIP). The oxidatively unstable diesel fuels studied are likely similar to unstable jet fuel when comparing the trace polar compounds present. After isolating the EIP, the material was characterized by elemental analysis, gas chromatography (GC), and pyrolysis/field ionization mass spectrometry (Py/FIMS). The GC analysis suggested that the EIP material contained significant amounts of higher molecular weight compounds that were not volatile enough to be analyzed by GC. Elemental analysis showed high amounts of oxygen and nitrogen in the EIP. The Py/FIMS data was very complex. However, they were able to show homologous series of a number of nitrogen and nitrogen/oxygen containing compounds. The variability of the homologous series detected by Py/FIMS across multiple fuel EIP samples supports the theory that reactive monomeric species (reactive trace polar compounds) oxidize and condense with each other to form larger, more polar, and less (but still) fuel soluble macromolecular species. An important observation is that the precursor oxidation is fast, but the deposit formation is slow.

Building off the SMORS model, a general mechanism for deposit formation has been proposed by Beaver, *et al.*[22] In their paper, they take ideas and results from academia and industry to suggest reactions of the trace polar molecules known to be involved in the TOD. In the mechanism (Figure 1.1, reprinted with permission from the American Chemical Society), the first step is oxidation of an alkyl phenol to an alkyl quinone. This is followed by electrophilic aromatic substitution (EAS) of the quinone with

an electron rich nitrogen heterocycle. The resulting product then undergoes oxidation reforming the quinone moiety. Two of these compounds can dimerize though EAS to form what would be the largest fuel soluble compound based on size and polarity. Interestingly, if the nitrogen heterocycle is a trimethyl substituted carbazole the empirical formula of the proposed reaction product would be $C_{21}H_{19}NO_2$ which is identical to the average empirical formula determined from the EIP in Hardy and Wechter's study, $C_{21}H_{19}NO_2$. Further reaction of this compound would likely lead to molecules that would be fuel insoluble and would precipitate. A second mechanism is also proposed to explain reactivity on stainless steel surfaces. The initiation step is an aromatic thiol binding to the steel surface followed by a SMORS electrophile reacting with the electron

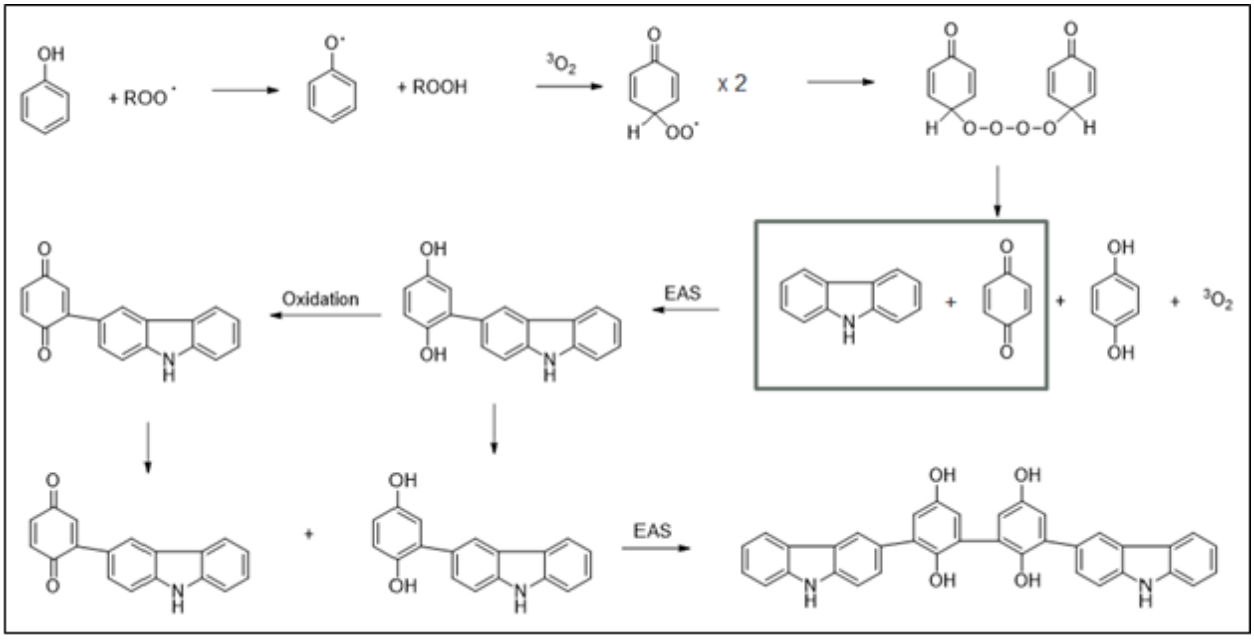

Figure 1.1 Proposed mechanism for the formation of SMORS during jet fuel thermal oxidation. Figure reprinted with permission from the American Chemical Society.[23]

rich aromatic ring through EAS. It is acknowledged that because these are proposed mechanisms, time will likely prove aspects of them incorrect. However, it is also pointed out that the mechanism explains the results from some studies. High levels of alkyl phenols and nitrogen containing aromatic heterocycles have been shown to lead to an increase in TOD by both ASTM D3241 and QCM.[8, 24]

Figure 1.2 shows the jet fuel autoxidation pathway that has been previously proposed.[23, 25] As can be seen, there are two pathways that lead to molecules responsible for deposit formation. The first fits with the SMORS model where an antioxidant molecule (alkyl phenol) reacts with a peroxy radical, formed during fuel oxidation, which can ultimately form the alkyl quinones that go on to react with the nitrogen heterocycles. Also, either through reaction with an antioxidant or another fuel molecule, hydroperoxides form in the fuel. If there are hydroperoxide decomposers, such as mercaptans, sulfides or disulfides, non-radical products, such as acidic sulfur oxides, can form leading to deposits.[6, 12-13, 26]

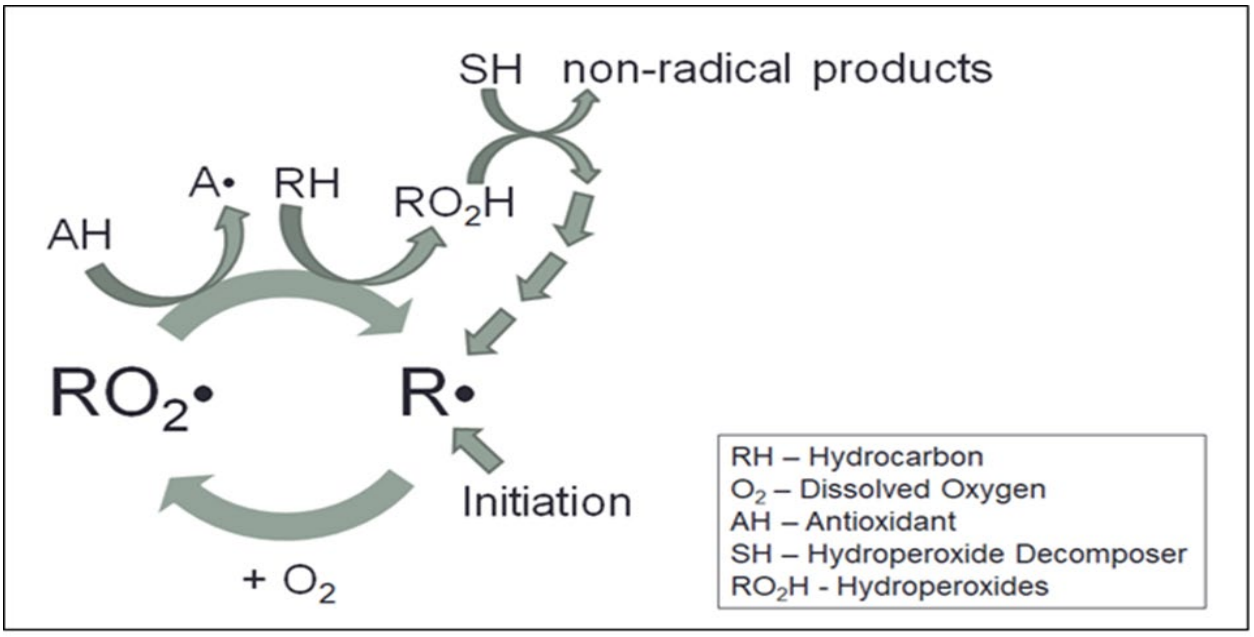

Figure 1.2 Jet fuel autoxidation pathway. The reaction of antioxidant molecules and peroxide decomposers is implicated in the formation of TOD. Reprinted with permission from the American Chemical Society.[23]

In addition to trace polar molecules, the bulk composition of a jet fuel may play an important part in thermal oxidative stability. Amara, *et al.* studied how the bulk composition of jet fuels affected their thermal oxidative stability as measured by RSSOT (temperature range 120-160°C) and ASTM D3241 (325°C).[27] The fuels that they studied were blends of a non-traditional fuel produced by the hydrogenation of fatty acids and esters (HEFA) with pure cyclic molecules. The cyclic molecules were cycloparaffins, aromatics and a cycloparaffin/aromatic hybrid, tetralin. The blends of HEFA and pure cyclic molecules were also blended at various levels with traditional jet fuel. HEFA fuels are almost entirely composed of alkanes and are allowed to be blended with traditional jet fuels at up to 50 volume % as long as they meet the ASTM D7566 specification (Standard Specification for Aviation Turbine Fuel Containing Synthesized Hydrocarbons).[28] These fuels tend to have poorer RSSOT stability and much better

ASTM D3241 stability than traditional jet fuels. The blends were analyzed by RSSOT and ASTM D3241 to determine the effect of the cyclic molecule's structure on thermal oxidative stability. In general, as normal alkane character increased, RSSOT performance decreased. They found that the addition of xylene, toluene, tetralin, and decalin up to certain levels improved or maintained the good thermal oxidative stability of HEFA by ASTM D3241.

Dewitt, et. al showed that diaromatics decrease performance of HEFA by ASTM D3241.[29] The effect of aromatic type on thermal oxidative stability was investigated by blending synthetic paraffinic kerosene (SPK) with aromatic solvents. The solvents were characterized by GC/MS and GCxGC to determine their chemical composition. Aromatic 100 was composed entirely of mononuclear aromatics. Aromatic 150 had 6 volume % dinuclear aromatics. Aromatic 200 had 82 vol % dinuclear aromatics. Blends of the aromatic solvents with SPK showed increasing TOD with increased total aromatic content. It was also observed that higher aromatic content delayed the onset of oxidation as measured by a QCM reactor system. Blends of 20 volume % of each aromatic solvent in SPK were made in order to understand how the aromatic type affected the TOD by QCM. The Aromatic 100 blend showed similar behavior to the neat SPK in total mass deposited although oxygen consumption increased. The Aromatic 150 and 200 blends significantly increased TOD.

Typically, the most abundant heteroatom in jet fuel is sulfur, with a max specification limit of 3000 ppm (m/m) in ASTM D1655.[1, 3] As can be seen in Figure 1.2, reactive sulfur-containing molecules can act as peroxide decomposers to form non-radical products.[12, 23, 25] The oxidation of jet range sulfur molecules through reaction with

hydroperoxides has been studied extensively.[6, 12] The most abundant sulfur species in conventional jet fuels are alkyl thiophenes.[30] Alkyl thiophenes tend to have stabilities similar to aromatic hydrocarbons and therefore do not tend to participate in the oxidation reactions that contribute to TOD.[30-31] It is likely that other, less abundant sulfur compounds that act as hydroperoxide decomposers such as mercaptans, sulfides, and disulfides.[12] There are a number of different products that can form through the oxidation of sulfur molecules by hydroperoxides; sulfoxides, sulfones, disulfides, and sulfonic acids.[6, 12-13, 32] Sulfonic acids have been shown to form deposits through acid-base reaction with basic nitrogen species.[26]

Kauffman suggested a pathway for deposit formation that has to do with the oxidation of sulfur species through hydroperoxide decomposition which is a part of the jet fuel autoxidation pathway shown in Figure 1.2.[26] This proposed deposition pathway is shown in Figure 1.3.

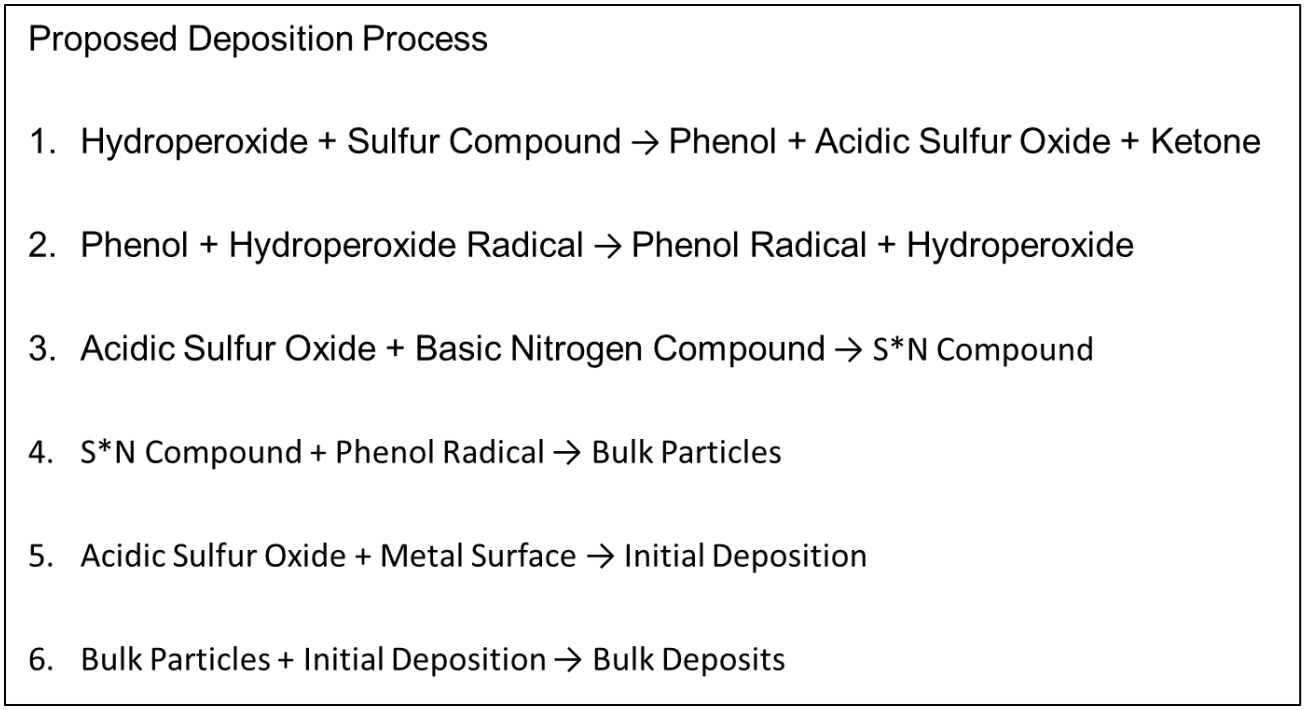

Figure 1.3 Proposed jet fuel TOD mechanism for hydroperoxide decomposer pathway. Adapted from Kauffman.[26]

In Step 1 of the deposition process proposed in Figure 1.3, a reaction between an oxidized fuel molecule that has formed a hydroperoxide and a reactive sulfur molecule goes to form a phenol, an acidic sulfur oxide, and a ketone. This can be illustrated by the oxidation of cumene to phenol using a mercaptan as the peroxide decomposer which is shown in Figure 1.4.[33] It takes 3 moles of cumene to oxidize the mercaptan to a sulfonic acid.[34] However, each oxygen added to the mercaptan increases its acidity and makes it more prone to the acid-base reaction shown in Step 3 of Figure 1.3.[35]

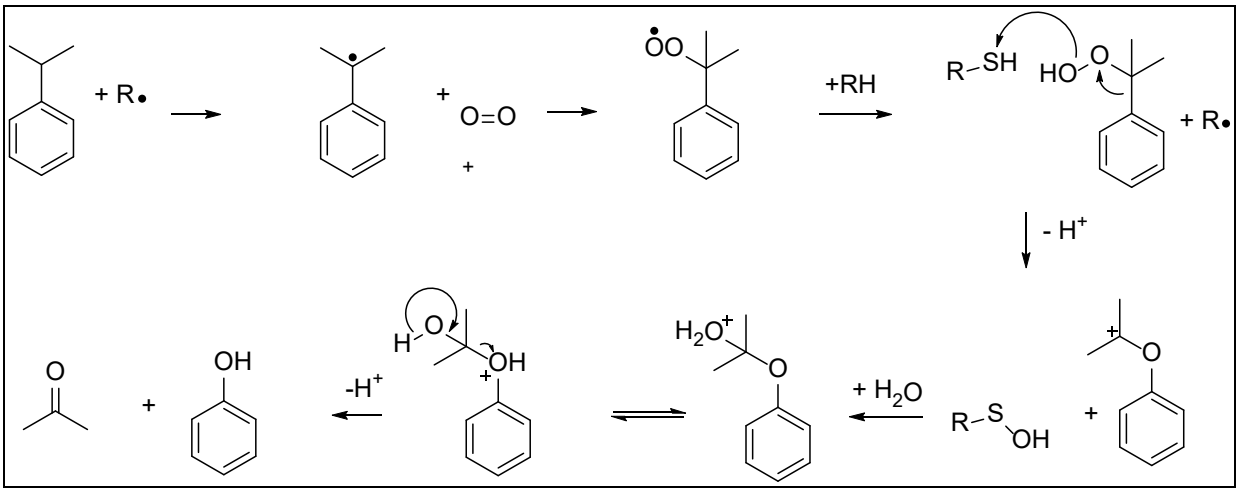

Figure 1.4 Formation of phenol, acetone, and acidic sulfur oxide from the oxidation of cumene and mercaptan molecules as proposed in Step 1 of Figure 1.3.

Step 2 of the deposition process proposed in Figure 1.3 has been previously discussed and is illustrated in Figure 1.2. The mechanism by which phenol radicals react with the S*N compounds in Step 4 has not been described. However, this step explains the fact that higher concentrations of alkyl phenols in jet fuel can lead to higher amounts of deposit formation.[26]

Research Goals of this Dissertation

As can be seen by the past research on jet fuel thermal oxidative stability, there are a number of different factors that can affect ASTM D3241 performance. In order to further the understanding of the molecules involved, the research presented here will investigate jet fuel thermal oxidative stability from a few different perspectives. Statistical analysis of LC/MS data will be used in order to identify molecules that show significance in relation to increased deposit formation by QCM and ASTM D3241. This will be done through differential analysis of fuels based on their thermal oxidative

stability and also through differential analysis of fuels before and after TOS in a QCM reactor. The molecular composition of the TOD will be explored through pyrolysis GC/MS (Py-GC/MS) of QCM deposits. Finally, to gain a deeper understanding of the variety of polar molecules that can be present in jet fuel, spent Attapulgus clay from refinery clay treaters will be extracted with solvents and then analyzed by comprehensive GCxGC/MS to speciate the molecules present. There are a number of supporting analyses that will be performed on the samples by outside laboratories following ASTM methods in addition to these primary experiments. For example, analysis of all samples for metals by ICP/MS will be done to ensure that poor thermal oxidative stability of the samples in the study are not attributable to dissolved metal ions.

By examining the possible causes of jet fuel thermal oxidative instability in a systematic way, it will be possible to identify significant molecular precursors to deposit formation and ASTM D3241 failures. The knowledge of these precursors will offer possible ways to prevent or mitigate jet fuels that fail ASTM D3241. This could be done through selective blending of refinery process streams to minimize precursor interactions, better refinery treatment operations, or possibly new refinery treatment processes.

Chapter 2 : Materials and Methods

Jet Fuels and Refinery Process Samples

To develop a deeper understanding of the complex interactions leading to poor thermal oxidative stability, it is necessary to analyze a large set of jet fuels from a variety of different sources. The largest possible set of petroleum derived jet fuel samples available was included in this study. Table 2.1 lists the samples that were analyzed in the various studies comprising this dissertation along with their description and their thermal oxidative stability as measured by ASTM D3241 and QCM (if available). Table 2.2 lists the physical properties of the samples that were measured.

It is important to note that samples were collected as they became available. They were often received as part of a specific project. Each project had specific requirements for the types of analyses that needed to be performed on the fuels. Oftentimes, the temperature of the ASTM D3241 analysis was dictated by the project needs. Due to sample volume limitations it was not possible to analyze all the fuels at the same temperature. Therefore, there are three temperatures settings for the ASTM D3241 analysis at which the samples were tested; 260 °C, 275 °C, and 280 °C.

The total volume received of each sample and the project requirements also limited the ability to test all fuels for all properties of interest. In general, ASTM D3241 analysis, QCM analysis, and LC/MS analysis were prioritized when sample volumes were limited. Running QCM analysis made Py-GC/MS of TOD also possible if enough deposit formed. Also, having these data allowed for statistical analysis to elucidate compounds significant to TOD formation.

Sample ID	Description	ASTM D3241 VTR	ASTM D3241 ITR, nm	ASTM D3241 dP, mmHg	ASTM D3241 Temperature, °C	QCM Max Mass, µg/cm^2	QCM, % O_2 at Max Mass
D9162	Diesel #1	1	8.031	0	260	0.63167	0
J2668	Jet A	1	11	0	275	7.2385	0.2
J2717	Straight Run	2A	69.45	0	275	7.2385	0.2
J2949	Hydroprocessed	1	0.1	0.1	280	1.3073	72.9
J2950	Hydroprocessed	<3	44.3	0.1	275	0.8827	0.0
J2954	Hydroprocessed	1	55.38	0	260	29.9977	2.0
J2969	Hydroprocessed	1	4.2	0	275	1.1889	0.0
J2971	Hydroprocessed	4P	N/A	0	260	4.2907	0.0
J2990	Hydroprocessed	1	N/A	0	260	0.7128	0.0
J3005	Hydroprocessed	2	33.3	0	275	8.8379	0.0
J3044	Straight Run	>4	188.8	250.2	260	16.3583	27.1
J3045	Hydroprocessed	<1	19.4	0	260	26.8261	0.4
J3070	Straight Run	<3A	44.6	0	275	2.5839	0.0
J3071	Hydroprocessed	1	41	0	275	1.0368	0.0
J3072	Straight Run	3P	61	251.5	275	10.679	0.0
J3091	Straight Run	>4P	155.4	252.2	280	20.3486	0.4
J3092	Straight Run	>4P	166.2	250.7	280	N/A	N/A
J3093	Jet A	4	53.8	0	280	N/A	N/A
J3094	Jet A	4	36	0	280	N/A	N/A
J3095	Jet A	4	105.1	0	280	N/A	N/A
J3096	Jet A	1	23.9	0	280	N/A	N/A
J3097	Jet A	1	34.1	0	280	N/A	N/A
J3098	Jet A	1	2.5	0	280	N/A	N/A
J3099	Jet A	1	28.1	0	280	N/A	N/A
J3100	Jet A	<3	63.6	0	280	N/A	N/A
J3101	Jet A	1	8.5	0	280	N/A	N/A
J3102	Jet A	4	47.3	0	280	N/A	N/A
J3103	Jet A	1	44.3	0	280	N/A	N/A
J3104	Jet A	1	45.2	0	280	N/A	N/A
J3105	Jet A	>4	134.95	0	280	N/A	N/A
J3188	Hydroprocessed	4P	164.7	251	275	16.3651	0.0
J3189	Jet A	<3	54	0	275	8.9052	0.1
J3190	Jet A	<3	50.5	0	275	13.9418	0.2
J3191	Hydroprocessed	3P	167.7	250.2	275	14.5895	0.3
J3192	Hydroprocessed	4P	113.4	0.8	275	31.2328	0.3
J3193	Straight Run	1	37.9	0	275	22.3591	5.8
J3194	Straight Run	3	75.1	0.7	275	13.4403	3.1
J3195	Hydroprocessed	1	47.7	0.1	275	8.1463	0.0

Table 2.1 Thermal oxidative stability measurements by ASTM D3241 and QCM for jet fuels in this dissertation. Fuels were analyzed at different temperatures depending on the project they were received for. If a test was not performed, it was due to sample volume. N/A means Not Analyzed.

Sample ID	Total Sulfur by XRF, ppm (m/m)	H_2S, ppm (m/m)	Mercaptan Sulfur, ppm (m/m)	Total Nitrogen, ppm (m/m)	Basic Nitrogen, ppm (m/m)	Detectable Metals by ICP/MS
D9162	<5	N/A	N/A	2.22	3	No
J2668	402	N/A	N/A	3.84	3	No
J2717	3008	N/A	N/A	1.13	2	No
J2949	<5	N/A	N/A	0.686	2	No
J2950	899	N/A	N/A	7.55	8	No
J2954	<5	N/A	N/A	2.02	1	No
J2969	<5	N/A	N/A	1.56	1	No
J2971	105	N/A	N/A	41.9	28	No
J2990	<5	N/A	N/A	0.662	<1	No
J3005	373	N/A	N/A	1.56	3	No
J3044	8633	N/A	N/A	99.2	70	No
J3045	1440	N/A	N/A	39.3	33	No
J3070	164	N/A	N/A	9.18	9	No
J3071	613	N/A	N/A	3.13	4	No
J3072	619	N/A	N/A	8.52	9	No
J3091	1173	0	82	11.3	11	No
J3092	N/A	N/A	N/A	N/A	N/A	No
J3093	N/A	N/A	N/A	N/A	N/A	No
J3094	N/A	N/A	N/A	N/A	N/A	No
J3095	N/A	N/A	N/A	N/A	N/A	No
J3096	N/A	N/A	N/A	N/A	N/A	No
J3097	N/A	N/A	N/A	N/A	N/A	No
J3098	N/A	N/A	N/A	N/A	N/A	No
J3099	N/A	N/A	N/A	N/A	N/A	No
J3100	N/A	N/A	N/A	N/A	N/A	No
J3101	N/A	N/A	N/A	N/A	N/A	No
J3102	N/A	N/A	N/A	N/A	N/A	No
J3103	N/A	N/A	N/A	N/A	N/A	No
J3104	N/A	N/A	N/A	N/A	N/A	No
J3105	N/A	N/A	N/A	N/A	N/A	No
J3188	164	0	4.4	27.1	22.5	No
J3189	369	0	4.6	78.8	59.2	No
J3190	367	0	4	77.4	59.2	No
J3191	429	0	5	61.9	48.9	No
J3192	1773	0	31	17.6	15.5	No
J3193	2435	0	62	15.4	14.1	No
J3194	2642	0	53	4.67	4.6	No
J3195	343	0	8.7	38.5	32	No

Table 2.2 Additional properties measured for jet fuels in this dissertation. If a test was not performed, it was due to limited sample volume. ICP/MS was prioritized due to dissolved metals effect on thermal oxidative stability. N/A means Not Analyzed.

All of the analyses described in Table 2.2 were carried out by contract laboratories. Only a brief description of the methodologies is provided here for context. Total sulfur was measured by X-ray fluorescence according to the standard test method ASTM D4294-16e1.[36] H_2S and mercaptan sulfur were determined by potentiometric titration according to the standard test method UOP163-10.[37] Total nitrogen was measured by oxidative combustion with chemiluminescence detection according to the standard test method ASTM D4629-17.[38] Basic nitrogen was determined by potentiometric titration according to the standard test method UOP269-10.[39] Trace dissolved metals were measured by inductively coupled plasma/mass spectrometry (ICP/MS) according to the standard test method UOP1005-14.[40]

Solvents and Chemicals

For LC/MS, 18 MOhm water was acquired from a Millipore Synergy UV water purification system (Model SYNSVHFOO) and used to make mobile phase solvents. Methanol and formic acid were Optima grade purchased from Fisher Scientific (Hampton, NH) and used as-is in mobile phase solvents. Isopropyl alcohol used for sample dilution was Optima grade and purchased from Fisher Scientific (Hampton, NH).

For the solvent extract of spent Attapulgus clay, hexane, toluene, methylene chloride (DCM), and methanol (MeOH) were Optima grade purchased from Fisher Scientific (Hampton, NH).

Solvent Extraction of Spent Attapulgus Clay

Attapulgus clay that had been used in refinery clay treaters was collected and removed from the filter bodies for analysis. Approximately 300 g of Attapulgus clay that

had been used in refinery service for the filtration of jet fuel was loaded into an open glass column with a fritted glass support above the stopcock. The clay was extracted with 400 mL of each; hexane, toluene, methylene chloride, 1:1 methylene chloride:methanol (DCM:MeOH), and methanol (MeOH). The effluent from each solvent wash was collected in individual fractions which were demarcated by the introduction of the next solvent. The solvents were then removed through evaporation utilizing a Reacti-Therm device (TS-18826, Thermo Fisher, Waltham, MA). The solutions were heated to 50 °C while under a stream of nitrogen gas open to the atmosphere in a fume hood for approximately 12 hours. The residue remaining after the solvent was removed was collected for analysis by comprehensive GCxGC-FID/MS.

Samples were prepared for GCxGC-FID/MS (GCxGC/MS) analysis by dissolving 1000 ppm (m/m) in Optima grade methylene chloride. This was determined to be an appropriate concentration after analyzing samples that were prepared at 100, 500, 1000, 1500, and 2000 ppm (m/m).

Liquid Chromatography/Mass Spectrometry

Positive ion ESI analysis. The following methodology was initially described in a manuscript written by the author of this dissertation.[23] An Agilent 1290 UHPLC was connected to an Agilent 6230 TOF MS instrument with a dual ESI source was used for the analysis of samples. 1 µL injections of samples diluted 1:1 with isopropyl alcohol were separated on an Agilent RRHD 2.1 × 50 mm C8 column with 1.8 µm particles. The mobile phase gradient went from 9:1 water/methanol with 0.1 vol % formic acid to 9:1 methanol/water with 0.1 vol % formic acid at a 0.300 mL/min flow rate. The initial

solvent was held for 1 min and then ramped to the final solvent over 10 min. The final solvent was held for 5 min.

The mass spectrometer was operated in positive ion mode. The drying gas temperature was 350 °C and the nebulizer pressure was 50 psi. Data were collected over the *m/z* range of 70−3600. The capillary voltage was set to 3000 V. The fragmentor voltage was 120 V. Data were collected at 4 GHz in high-resolution mode. A solution of API-TOF reference masses (Agilent Technologies, Santa Clara, CA) was introduced through the second ESI nebulizer to allow for real-time mass accuracy calibration during the analysis.

To minimize the number of samples being analyzed sequentially, all samples were run in a randomly generated order in triplicate. The technical replicates help to reinforce confidence during statistical analysis. The column was equilibrated to the solvent system by running the method three times with no injection at the beginning of the sequence. J2990 was chosen to be used as a quality control (QC) sample due. Analysis of the QC sample was performed 3 times after the blank runs. The QC was then run again after every third sample in order to monitor the drift of retention times and the change in peak intensities across the sequence.

Negative ion ESI analysis. An Agilent 1290 UHPLC was connected to an Agilent 6230 TOF MS instrument with a dual ESI source was used for the analysis of samples. 1 µL injections of samples diluted 1:1 with isopropyl alcohol were separated on an Agilent RRHD 2.1 × 50 mm C8 column with 1.8 µm particles. The mobile phase gradient went from 9:1 water/methanol with 0.1 vol % ammonium hydroxide and 5 mM

ammonium fluoride to 9:1 methanol/water with 0.1 vol % ammonium hydroxide and 5 mM ammonium fluoride at a 0.300 mL/min flow rate. The initial solvent was held for 1 min and then ramped to the final solvent over 10 min. The final solvent was held for 5 min.

The mass spectrometer was operated in negative ion mode. The drying gas temperature was 350 °C and the nebulizer pressure was 50 psi. Data were collected over the *m/z* range of 70−3600. The capillary voltage was set to -3000 V. The fragmentor voltage was -120 V. Data were collected at 4 GHz in high-resolution mode. A solution of API-TOF reference masses (Agilent Technologies, Santa Clara, CA) was introduced through the second ESI nebulizer to allow for real-time mass accuracy calibration during the analysis.

The same random ordering sequence was used in negative mode that was employed in positive ion mode in order to allow for confidence during statistical analysis of the data.

Statistical Analysis of LC/MS Data

Data preprocessing. The following methodology was initially described in a manuscript written by the author of this dissertation.[23] LC/MS Data were preprocessed by batch molecular feature extraction (MFE) with recursive analysis in *Profinder*® (version B08.00, Agilent Technologies, Santa Clara, CA). The algorithm employed during the molecular feature extraction identified ions in the data that displayed chromatographic behavior. Chromatographic behavior can be defined as an ion that exhibits a normal distribution of intensity over time; plotting the intensity over time yields

a chromatographic peak. The Profinder recursive analysis then examines the list of identified ions from all of the samples and performed a find-by-ion algorithm on each individual sample using the entire list allowing for the detection of ions that may have been missed during the initial MFE. The result was an entity list of ions defined by their *m/z* values and the retention time at their chromatographic peak maxima. Alignment of the entities was performed by saving them with their average *m/z* and retention time values.

Statistical analysis of preprocessed data for differential analysis of jet fuels based on thermal oxidative stability. Preprocessed data were imported into *Mass Profiler Professional*® (MPP) (version 14.9.1, Agilent Technologies, Santa Clara, CA). When data are imported into MPP, the software automatically transforms the raw abundance values by applying a log2 transformation. The purpose of this transformation is to help ensure a normal distribution which is necessary to meet the assumptions of most statistical tests. A 75-percentile shift was utilized to normalize the entities. This normalization is done by taking the log2 intensity at the 75th percentile and subtracting it from the log2 intensity of itself and every other entity. The 75th percentile normalization helps to eliminate small variations due to experimental factors by assuming the total intensity from each sample is approximately the same. After 75th percentile normalization, each entity was baselined to the median intensity value for that entity across all samples.

In order to perform differential analysis in the small-scale study, the samples were grouped according to their ASTM D3241 results. Statistical tests were applied to the different groups of samples to find entities that were significant to each group.

Filtering the entities by frequency removed entities that were not present in 100% of the samples in at least one group. Filtering the entities on variability removed all entities that had a coefficient of variation that was ≤25%. This coefficient of variation was selected to eliminate some of the entities that did not show variability without removing too many entities. An analysis of variance (ANOVA) $p \leq 0.01$ was performed across the groups on the list of entities remaining after the initial data filtration steps. A filter by fold change was applied to the statistically significant entity list that remained after the ANOVA looking for entities that were present ≥16-fold higher in the fuel that failed ASTM D3241. This is the maximum allowable fold change filter in MPP which allowed for the maximum reduction of entities that didn't show large variation across the sample groups. Principal component analysis (PCA) was used to visualize the sample groupings after data processing and to confirm that the samples still cluster with logical groups relating to the ASTM D3241 results. The final entity list was processed in the ID browser imbedded in MPP allowing for elemental compositions to be generated which were then searched against a proprietary database built in the *Personal Compound Database Library (PCDL)* (Version B.07.00 2017, Agilent Technologies, Santa Clara, CA).

For the large-scale study, it was necessary to process the data differently. Samples were grouped based on their ASTM D3241 results. For visualization purposes prior to statistical analysis, the entities were grouped by their average value in the passing and failing ASTM D3241 groups. The QC samples were omitted from the statistical analysis to simplify the analysis however it was determined that they showed equivalent results across the entire sequence. For the two-group set it was possible to use a moderated T-test ($p \leq 0.05$) to determine significance in the entities. Then a filter

by fold change (>4 fold) was applied to determine entities that either increased or decreased based on ASTM D3241 results.

Statistical analysis of preprocessed data for differential analysis of jet fuel samples before and after thermal oxidative stressing in a QCM. LC/MS ESI data was batch processed in *Profinder*® (Agilent Technologies, v. B08.00) by a recursive molecular feature extraction algorithm as previously discussed. The pre-processed data were then imported into *Mass Profiler Professional*® (MPP) (version 14.9.1, Agilent Technologies, Santa Clara, CA) for statistical analysis. Each fuel was analyzed separately to look at the changes that occurred after thermal oxidative stressing in the QCM reactor. For this type of data, a moderated T-test with a 95% confidence interval was utilized to find entities that changed significantly.

After identifying significant entities, elemental compositions were generated based on *m/z* values and isotope abundance utilizing the ID browser embedded in MPP. These were searched against a proprietary database utilizing the *Personal Compound Database Library (PCDL)* (Version B.07.00 2017, Agilent Technologies, Santa Clara, CA).

Comprehensive GCxGC/MS

All comprehensive GCxGC/MS measurements were carried out on an Agilent 7890B gas chromatograph with a Zoex ZX-1 thermal modulator coupled to a JEOL AccuTOF GCv 4G. The transfer line temperature was 300 °C. The mass spectrometer had an electron ionization (EI) source installed with a photoionization (PI) source attached (MS-53120PI, JEOL USA, Peabody, MA) allowing for either ionization mode to

be utilized. The transfer line temperature was 250 °C. Samples were analyzed in both EI and PI mode to allow for different types of data processing. EI mode allowed for searching the NIST 17 Library with MS Search v2.3 to determine the identity of compounds.[41-42] For both EI and PI mode analysis, the ion source had a temperature of 250 °C. PI mode allowed for the measurement of molecular ions and the determination of elemental compositions based on the measured *m/z* values and isotope abundance.[43]

The mass spectrometer was set to collect data in the *m/z* range of 29-500. The sampling interval was set to 0.25 ns. The recording interval was set to 0.04 s, which was sufficient for the narrow peaks produced by comprehensive GCxGC analyses. For EI mode, the detector voltage was set to 1900 volts. For PI mode, the detector voltage was set to 2300 volts. The instrument's mass accuracy was tuned by analyzing perfluorokerosene in EI mode and utilizing a 3rd degree polynomial calibration curve. Each data file had a drift compensation performed by finding a compound of known exact mass and performing a single point calibration which is a feature in the *MassCenter* software (version 2.6.6b, JEOL USA, Peabody, MA).

The column setup utilized for these analyses was a reverse column set where the first column was more polar than the second column which has been shown to be useful for the analysis of polar compounds in a non-polar bulk matrix.[44] The first column was a 30 m x 0.25 mm x 0.25 µm DB-17ms column (Agilent Technologies, Santa Clara, CA). The first column was connected to a 1.5 m x 0.1 mm loop of high temperature fused silica (Agilent Technologies, Santa Clara, CA) using an SGE micro union connector (Trajan Scientific, Australia). The loop sits inside the thermal modulator

allowing for the trapping of effluent from the first column with liquid nitrogen and the introduction of the trapped compounds to the second column by a jet of hot nitrogen gas. The liquid nitrogen was flowed over the loop at approximately 5 mL/min. The hot jet pulsed every 10 seconds for 0.35 seconds. The temperature of the hot jet was initially 200 °C which was held for 10 minutes prior to being ramped at a rate of 3 °C to a final temperature of 330 °C which was then held for 10 minutes.

The effluent from the second column went into a 2-way purged capillary flow splitter. The purged flow was set to 12 psi. This setting allowed for a 1:1 split over the entire temperature gradient for the method. A 1.02 m x 100 μm high temperature fused silica column (Agilent Technologies, Santa Clara, CA) connected one of the effluent ports of the splitter to the mass spectrometer. A 0.73 m x 100 μm high temperature fused silica column (Agilent Technologies) connected the other effluent port to a flame ionization detector (FID). The FID was at a temperature of 300 °C. The air flow was 320 mL/min. The hydrogen gas flow was 38 mL/min. The He makeup flow was 61 mL/min. Data was acquired at 100 Hz which was sufficient for the narrow peaks from comprehensive GCxGC analysis.

1 μL of sample was injected into the split/splitless inlet at 300 °C. The inlet had a dual taper ultra-inert split liner packed with glass wool (5190-3165, Agilent Technologies, Santa Clara, CA). The inlet was operated at a split ratio of 100:1. The column flow rate was set to 1.5 mL/min. The initial oven temperature was 40 °C, which was held for 5 minutes. The oven was then ramped at a rate of 3 °C/minute until a final temperature of 250 °C. The final temperature was held for 10 minutes.

ASTM D3241 – Jet Fuel Thermal Oxidation Test

ASTM D3241 analyses were performed according to the standard test method on a JFTOT Mark IV instrument manufactured by PAC (Houston, TX) (ASTM D3241-18[4]). There has been discussion in the aviation industry suggesting that different versions of ASTM D3241 compliant instruments can produce different results for the same fuel due to design differences.[45] There is an effort underway within a working group at the Coordinating Research Council to develop a reference fluid to develop a reference fluid with known ASTM D3241 values to allow for calibration across different models of instruments.

There are two different ways that samples can fail ASTM D3241 analysis. They can fail from excessive deposit formation on the aluminum heater tube or by excessive differential pressure across a nominal 17 μm steel filter. Excessive deposit formation can be determined either by visual tube rating (VTR) where the color of the tube is compared to the ASTM color standard for heater tube deposits. A VTR of 3 or greater or any tube that has an abnormal or peacock deposit fails. It can also be determined by metrology such as interferometer tube rating (ITR) where the thickness of the deposit is measured. Any tube with an ITR of 85 nm or greater fails. The fuel is filtered by a 0.45 μm nitrocellulose filter before it enters the heater tube region of the instrument. If pressure builds across the 17 μm filter it is likely due to insoluble material that forms in the heater tube region. If the differential pressure reaches 25 mmHg at any time during the analysis, the sample fails.

Quartz Crystal Microbalance

Thermal oxidative stressing (TOS) was carried out in a QCM system built by the University of Dayton Research Institute (Dayton, OH) conforming to ASTM D7739,[20] similar to what has been described previously in the literature for the study of jet fuel.[46] A 5 MHz crystal (Inficon, 149211-1) was submerged in 60 mL of sample in a 100 mL Parr reactor with continuous stirring. The sample was sparged with air for 15 min then the reactor was sealed and heated to 140 °C. Once the system reached the test temperature, the 15-hour reaction time began and the pressure, relative % oxygen, and frequency of the crystal were recorded. After the analysis was completed, the system was allowed to cool, and the residual fuel was collected and saved for further analysis. Any residual deposits that formed were washed out of the QCM reactor with heptane and retained for Py-GC/MS analysis. The mass deposition was calculated using a modified Saurbrey's equation (Figures 2.1 and 2.2). The theory behind the relationship between the mass deposition and change in frequency has been described in detail previously.[46-47]

$$\Delta F_M \approx \frac{-2F_o^2 \Delta m}{A\sqrt{\rho_q \mu_q}}$$

Figure 2.1 Modified Saurbrey's equation relating the change in frequency of a quartz crystal with its initial frequency (Fo), change in mass (Δm), surface area (A), density of the crystal (ρq), and rigidity of the crystal (μq).

QCM mass deposition results are reported in μg/cm^2. In order to get this value, the modified Saurbrey's equation is rearranged.

$$\Delta m/A \approx \frac{\Delta F_M \sqrt{\rho_q \mu_q}}{-2F_o^2}$$

Figure 2.2 Modified Saurbrey's equation solved for the change in mass of the crystal over its unit area. Values are reported in units of μg/cm^2.

Pyrolysis Gas Chromatography/Mass Spectrometry

All Py-GC/MS analyses were carried out using a Frontier auto-shot sampler (AS-1020E) with a multi-shot pyrolyzer (EGA/Py-3030D) and a selective sampler (SS-1010E) utilizing a micro jet cryo trap (MJT-1030Ex) on an Agilent 7890A gas chromatograph coupled to an Agilent 7010 GC-TQ mass spectrometer with an electron ionization source.

Evolved Gas Analysis (EGA) is used to determine the temperature ranges at which thermal desorption and pyrolysis occur. Prior to EGA analysis of TOD the furnace was held at 100 °C for two minutes while venting to desorb trace solvent from the sample. For EGA of the TOD the furnace was ramped from 100 °C to 800 °C at 20 °C/min while the GC oven was held at 300 °C and an inert capillary directly introduced evolved sample vapors into the ion source without chromatographic separation. A split

ratio of 50:1 was utilized and the mass range monitored was *m/z* 29 to *m/z* 650. The GC inlet temperature was 300 °C, the mass spectrometer transfer line temperature was 320 °C, the EI source temperature was 230 °C, and the quadrupole temperature was 150 °C.

A heart-cut single shot experiment was used to perform GC/MS analysis on pyrolysis vapors products. First, the furnace was held at 310 °C for 3 minutes while volatile components were desorbed and vented. The lower temperature of 310 °C was selected to avoid unintentional pyrolysis during venting. Then, the furnace was ramped from 310 °C to 800 °C at 40 °C/min and the produced pyrolysis product vapors were directed with a split ratio of 25:1 onto the cryogenic trap inside the GC oven. For GC/MS analysis of the trapped vapors the GC oven containing a UA-5 column (5% phenyl/95% poly dimethyl siloxane) 30 m x 0.25 mm (0.25 μm film) was held at 40 °C for 2 minutes, then ramped to 180 °C at 2.5 °C/min, then ramped to 300 °C at 20 °C/min, then held at 300 °C for 3.5 min. The GC inlet temperature was 300 °C, the mass spectrometer transfer line temperature was 320 °C, the EI source temperature was 230 °C, and the quadrupole temperature was 150 °C.

Chapter 3 : Statistical Analysis of LC/MS ESI Data from Jet Fuels with Varying Thermal Oxidative Stability

Initial Small-Scale Pilot Study

Positive ion ESI. To determine the efficacy of utilizing statistical analysis of LC/MS ESI data to determine the compounds significant to jet fuel thermal oxidative stability a small-scale study utilizing 7 fuels was performed. The results of this study have been previously published.[23] Table 3.1 (reprinted with permission from the American Chemical Society) shows the subset of fuels that were used in this set of experiments. All fuels meet the requirement of ASTM D1655 for use as Jet A with the exception of J2971 which does not meet the ASTM D3241 thermal oxidative stability requirement. This set of fuels was analyzed by ASTM D3241 at 260 °C which was the temperature of interest for the original study. Detailed properties for these fuels can be found in Tables 1.1 and 1.2.

Fuel Sample ID	Sample Type	ASTM D3241 VTR, 260 °C	ASTM D3241 Pass/Fail	Detectable Metals by ICP/MS?
J2949	Jet A	<1	Pass	No
J2950	Jet A	<1	Pass	No
J2954	Jet A	<1	Pass	No
J2971	Jet A	4P	Fail	No
J2990	Jet A	<1	Pass	No
J3005	Jet A	<1	Pass	No
D9162	Diesel #1	<1	Pass	No

Table 3.1 Samples analyzed for initial small-scale pilot study with ASTM D3241 results at 260 °C. No metals were detected in these fuels. Table reproduced with permission from the American Chemical Society.[23]

The fuels in Table 3.1 were analyzed by liquid chromatography/mass spectrometry electrospray ionization (LC/MS ESI) in positive ion mode by the methodology previously described in Chapter 2. ESI has the disadvantage of large differences in ionization efficiencies between compounds along with the possibility of ion suppression from solvents, additives, or co-eluting compounds.[42] The effect of this can be bias in interpretation of LC/MS ESI data due to the analyst seeing large reconstructed total ion current chromatographic (RTICC) peaks and assuming that means those RTICC peaks are significant. Baselining the relative intensity values for entities extracted from the LC/MS ESI data to their median value puts all entities on the

Figure 3.1 Log 2 normalized plot of all entities in unprocessed data. Each line represents an entity detected. The legend relates the intensity of the entity in J2971 relative to the median value for the entity. Image reproduced with permission from the American Chemical Society.[23]

same scale. The statistical analysis of the data along with the data filtration steps reduced the number of entities in the data set from 1669 to 284. Figure 3.1 shows a graphical representation of the unprocessed entity list with 1669 entities and Figure 3.2 shows the final entity list after the final filter by fold change step of data processing. The charts from the other data processing steps can be found in Appendix A (Supplemental Figures 3.1-3). The remaining entities were statistically significant ($p \leq 0.01$) when

comparing the fuel that failed ASTM D3241 at 260 °C with the fuels that passed ASTM D3241 at 260 °C.

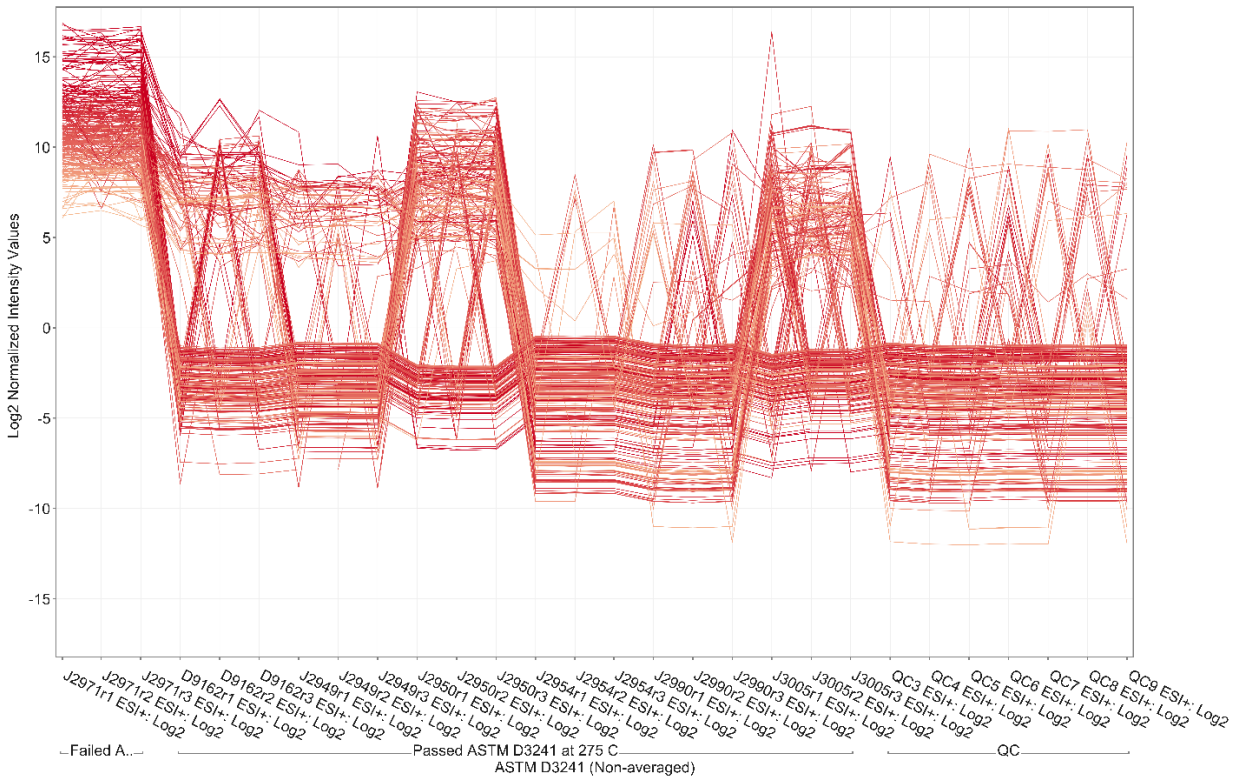

Figure 3.2 Log 2 normalized plot of all entities after ANOVA and Filter by Fold Change (>16 fold) (entities increase in Poor ASTM D3241 sample. The legend in Figure 3.1 applies to this chart as well. Image reproduced with permission from the American Chemical Society.[23]

Figure 3.3 is a 3-D graphical representation of the results from a principal component analysis (PCA) of the remaining entities which shows that the samples cluster with themselves and also along ASTM D3241 results (Image reproduced with permission from the American Chemical Society).

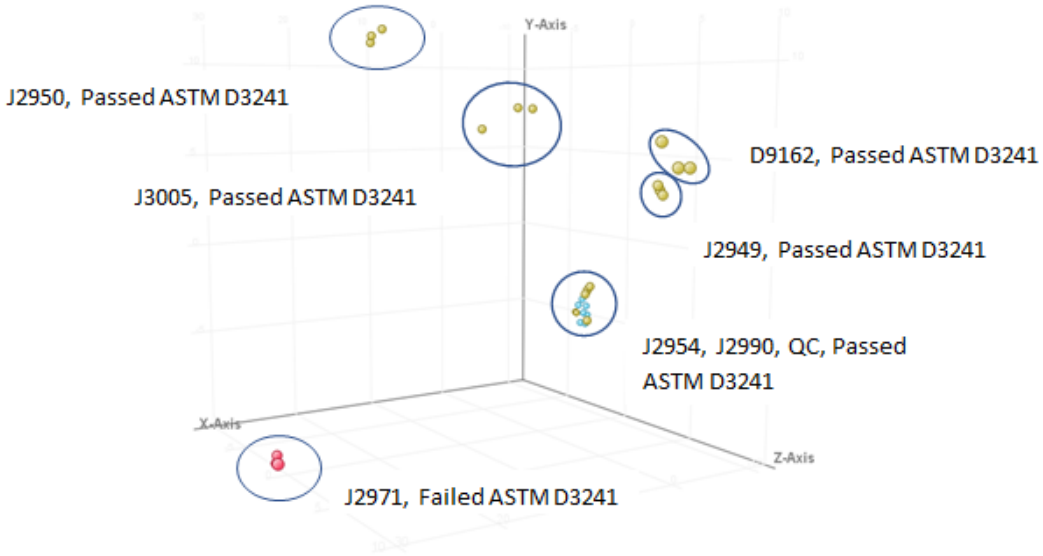

Figure 3.3 3-D graphical representation of the principal component analysis for the final entity list. All samples cluster with themselves. The failing sample (red dots) is well separated from the other samples. The x-axis represents the first principal component, the y-axis represents the second principal component, and the z-axis represents the third principal component. Image reproduced with permission from the American Chemical Society.[23]

From this chart, it is clear that most of the variation in the data occurs along the first two principal components which are represented by the x-axis and y-axis as shown in the 2D PCA (Figure 3.4, image reproduced with permission from the American Chemical Society). In the 2D PCA, J2971 sits outside the T^2 Hotelling Ellipse with a 95% confidence interval, which suggests there is significant variance between this sample and the rest along the first two principal components.

Exporting the final entity list to the IDBrowser embedded in the MPP software package allowed for the generation of elemental compositions and searching against a library of compounds created in the *Personal Compound Database Library (PCDL)*

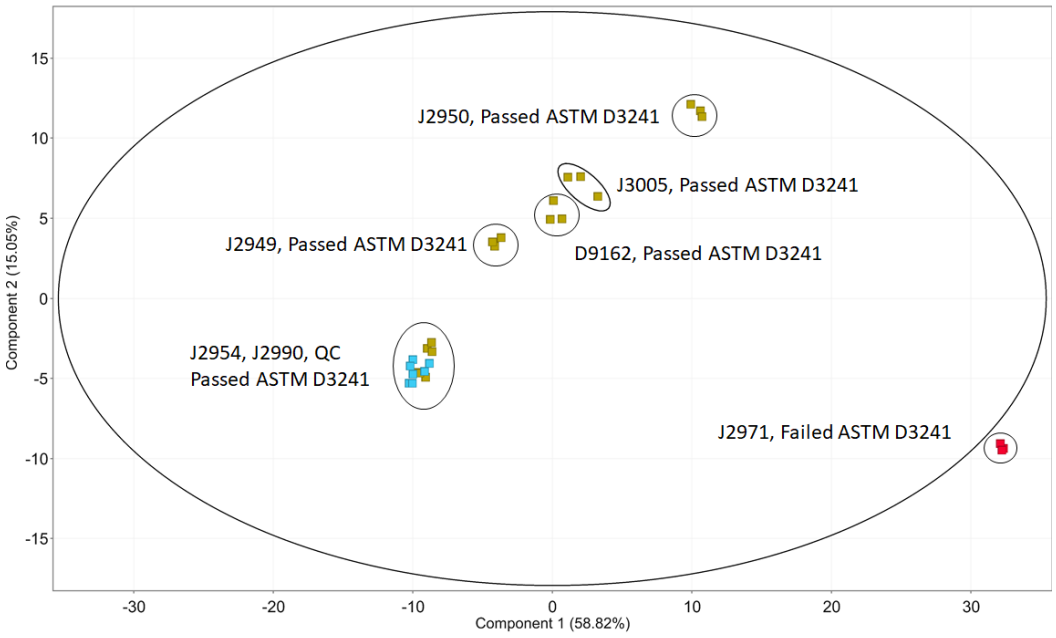

Figure 3.4 2-D graphical representation of the principal component analysis for the final entity list. All samples cluster with themselves. The failing sample (red dots) is well separated from the other samples. Image reproduced with permission from the American Chemical Society.[23]

(Version B.07.00 2017, Agilent Technologies, Santa Clara, CA) built using the previously described LC/MS ESI method. The IDBrowser utilizes the *m/z* values, isotope abundance, and isotope spacings of the entities to generate possible elemental compositions based on how closely they match the actual values. The PCDL can match library entries to entities based on their elemental composition or the *m/z* value and isotope abundance and isotope spacings along with their retention time. Table 3.2 lists identified compounds and generated elemental compositions. Duplicate elemental compositions (isomers) have been eliminated in the table so each elemental composition only appears once. This process identified homologous series of compounds consistent with those that have been previously implicated in jet fuel thermal oxidative stability issues. Specifically, homologous series with elemental

Identity	Mass	Score (DB)	Score (MFG)
$C_nH_{2n-5}N$ (Anilines)			
N-ethylaniline	121.0889	99.1	0
2-propylaniline	134.0956	86.6	0
C10 H15 N	149.1202	0	86.5
C11 H17 N	163.1361	0	85.7
C12 H19 N	177.1515	0	85.5
C13 H21 N	191.1671	0	85.6
4-octylaniline	205.1828	98.9	0
C15 H25 N	219.1982	0	0
4-decylaniline	233.2136	87	0
$C_nH_{2n-9}N$ (Indoles)			
2,3,7-trimethylindole	159.1061	84.9	0
2-methyl-3-propylindole	173.1203	84.6	0
C13 H17 N	187.1356	0	87.3
C14 H19 N	201.1513	0	87.4
C16 H23 N	229.1818	0	87.1
C_nH_{2n-7N} (Indolines)			
$C_{13}H_{19}N$	189.1514	0	87.5
$C_nH_{2n-11}N$ (Quinolines)			
2,6-dimethylquinoline	157.089	87.8	0
C12 H13 N	169.183	0	84
$C_nH_{2n-13}N$			
C12 H11 N	169.089	0	84.5
$C_nH_{2n-6}O$ (Phenols)			
m-cresol	90.0475	87.5	0
C7 H8 O	90.0475	0	85.7
2,5-dimethylphenol	121.089	87.1	0
2,6-di-tert-butylphenol	223.1943	79.8	0
$C_nH_{2n-8}O$			
C9 H10 O	134.0715	0	86.8
C11 H14 O	162.1042	0	87.2
$C_nH_{2n-10}O$			
C10 H10 O	146.0699	0	80.4
C_nH_yOS			
C7 H14 O S	146.0767	0	79.7
C8 H16 O S	160.0897	0	79.5
C9 H18 O S	174.105	0	98.8
C10 H18 O S	186.1059	0	99.6

Table 3.2 Identified compounds and generated elemental compositions for entities in the final list. Duplicate entities (isomers) have been omitted. Table reproduced with permission from the American Chemical Society.[23]

Identity	Mass	Score (DB)	Score (MFG)
C_nH_yNO			
C8 H11 N O	137.0838	0	87.6
C9 H17 N O	155.1309	0	87
C10 H17 N O	167.1309	0	87.6
C11 H13 N O	175.0996	0	99.5
C12 H19 N O	193.1487	0	86.8
C13 H15 N O	201.1148	0	85
C13 H17 N O	203.1306	0	77.6
C13 H23 N O	209.1779	0	85.2
C15 H19 N O	229.1469	0	76.2
C15 H23 N O	233.181	0	75.9
C15 H27 N O	237.2092	0	86.6
C17 H23 N O	257.1813	0	76.5
C17 H27 N O	261.2036	0	98.3
C18 H29 N O	275.2247	0	99.3
C19 H29 N O	287.2246	0	86.1
C19 H31 N O	289.2401	0	99.3
C20 H25 N O	295.214	0	82.1
C20 H29 N O	299.2242	0	77.1
C20 H31 N O	301.234	0	82.2
C22 H33 N O	327.2558	0	83.7
C23 H39 N O	345.3026	0	99.3
C24 H33 N O	351.2524	0	81.2
C25 H41 N O	371.3031	0	82.8
C_nH_yNOS			
C11 H25 N O S	219.1654	0	98.8
C12 H27 N O S	233.1811	0	78
C14 H29 N O S	259.1961	0	71.8
$C_nH_yO_2S$			
C16 H26 O2 S	282.1659	0	98.1
C18 H30 O2 S	310.1957	0	91.3
$C_nH_yNO_2S$			
C22 H41 N O2 S	383.2871	0	63.3
$C_nH_yNO_2$			
C7 H17 N O2	147.1271	0	81.6
C11 H13 N O2	191.0943	0	89.3
C19 H21 N O2	295.1578	0	85.1
C24 H33 N O2	367.2547	0	83.6
C26 H37 N O2	395.2825	0	85.2

Table 3.2 (continued) Identified compounds and generated elemental compositions for entities in the final list. Duplicate entities (isomers) have been omitted. Table reproduced with permission from the American Chemical Society.[23]

compositions consistent with alkyl phenols, alkyl indoles, and alkyl indolines were found to be at significantly higher concentrations in the sample that failed ASTM D3241. Homologous series consistent with other nitrogen containing species, alkyl anilines and alkyl quinolines, were also shown to be present at significantly higher concentrations in the sample that failed ASTM D3241. It has been shown elsewhere that alkyl anilines and alkyl quinolines, which are basic amines, can have a negative correlation with thermal oxidative deposit formation.[24] There are also groups of compounds identified that are not necessarily homologous series with the general elemental compositions of C_nH_yOS, C_nH_yNO, C_nH_yNOS, and $C_nH_yNO_2$. Because this is a small-scale study, it is important to be aware of the fact that there is only one fuel included that fails ASTM D3241; therefore, not all of the entities identified are necessarily significant to the failure in the jet fuel thermal oxidation test.

The elemental composition $C_nH_yNO_2$ is notable because it could fit the first electrophilic aromatic substitution reaction product described in the SMORS model. A compound with this elemental composition could form as a result of an alkyl phenol that has oxidized to a quinone undergoing electrophilic aromatic substitution with a nitrogen heterocycle. The raw abundance plot for 2,5-dimethylphenol (Figure 3.5) shows it to be at a higher abundance in J2971, the fuel that failed ASTM D3241.

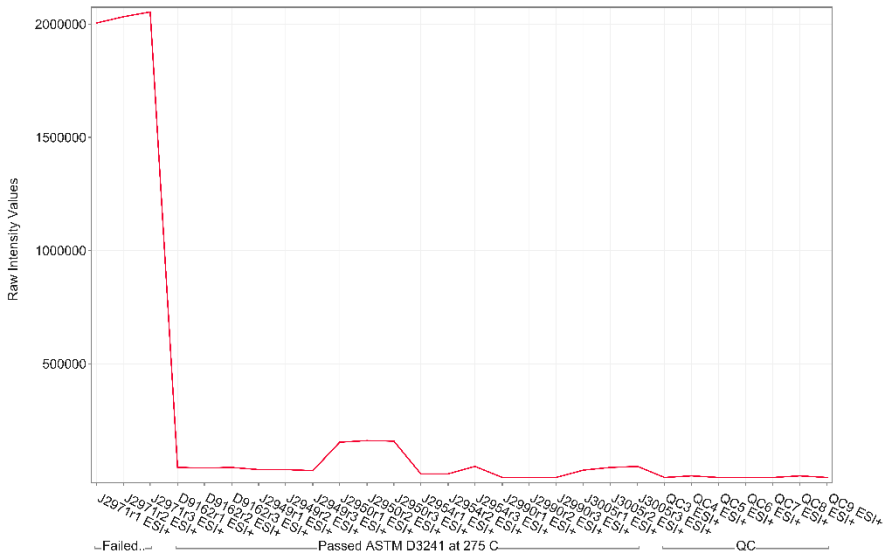

Figure 3.5 Profile plot of the raw intensity values for 2,5-dimethylphenol. Image reproduced with permission from the American Chemical Society.[23]

The raw intensity profile plot of 2,3,7-trimethylindole (Figure 3.6) has a similar profile to the raw intensity profile plot for 2,5-dimethylphenol with the raw abundance for this compound much higher in J2971 than any of the other fuels. This is also true with

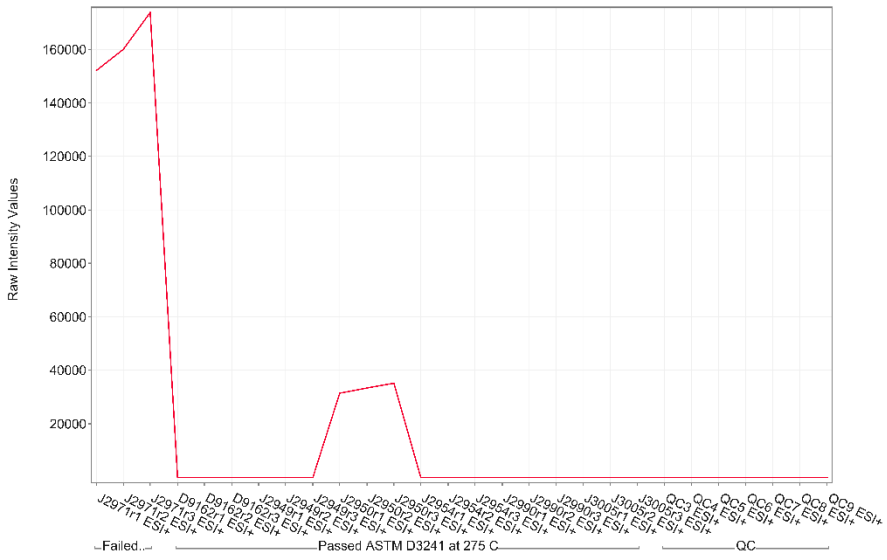

Figure 3.6 Profile plot of the raw intensity values for 2,3,7-trimethylindole. Image reproduced with permission from the American Chemical Society.[23]

the raw abundance plot for the elemental composition of $C_{19}H_{21}NO_2$ where the raw abundance is higher in J2971 than the rest of the jet fuels analyzed (Figure 3.7).

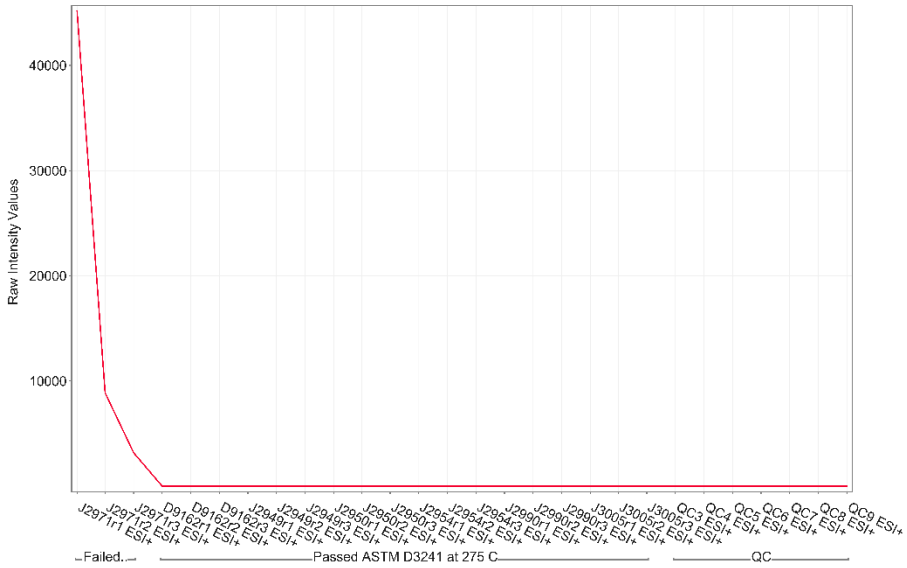

Figure 3.7 Profile plot of the raw intensity values for $C_{19}H_{21}NO_2$. Image reproduced with permission from the American Chemical Society.[23]

The soft ionization LC/MS ESI method used in this study does not offer insight into the structure of the entities detected, however, using the SMORS model as a guide the elemental composition $C_{19}H_{21}NO_2$ could be the reaction product of a quinone that formed from the oxidation of 2,5-dimethylphenol which could then undergo electrophilic aromatic substitution with 2,3,7-trimethylindole (Figure 3.8).

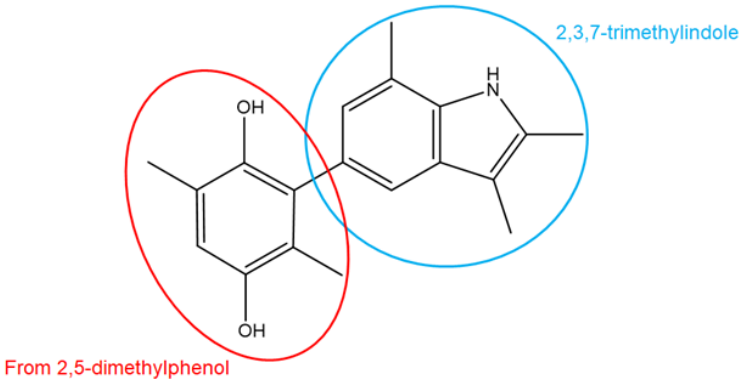

Figure 3.8 Hypothetical structure of $C_{19}H_{21}NO_2$ based on the SMORS model. Image reproduced with permission from the American Chemical Society.[23]

A similar process can be applied to the entity with the elemental composition $C_{13}H_{19}N$ which is consistent with a C5 alkyl indoline (5 saturated carbons attached to the indoline moiety). The raw intensity profile plot for $C_{13}H_{19}N$ is shown in Figure 3.9.

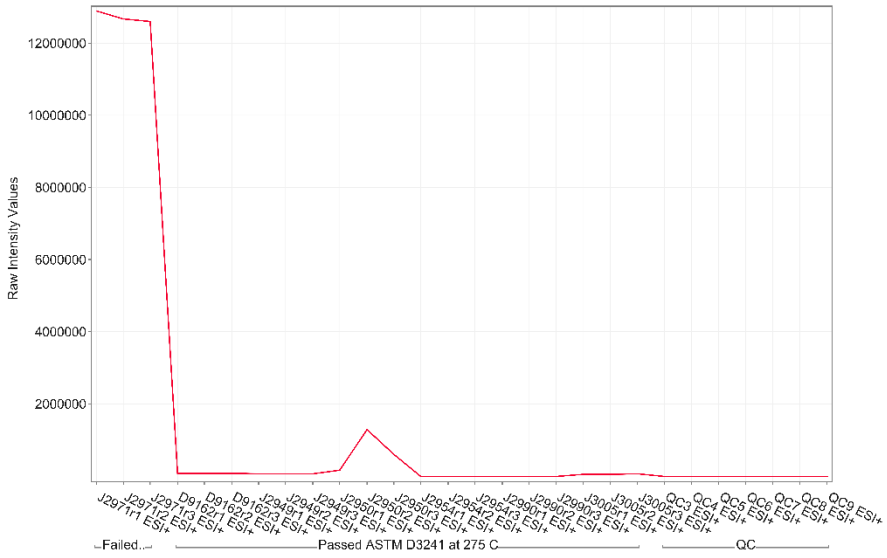

Figure 3.9 Profile plot of the raw intensity values for $C_{13}H_{19}N$ which is consistent with a C5 alkyl indoline. Image reproduced with permission from the American Chemical Society.[23]

Figure 3.10 shows the raw intensity profile plot for $C_{24}H_{33}NO_2$.

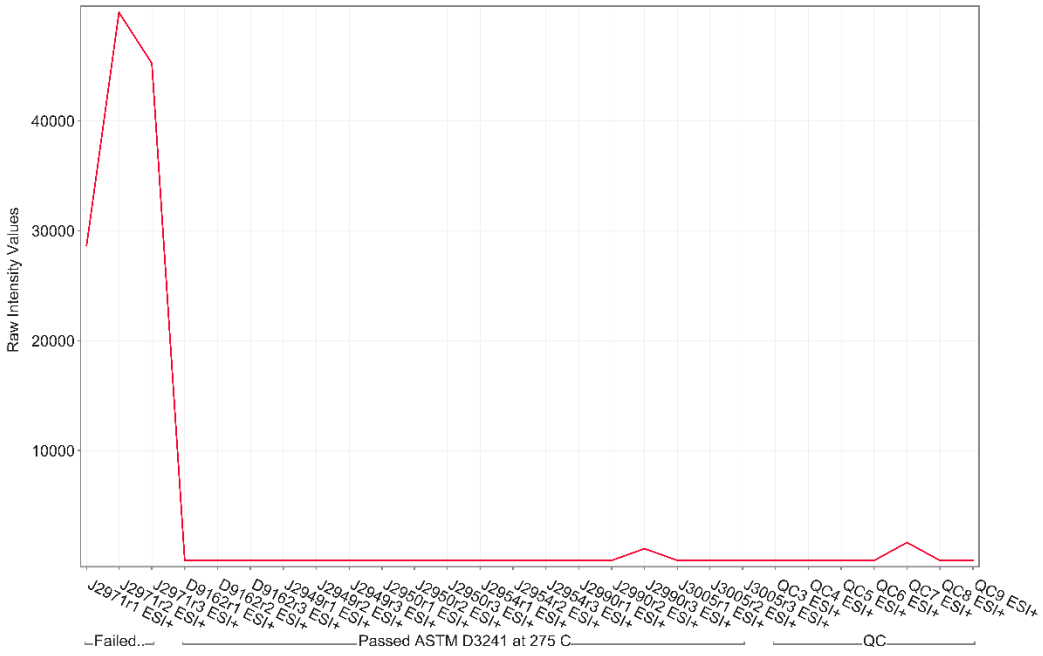

Figure 3.10 Profile plot of the raw intensity values for $C_{24}H_{33}NO_2$. Image reproduced with permission from the American Chemical Society.[23]

Although there were no C5 alkyl phenols detected which makes the argument for the occurrence of the SMORS reaction product shown in Figure 3.11 less compelling than the one previously discussed, it is still possible to imagine its formation from the EAS of a quinone from the oxidation of a C5 alkyl phenol and a C5 alkyl indoline

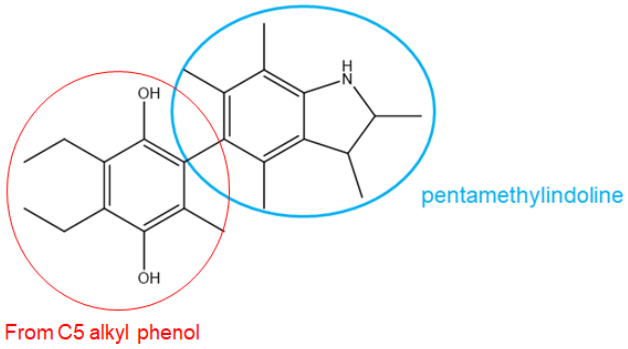

Figure 3.11 Hypothetical structure of C24H33NO2 based on the SMORS model. Image reproduced with permission from the American Chemical Society.[23]

It would also be logical to expect that the other alkyl phenols and alkyl indolines shown to be statistically significant to poor thermal oxidative stability as measured by ASTM D3241 would react in this manner as well, however elemental compositions consistent with those reactions were not detected. It is possible that the absence of various compounds could be due to differing response factors leading some compounds to be below their detection limits. Alkyl phenols and neutral nitrogen containing compounds are slightly acidic and may have higher ionization efficiencies by negative ion ESI compared to the positive ion ESI methodology employed here.[48]

It is uncertain from this small-scale pilot study whether the compounds with the general elemental compositions of C_nH_yOS, C_nH_yNO, and C_nH_yNOS are truly significant to poor thermal oxidative stability as measured by ASTM D3241. The elemental compositions related to the homologous series of $C_nH_{2n}OS$ could be the result of the oxidation of tetrahydrothiophene compounds. These oxidation products may then become prone to reaction with basic nitrogen compounds possibly leading to the formation of compounds with the general elemental composition of C_nH_yNOS.

Hydroxybenzenethiols, possibly reactants with quinones to form deposits,[11] could fit with the general elemental composition C_nH_yOS although none of the specific compositions detected directly fit this compound class in this sample set. There are other compound classes that fit with this general elemental composition as well. The entity with the elemental composition of $C_{11}H_{14}OS$ is consistent with a sulfur-containing analog of quinone. This C5 alkyl monothioparabenzoquinone could fit as a reactant in the SMORS model replacing quinone. This is purely hypothetical because there is no structural information provided from the soft ionization ESI method utilized. Tandem mass spectrometry experiments with a tandem quadrupole, ion trap, or quadrupole time-of-flight could offer insight into the structures of the entities by providing fragmentation.[42, 49]

Negative ion ESI. Negative ion ESI analysis offers a way to ionize and detect some compounds that were not amenable to positive ion ESI and can form negative ions in solution. Compounds that do not ionize, have low ionization efficiency, or suffered from ion suppression in positive ion mode may ionize better in negative mode and be detectable. Therefore, the same 7 fuels that were analyzed in positive ion mode were also analyzed in negative ion mode (Table 3.1).

The negative ion ESI method and statistical analysis of the resulting data were performed by the method discussed in Chapter 2. The total number of entities detected after performing a molecular feature extraction was 104, shown in Figure 3.12, which is significantly fewer entities than were detected in positive ion ESI.

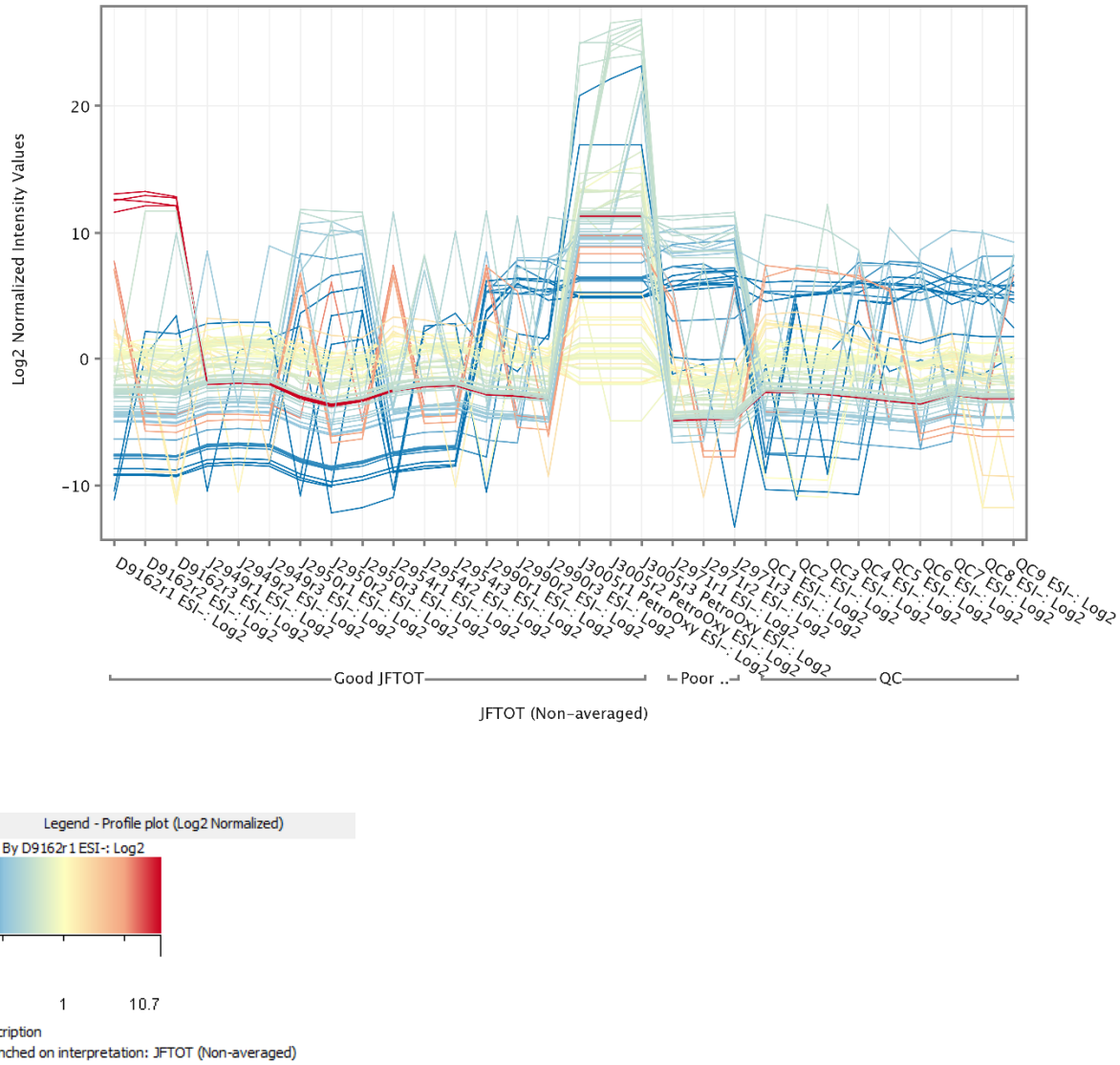

Figure 3.12 Log 2 normalized plot of all entities in unprocessed data. Each line represents an entity detected. The legend relates the intensity of the entity in D9162 relative to the median value for the entity.

This is likely due to the fact that fewer compounds form negative ions by ESI.[42] After performing an analysis of variance (ANOVA) and a filter by fold change, looking at the significant entities that increase in the fuel that failed ASTM D3241 (J2971), the number of significant compounds remaining was 26 which can be seen in Figure 3.13. The charts from other data processing steps can be found in Appendix A.

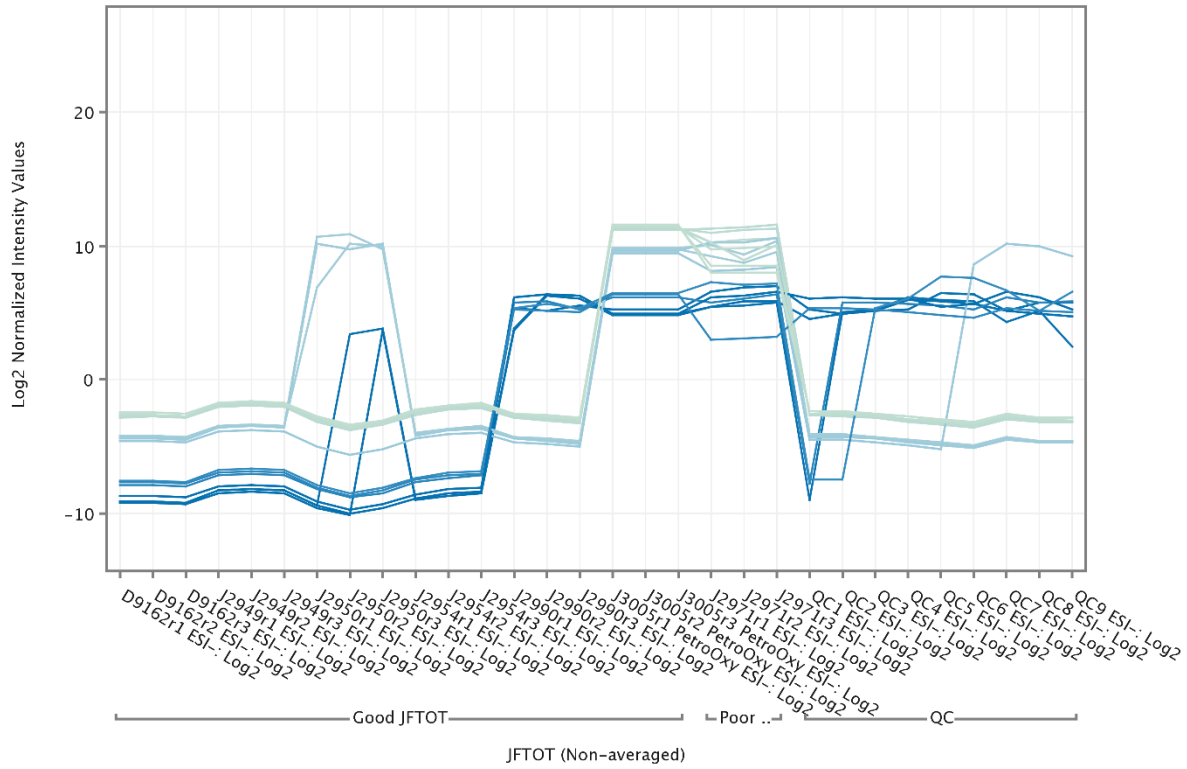

Figure 3.13 Log 2 normalized plot of entities in remaining after statistical analysis. Each line represents an entity detected. The legend for Figure 3.12 applies to this data as well.

The remaining 26 entities were submitted to the IDBrowser embedded in the MPP software as discussed in the previous section. Compounds were searched against a proprietary library and assigned elemental compositions based on their accurate *m/z* values and isotope abundance. Table 3.3 lists identified compounds and generated elemental compositions. Duplicate elemental compositions (isomers) have been eliminated in the table so each elemental composition only appears once.

Identity	Mass	Score (DB)	Score (MFG)
$C_nH_{2n-6}O$ (Phenols)			
o-cresol	108.0576	87.11	0
2,5-dimethylphenol	122.0731	87.38	0
2,4,6-trimethylphenol	136.0886	87.35	0
2,4,6-trimethylphenol	136.0887	87.35	0
C10 H14 O	150.1041	0	87.06
C11 H14 O	162.1041	0	87.25
C12 H16 O	176.1199	0	86.56
C13 H20 O	192.1511	0	87.06
2,6-di-tert-butylphenol	206.1668	86.55	0
C15 H24 O	220.1823	0	85.25
$C_nH_{2n-8}O$			
C10 H12 O	148.0886	0	81.88
$C_xH_yO_2$			
C18 H22 O2	270.1618	0	82.76
C20 H26 O2	298.1933	0	83.90
C20 H30 O2	302.2245	0	84.07

Table 3.3 Identified compounds and generated elemental compositions for entities in the final entity list in negative ion ESI. Duplicate entities (isomers) have been omitted.

As can be seen from the results in Table 3.3, the negative ion ESI analysis detected primarily alkyl phenols and there was a wider distribution of the homologous series identified. In the positive ion analysis, the range of alkyl phenols detected was 7-8 carbons although 2,6-di-tert-butyl phenol was detected in both analyses which was probably added as an antioxidant. In the negative ion analysis, the range of alkyl phenols detected was 7-13 carbons. Figure 3.14 shows the profile plot for 2,5-dimethylphenol illustrating that this compound is significantly higher in abundance in J2971. The profile plots for the other alkyl phenols all exhibit similar behavior.

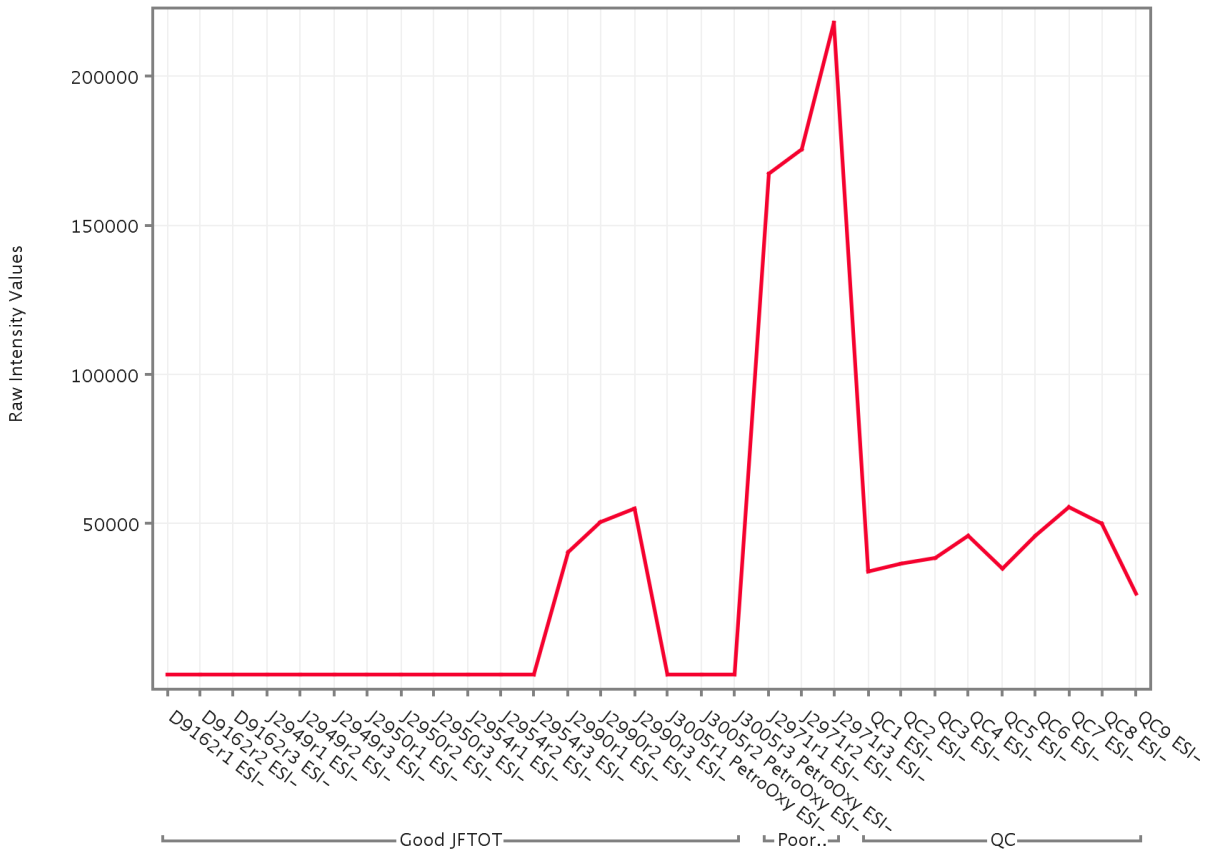

Figure 3.14 Profile plot of the raw intensity values for 2,5-dimethylphenol in negative ion ESI.

Additionally, compounds with the general elemental composition $C_xH_yO_2$ were shown to be significant to the fuel that failed ASTM D3241. Figure 3.15 shows the profile plot for $C_{20}H_{26}O_2$. As can be seen, the behavior of this entity across the sample set is similar to that of the alkyl phenols suggesting that they may be related. It is also possible that whatever process the fuels are exposed to during refining removes alkyl phenols and the $C_xH_yO_2$ with similar efficiency.

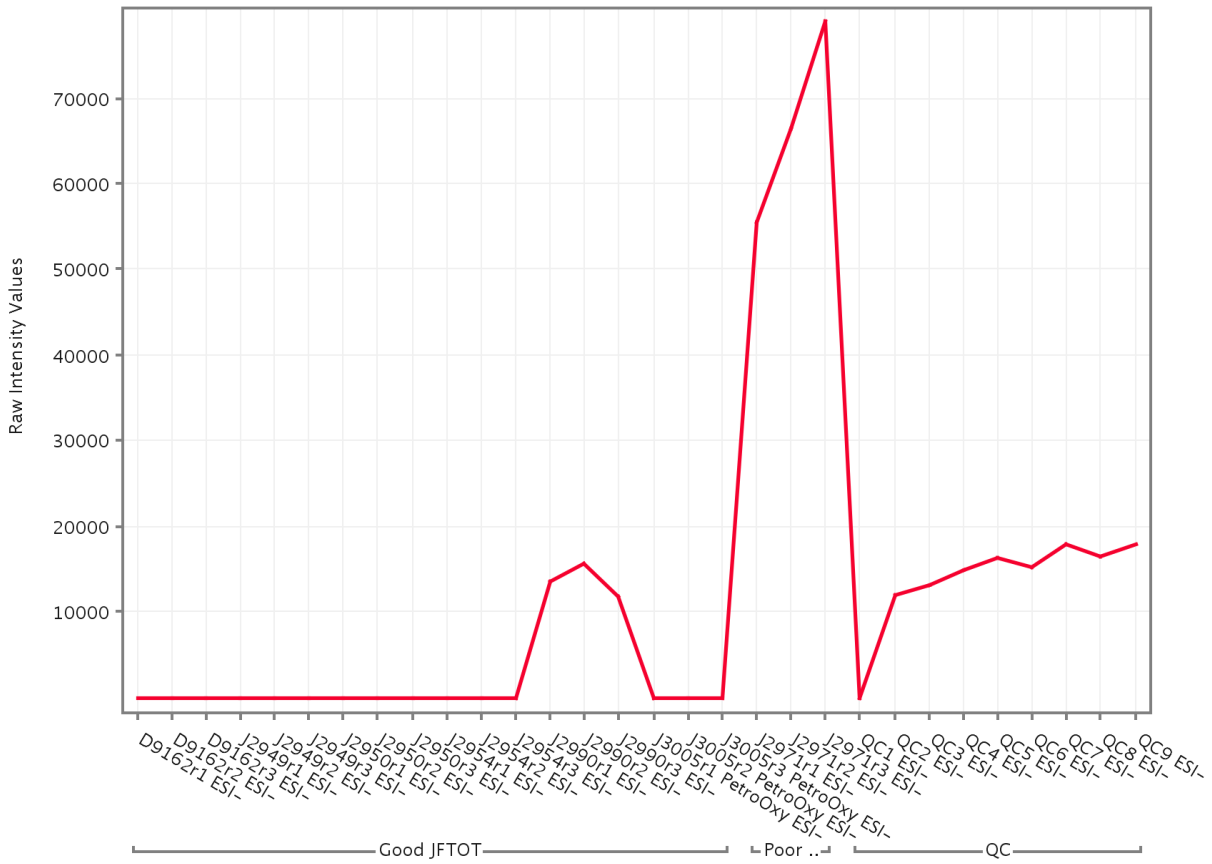

Figure 3.15 Profile plot of the raw intensity values for $C_{20}H_{26}O_2$ in negative ion ESI.

No alkyl carbazoles were detected in the negative ion ESI analysis adding further confidence to their absence in these samples because this is in agreement with the results from the positive ESI analysis. It does appear that the negative ion analysis is a useful complimentary technique to the positive ion analysis and allows for the detection of additional compounds.

Full-Scale Study

Positive ion ESI. There is a primary advantage to including a larger number of samples for statistical analysis, increasing the statistical power of the experiment.[50] However, there are some complications that could arise from this approach as it relates to jet fuel TOD. There are likely different pathways to deposit formation through the previously discussed SMORS, reactive sulfur species,[13] and dissolved metal ions or possibly other undiscovered mechanisms. By approaching the statistical analysis from the perspective of whether the individual samples pass or fail ASTM D3241 or form large amounts of TOD in the QCM reactor, the pathway to TOD formation is not addressed. Although, for both of the major deposition pathways previously discussed, alkyl phenols are involved and are likely always going to be found to be significant. Therefore, what is significant to TOD formation for one subset of the fuels may be different than what is significant for a different subset of the fuels. It may be possible to tease these differences out by looking at the data from different perspectives and focusing on different ways of grouping the samples. It may also be possible to see commonalities between the different subsets of fuels leading to the identification of compounds significant to TOD formation regardless of mechanistic pathway, like for alkyl phenols as previously mentioned.

For the full-scale study, the fuels analyzed can be seen in Table 3.4. This is a subset of the fuels that can be found in Table 2.1 and additional properties can be found in Table 2.2. No dissolved metal ions were detected in these fuels. There is some variation in the ASTM D3241 test temperatures, so some assumptions were made for the statistical analysis. Results at 275 °C and 280 °C were assumed to be equivalent.

Sample ID	ASTM D3241 VTR	ASTM D3241 ITR, nm	ASTM D3241 dP, mmHg	ASTM D3241 Temperature, °C	QCM Max Mass, µg/cm^2	QCM, % O_2 at Max Mass
D9162	1	8.031	0	260	0.63167	0
J2668	1	11	0	275	7.2385	0.2
J2717	2A	69.45	0	275	7.2385	0.2
J2949	1	0.1	0.1	280	1.3073	72.9
J2950	<3	44.3	0.1	275	0.8827	0.0
J2954	1	55.38	0	260	29.9977	2.0
J2969	1	4.2	0	275	1.1889	0.0
J2971	4P	N/A	0	260	4.2907	0.0
J2990	1	N/A	0	260	0.7128	0.0
J3044	>4	188.8	252.1	260	16.3583	27.1
J3091	>4P	155.4	252.2	280	20.3486	0.4
J3095	4	105.1	0	280	N/A	N/A
J3096	1	23.9	0	280	N/A	N/A
J3097	1	34.1	0	280	N/A	N/A
J3098	1	2.5	0	280	N/A	N/A
J3099	1	28.1	0	280	N/A	N/A
J3100	<3	63.6	0	280	N/A	N/A
J3101	1	8.5	0	280	N/A	N/A
J3102	4	47.3	0	280	N/A	N/A
J3103	1	44.3	0	280	N/A	N/A
J3104	1	45.2	0	280	N/A	N/A
J3105	>4	134.95	0	280	N/A	N/A
J3192	4P	113.4	0.8	275	31.2328	0.3
J3193	1	37.9	0	275	22.3591	5.8
J3194	3	75.1	0.7	275	13.4403	3.1
J3195	1	47.7	0.1	275	8.1463	0.0

Table 3.4 Samples analyzed by LC/MS ESI for full-scale study.

Passing fuels with low ITR values at 260 °C were assumed to be passing at 280 °C. If the ITR value was >50 nm at 260 °C it was assumed that the sample would fail ASTM D3241 at 275 °C or higher. It is possible to interrogate whether these assumptions were valid by looking at the PCA of the statistically treated data. If the samples cluster along the ASTM D3241 results, then it is likely that the assumptions are valid. If they do not cluster appropriately then it suggests that the assumptions may not be correct although

there are other reasons that they would not cluster such as variation in the data that is not related to entities that affect ASTM D3241 performance.

The motivation behind selecting this subset of samples for the full-scale study was one of practicality. It was the largest set of samples that could all be analyzed at the same time in both positive and negative ion mode. All of the samples had been analyzed by LC/MS ESI in positive ion mode at one time or another. However, negative ion ESI was determined to be of interest once more detail into the possible mechanisms was discovered. Because the statistical analysis is very sensitives to changes in chromatographic behavior and ion intensities, it is best to analyze all of the samples at the same time. Therefore, once the final experiment was determined for the full-scale study, the largest group of samples with enough volume to analyze still remaining was selected.

It is worth mentioning that there is not always a direct correlation between mass deposition by QCM and ASTM D3241 results. For example, J3194 fails ASTM D3241 at 275 °C and J3193 passes ASTM D3241 at 275 °C but J3193 shows higher mass accumulation by QCM. This is likely due to the differing temperature and time regimes along with the fact that the QCM is a batch process and ASTM D3241 is a flow process coupled with the type of precursors present in the different samples.[51] From an industry perspective, it is necessary to pass ASTM D3241 in order to be able to sell jet fuel. Therefore, the statistics are focused on relating entities to ASTM D3241 results and not QCM results. There are opportunities in the future to explore why there are differences between the two different methods and if it relates to different TOD mechanisms.

Figure 3.16 shows a graphical representation of the Log 2 normalized intensity values for all the entities identified during molecular feature extraction with recursive analysis (explained in Chapter 2) prior to statistical analysis. There were 1728 entities detected in this sample set. The chart is showing the average values for the entities across 2 different groups, the samples that failed ASTM D3241 at 275 °C and the samples that passed ASTM D3241 at 275 °C. Due to the large number of samples, it is necessary to show the average values in order to visualize trends in the data. The legend shows how the entities for the log 2 normalized average value of ASTM D3241 failing sample relates to the median value for the entire data set. Blue indicates that the log 2 normalized average value for the entity in the ASTM D3241 samples is lower than the median value for the entire data set. Yellow indicates the log 2 normalized average value for the ASTM D3241 failing sample and the median value for the entire data set are approximately the same. Red indicates that the log 2 normalized average value for the entity in the ASTM D3241 failing samples is higher than the median value for the entire data set.

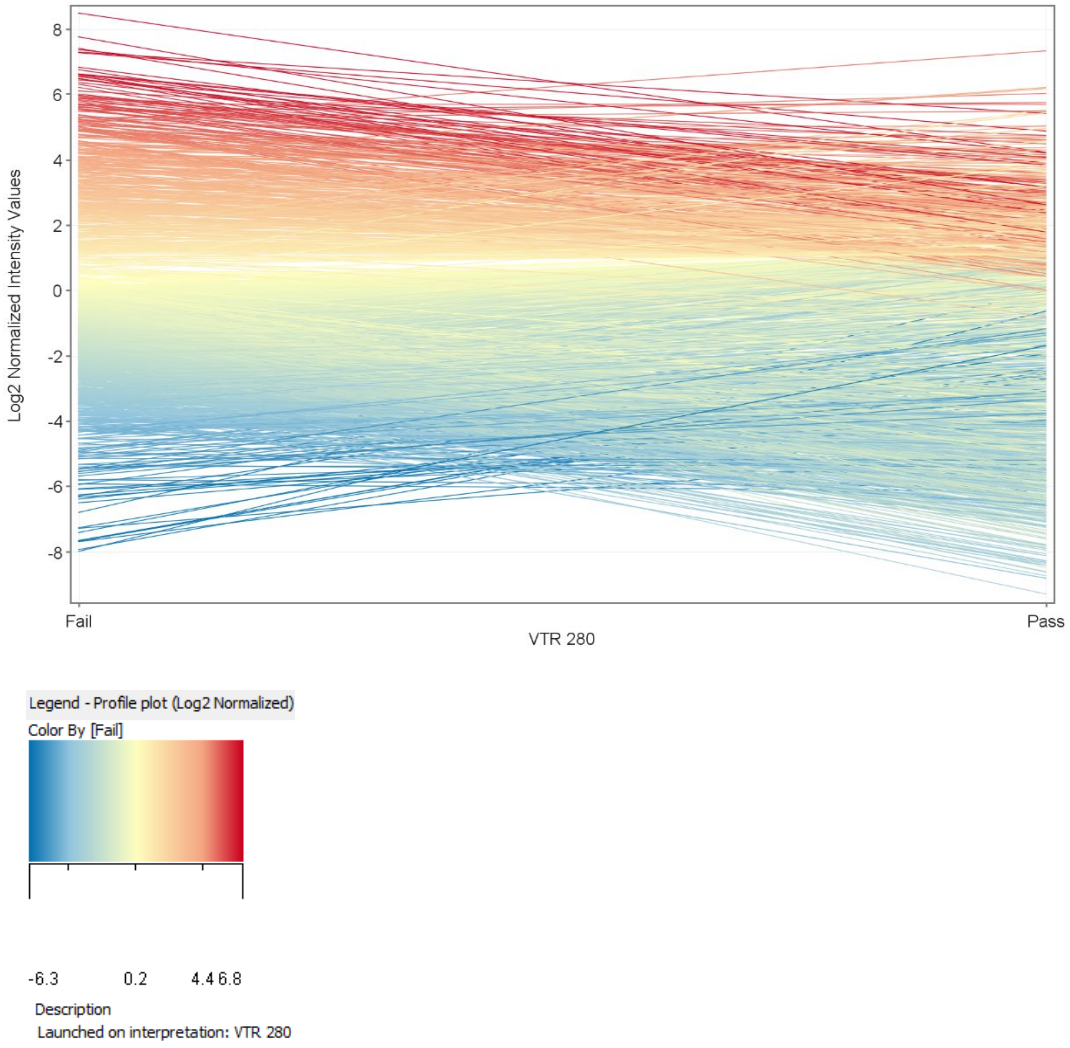

Figure 3.16 Log 2 normalized plot of the average values in the ASTM D3241 passing and failing samples for all entities in unprocessed data. Each line represents an entity detected. The legend relates the average intensity of the entity in failing samples relative to the median value for the entire data set.

Statistical analysis was performed on the data set in order to determine the entities that had significance when comparing the passing and failing sample groups. Details of the analysis can be found in Chapter 2. There were 540 entities remaining that had significantly higher intensity values in the samples that failed ASTM D3241

than the samples that passed. Figure 3.17 shows the entities remaining after statistical analysis looking at the entities that are higher in abundance in the failing samples.

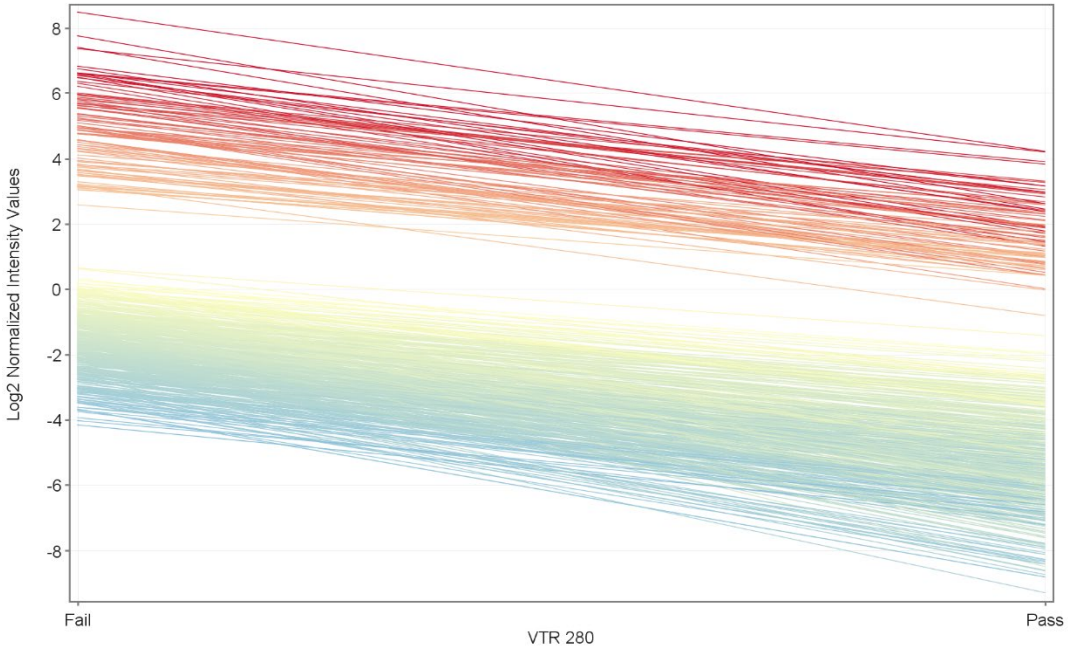

Figure 3.17 Log 2 normalized plot of the average values in the ASTM D3241 passing and failing samples for all entities after statistical analysis. Each line represents an entity detected. The legend for Figure 3.16 applies to this chart as well.

Table 3.5 shows the identified compounds and generated elemental compositions for the entities that were determined to be significant to ASTM D3241 results. Duplicate entities have been eliminated so each compound or elemental composition is only shown once. There were also a number of entities for which no elemental composition was generated and those are omitted as well. As can be seen from the results, similar sets of homologous series and general elemental compositions

Identity	Mass	Score (DB)	Score (MFG)
$C_nH_{2n+3}N$ (Aliphatic)			
C16 H35 N	241.2792	0	85.50
$C_nH_{2n+1}N$			
C12 H25 N	183.1993	0	99.69
C13 H27 N	197.2159	0	98.82
C14 H29 N	209.181	0	47.59
C15 H31 N	225.2519	0	87.34
$C_nH_{2n-1}N$			
C12 H27 N	185.215	0	83.42
$C_nH_{2n-3}N$			
C12 H21 N	179.167	0	98.68
C16 H29 N	235.2243	0	85.72
$C_nH_{2n-5}N$ (Anilines)			
N-ethylaniline	121.0876	87.13	0
N-ethyl-N-methylaniline	135.1044	99.24	0
C10 H15 N	148.0878	0	99.20
C11 H17 N	163.1356	0	98.29
C12 H19 N	177.1518	0	96.78
4-octylaniline	205.1826	95.03	0
C15 H25 N	219.1985	0	87.04
4-decylaniline	233.2172	50.87	0
$C_nH_{2n-9}N$ (Indoles)			
7-methylindole	149.0843	47.30	0
2,3,7-trimethylindole	177.1165	62.43	0
2-methyl-3-propylindole	173.1227	33.63	0
C13 H17 N	187.1354	0	75.86
C15 H21 N	215.1668	0	85.60
C16 H23 N	229.1828	0	96.50
C_nH_{2n-7N} (Indolines)			
C10 H13 N	147.1049	0	86.62
C11 H15 N	161.1204	0	86.26
C12 H17 N	175.1355	0	85.52
C13 H19 N	189.1512	0	84.54
C14 H21 N	203.1962	0	81.21

Table 3.5 Identified compounds and generated elemental compositions for entities in the final list. Duplicate entities (isomers) have been omitted.

Identity	Mass	Score (DB)	Score (MFG)
$C_nH_{2n-11}N$ (Quinolines)			
2,6-dimethylquinoline	157.0894	86.29	0
Trimethylquinoline	171.1046	99.69	0
C13 H15 N	185.1199	0	82.14
C14 H17 N	199.1355	0	84.27
$C_nH_{2n-13}N$			
C12 H11 N	169.089	0	84.5
$C_nH_{2n-6}O$ (Phenols)			
C8 H10 O	122.07	0	47.61
C11 H16 O	164.121	0	66.13
$C_nH_{2n-8}O$			
C9 H10 O	134.0737	0	86.01
C11 H14 O	162.1016	0	86.99
$C_nH_{2n-10}O$			
C10 H10 O	146.0769	0	86.95
C11 H12 O	160.0914	0	79.67
C12 H14 O	174.1082	0	83.74
C13 H16 O	188.1532	0	84.56
C_nH_yOS			
C7 H14 O S	146.0766	0	79.54
C8 H14 O S	158.0766	0	98.7
C8 H16 O S	160.092	0	86.09
C9 H10 O S	166.0455	0	94.61
C9 H18 O S	174.107	0	96.33
C10 H12 O S	180.061	0	93.14
C10 H16 O S	184.092	0	92.89
C10 H18 O S	186.1072	0	91.77
C10 H20 O S	188.1224	0	98.08
C11 H14 O S	194.078	0	97.72
C11 H18 O S	198.1086	0	97.16
C11 H20 O S	200.1523	0	97.61
C11 H22 O S	202.1386	0	96.36
C12 H20 O S	212.1233	0	95.28
C15 H28 O S	256.1889	0	94.25

Table 3.5 (continued) Identified compounds and generated elemental compositions for entities in the final list. Duplicate entities (isomers) have been omitted.

Identity	Mass	Score (DB)	Score (MFG)
C_nH_yNO			
C8 H11 N O	137.0841	0	86.62
C9 H11 N O	149.0837	0	99.22
C10 H11 N O	161.0854	0	75.31
C10 H15 N O	165.115	0	46.75
C10 H17 N O	167.1306	0	99.37
C10 H19 N O	169.1464	0	99.60
C10 H21 N O	171.1309	0	87.40
C11 H19 N O	181.1485	0	85.36
C11 H21 N O	183.1651	0	99.60
C12 H21 N O	195.1603	0	80.08
C13 H23 N O	209.1769	0	75.89
C15 H23 N O	233.1798	0	79.04
C15 H29 N O	239.226	0	71.83
C17 H25 N O	259.1888	0	88.77
C18 H25 N O	271.1975	0	93.58
C19 H27 N O	285.2104	0	84.06
C_nH_yNOS			
C13 H24 N O S	242.1696	0	97.53
C13 H27 N O S	245.1891	0	42.70
C14 H31 N O S	261.2118	0	98.14
C17 H35 N O S	301.2369	0	97.49
C19 H41 N O S	331.2852	0	90.21
$C_nH_yO_2S$			
C22 H32 O2 S	360.2175	0	91.78
$C_nH_yO_3S$			
C15 H28 O3 S	288.2309	0	69.69
$C_nH_yNO_2$			
C8 H17 N O2	159.0679	0	82.35
C11 H15 N O2	192.1403	0	57.74
C12 H15 N O2	205.0927	0	85.24
C13 H19 N O2	221.1765	0	75.46
C13 H22 N O2	224.1755	0	78.43
C16 H21 N O2	259.1957	0	79.30
C17 H35 N O2	285.2581	0	47.00

Table 3.5 (continued) Identified compounds and generated elemental compositions for entities in the final list. Duplicate entities (isomers) have been omitted.

are identified during this analysis. Elemental compositions consistent with basic nitrogen species are still prevalent; alkyl aniline, alkyl indoline, and alkyl quinolines. Additional homologous series of compounds with elemental compositions consistent with amine compounds that are likely basic were identified as well; $C_nH_{2n-3}N$, $C_nH_{2n-1}N$, $C_nH_{2n+1}N$, and $C_nH_{2n+3}N$ (consistent with aliphatic amine). Notably, alkyl indoles are identified as significant in this data set whereas they were not identified during the pilot study. Also, of note is the fact that only a couple of elemental compositions consistent with alkyl phenols have been identified in the larger data set. It is possible that due to the fact that a) alkyl phenols are frequently present in jet fuel, b) can be present without causing ASTM D3241 to fail, and c) can be generated through decomposition of hydroperoxides formed from alkyl benzenes they do not appear to be statistically significant when analyzing a large set of samples that may have different failure pathways.

The general elemental compositions of C_nH_yNO, C_nH_yOS, $C_nH_yO_2S$, C_nH_yNOS, and $C_nH_yNO_2$ are still identified as being significant to samples that fail ASTM D3241. Additionally, a compound with the elemental composition of $C_{15}H_{28}SO_3$ is identified as being significant in this data set. It is possible that these compounds are initial oxidation products that are significant to forming deposits and the fuels that fail ASTM D3241 have these deposit precursors present in significantly higher amounts.

Negative ion ESI. Negative ion analysis was attempted with the larger sample set. There were 110 runs in the sequence for this analysis. Consistently, the sequence would fail due to backpressure on the HPLC pump (1200 bar limit). It is likely that insoluble salts are forming as a result of the high pH solvent system leading to the column plugging. Therefore, it was not possible with the given methodologies to acquire

results with enough consistency to perform statistical analysis of the data and there are no results presented here. It may be possible with further method development to find a set of conditions that allow for this analysis.

Chapter 4 : Statistical Analysis of LC/MS ESI Data from Jet Fuels Before and After Thermal Oxidative Stressing in a QCM Reactor

A different way to utilize statistical analysis of mass spectral data is to look at the change in jet fuel samples after they undergo thermal oxidative stressing in the QCM reactor. There should be a correlation between the entities that were identified to be significant to poor thermal oxidative stability and the entities that significantly increase or decrease after thermal oxidative stressing in the QCM reactor. This could provide some insight into which significant compounds are being formed during thermal oxidative stress and which compounds are being consumed during thermal oxidative stress, something that is not determined by the previous analyses.

Positive Ion ESI

Table 4.1 shows the ASTM D3241 and QCM results for the jet fuel samples that were analyzed for this study. The samples came from a variety of different sources. Some were hydroprocessed and some went through other types of refinery process units. Not all of the samples would be considered finished Jet A fuels meeting all of the requirements of ASTM D1655. The samples J2668 and J2950 are finished Jet A fuels meeting the requirements of ASTM D1655. J3192 is an intermediate refinery stream that has both hydroprocessed and straight run components blended together. J3193 and J3194 are both straight run jet samples with different levels of processing but no hydroprocessing. J3195 is a hydroprocessed component. The severity of the hydroprocessing units that processed these samples is unknown. It is possible that there are a range of severities from mild hydrotreating all the way to hydrocracking. The

composition of the feed will have an effect on the types of molecules in the product.[52] Differing the severity of the hydroprocessing units is expected to have an effect on the types and quantities of heteroatom molecules remaining in the samples.[53] All samples were tested for metals by ICP/MS and there were no detectable metals that would have a negative impact on any of the fuel's thermal oxidative stability.

	ASTM D3241 275 °C			QCM	
Sample ID	**VTR**	**ITR, nm**	**dP, mmHg**	**mass accumulation, µg/cm²**	**% Oxygen at max mass**
J2668	1	11.0	0.0	7.2385	0.22712
J3195	1	47.7	0.1	8.1463	0.0000
J2950	<3	44.3	0.0	29.9977	2.0323
J3192	4P	113.4	0.8	31.2328	0.27107
J3193	1	37.9	0.0	22.3591	23.5882
J3194	3	75.7	1.5	13.4403	14.0314

Table 4.1 ASTM D3241 and QCM Results Organized by Decreasing ASTM D3241 Stability and Sample Type

Table 4.1 is organized by decreasing ASTM D3241 stability, first for the fuels that contain hydroprocessed components followed by the straight run samples. For the samples that contain hydroprocessed components, there appears to be a direct correlation between decreasing ASTM D3241 stability and increasing QCM mass accumulation. For the two straight run samples, the inverse is true and as the ASTM D3241 stability decreases the QCM mass accumulation decreases as well. Another difference between the two different sample types is that for the fuels containing hydroprocessed components, nearly all of the oxygen has been consumed once the maximum mass deposition is observed whereas for the straight run samples there is still

a significant amount of oxygen remaining in the reactor. This suggests that there are either two different mechanisms of deposit formation for the two different sample types or there is something present in one or both straight run samples which causes different behavior. The different temperature and time conditions that the samples experience in the different analyses likely influence the different stability trends. The temperature is 135 °C higher in the ASTM D3241 analysis for this study. However, because ASTM D3241 flows the sample over the heater tube at 3 mL/min the fuel only experiences the elevated temperature condition for seconds.[51] Conversely, the QCM is operated as a batch reactor keeping the fuel at the test temperature for 15 hours while being stirred.

Statistical analysis of the LC/MS ESI data for the samples before and after thermal oxidative stressing (TOS) in the QCM reactor utilizing *Mass Profiler Professional*® (MPP) (version 14.9.1, Agilent Technologies, Santa Clara, CA) highlights significant entities that either increase or decrease in concentration. Looking at the results for J3192, which is the most unstable fuel as measured by both ASTM D3241 and QCM, there are 85 significant entities identified as decreasing in intensity and 139 significant entities identified as increasing in intensity after TOS in the QCM reactor (Appendix A, Supplemental Figure 4.1). Generating elemental compositions for the entities based on their *m/z* values and isotope abundance utilizing the ID Browser imbedded in MPP, there are homologous series identified that are consistent with some of the compounds that were shown to correlate with instability as measured by ASTM D3241 in Chapter 3.[23]

Entities consistent with alkyl phenols were identified as decreasing in abundance during TOS in the QCM for J3192. This behavior was also observed for the other fuels

to some degree although the distribution of the homologous series became narrower as stability increased in the samples for the hydroprocessed components and was also narrow for the straight run samples, possibly due to lower abundance of the phenolic compounds in these fuels. Figure 4.1 shows the change in the average raw intensity values of $C_9H_{12}O$ in J3192 which is consistent with a C3 alkyl phenol (C3 denotes 3 saturated carbons attached to the phenol) for the three technical replicates of J3192 before and after TOS. The absolute raw intensity values shown are not significant and can't be compared to the values for other entities detected. However, the trends in the data are informative. The behavior observed is not surprising because phenols are natural antioxidants and will likely be consumed during oxidation. Therefore, if alkyl phenols are present, they will likely decrease in concentration after thermal oxidation regardless of whether or not their oxidation products go on to form TOD.

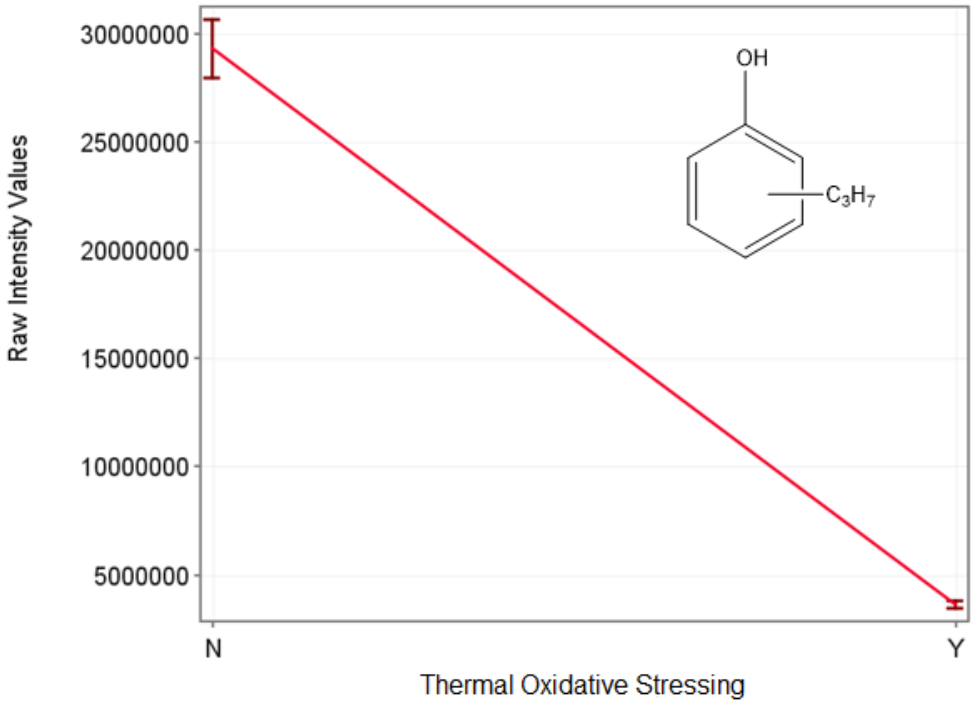

Figure 4.1 Log 2 normalized plot of the average raw intensity values of entities consistent with C3 Alkyl Phenol Before and After TOS.

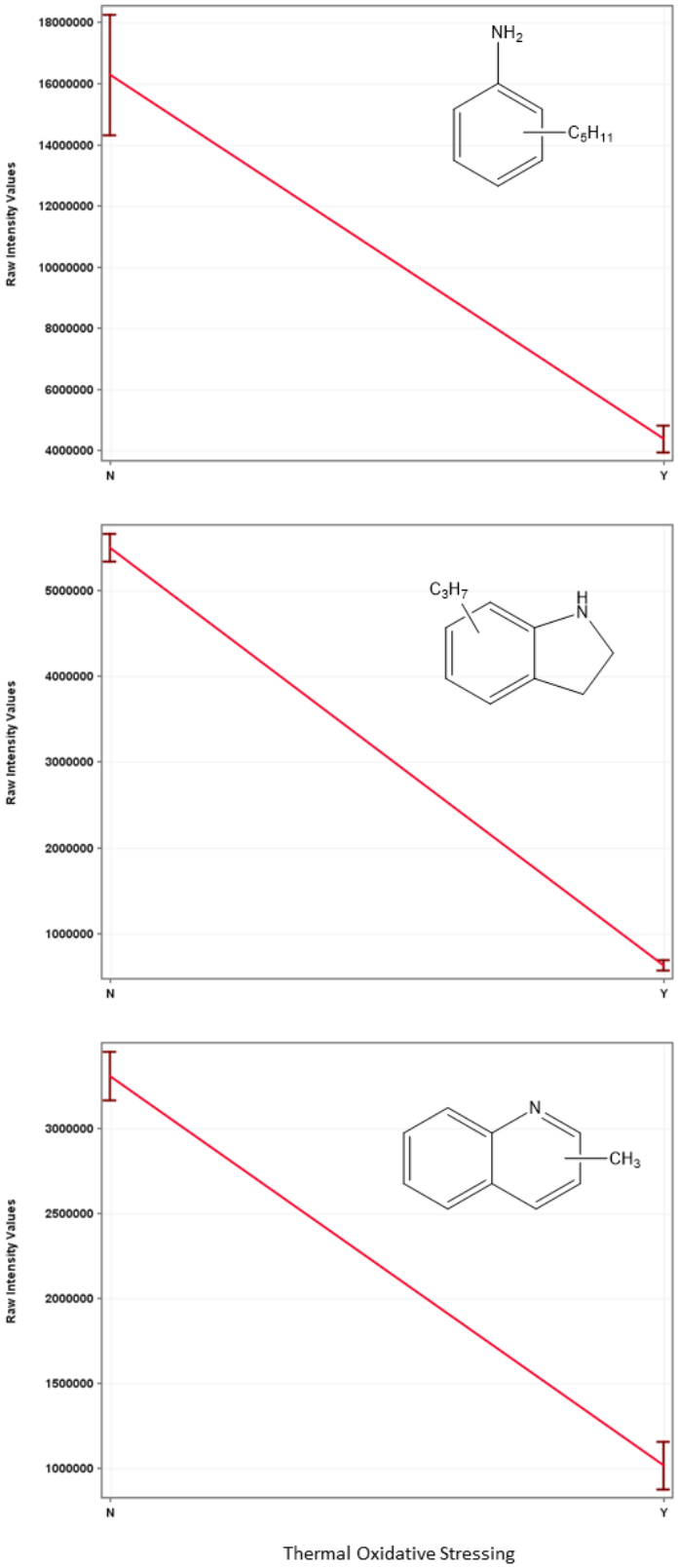

Figure 4.2 Log 2 normalized plot of the average raw intensity values of entities consistent with alkyl anilines/pyridines, alkyl indolines, and alkyl quinolines before and after TOS.

Three homologous series of nitrogen containing compounds were also identified as decreasing in abundance after TOS in the QCM reactor; $C_nH_{2n-5}N$ (consistent with alkyl anilines/pyridines), $C_nH_{2n-7}N$ (consistent with alkyl indolines), and $C_nH_{2n-11}N$ (consistent with alkyl quinolines). Figure 4.2 shows the average change in intensity of the most abundant compounds from each of the 3 homologous series in J3192, similar to what was shown for the alkyl phenol in Figure 4.1.

Notably, there were no entities consistent with alkyl indoles or alkyl carbazoles identified as decreasing after thermal oxidative stressing. All 3 of the homologous series that were identified are basic amines which means that they should have higher ionization efficiencies than the neutral amines like alkyl indole and alkyl carbazole by the positive ESI LC/MS method utilized here.[54] It is possible that due to their lower ionization efficiency, the neutral amines are present but at concentrations below their detection limit in these samples. All of the samples analyzed show similar behavior for the entities with elemental compositions that correlate to the basic amines in that they are shown to be significantly decreasing. Utilizing a negative ionization ESI LC/MS method may help to achieve a lower detection limit for the neutral amine compounds and the alkyl phenols both of which are slightly acidic.[48]

There are three sets of series of compounds, which are not necessarily homologous, that are shown to significantly increase after TOS in the QCM reactor. These have the general elemental compositions C_nH_yOS, C_nH_yNO, and C_nH_yNOS which have also been correlated to elemental compositions. These general elemental compositions were determined to have a statistically significantly correlation to poor thermal oxidative stability as measured by ASTM D3241 (Chapter 3).[23]

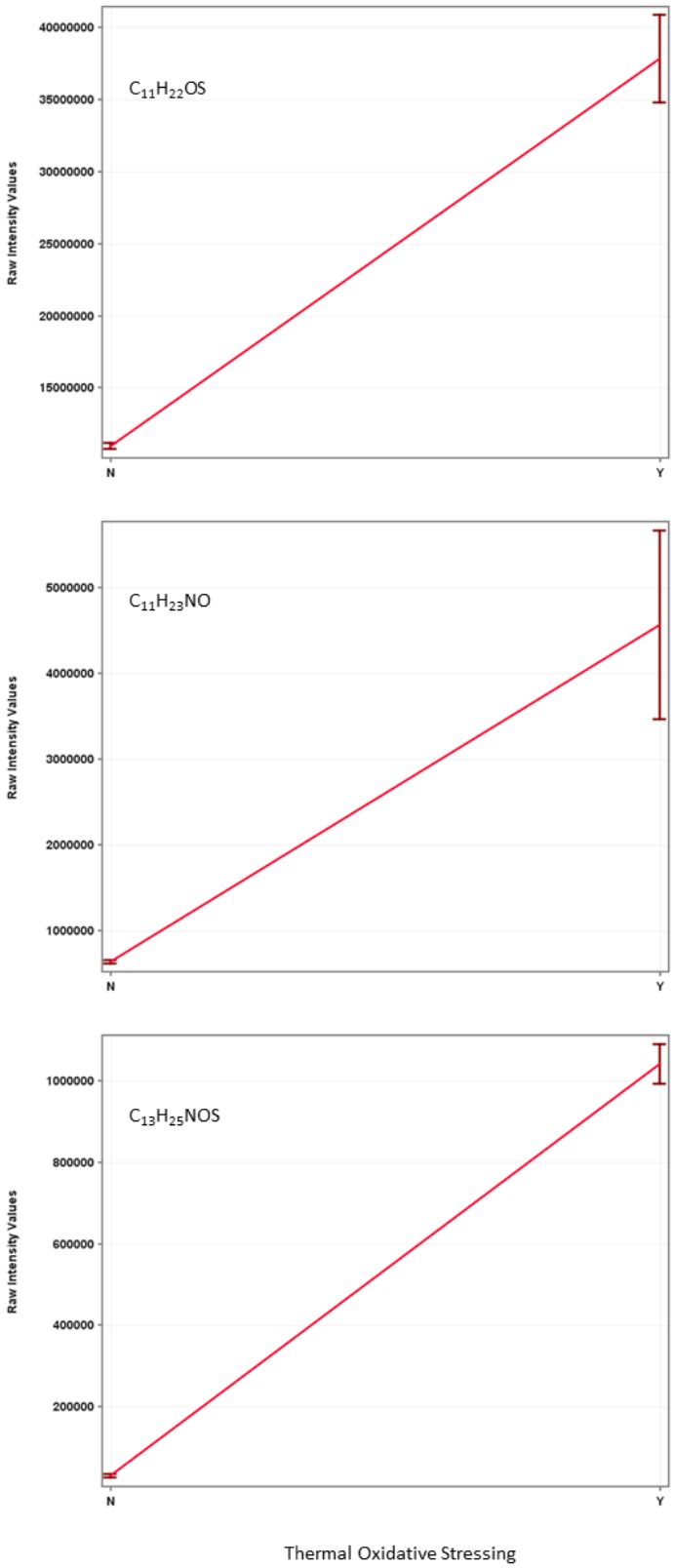

Figure 4.3 Log 2 normalized plot of the average raw intensity values of entities with general elemental compositions of CnHyOS, CnHyNO, and CnHyNOS before and after TOS.

This means that in addition to forming during TOS in the QCM reactor, they were present at significantly higher abundance in unstressed jet fuels that had poor stability when compared to fuels that had good stability as measured by ASTM D3241. Figure 4.3 shows the average changes in intensity for $C_{11}H_{22}OS$, $C_{11}H_{23}NO$, and $C_{13}H_{25}NOS$ after TOS for J3192. Similar behavior for compounds with these general elemental compositions is observed in all of the samples analyzed. It is plausible that these compounds are formed as a result of the oxidation of reactive sulfur species, reactive nitrogen species, sulfur/nitrogen containing compounds, or possibly the reaction between an oxidized sulfur compound and a basic amine. However, it is reasonable to expect that there would be series of reactive sulfur and nitrogen compounds with corresponding elemental compositions significantly decreasing as well, which is not observed. For the reactive sulfur species, these compounds are often present in jet fuel in the form of mercaptans, sulfides such as tetrahydrothiophenes, and possibly in other forms.[55] Their decrease due to oxidation may not be seen as statistically significant because the amount of oxidation product might be small relative to the total amount of reactive sulfur species present or they may have poor ionization efficiency by the positive ion ESI method. This may also be true for the amine compounds that oxidize as well.

Negative Ion ESI

The samples detailed in Table 4.1 were also analyzed by the negative ion ESI method described in Chapter 2. Focusing on J3192, the sample that had poor stability by both ASTM D3241 and QCM (the other samples exhibited similar behavior to some degree), after processing the raw data in Profinder® and performing a moderated T-test

(p>0.05) there were 181 entities identified as changing significantly after TOS (108 increasing in intensity and 73 decreasing in intensity, Appendix A, Supplemental Figure 4.2). As expected, alkyl phenols decrease in abundance after TOS. Figure 4.4 shows the raw intensity plot for the average intensities of 2,5-dimethylphenol before and after TOS. Other alkyl phenols are seen to exhibit this behavior as well; isomers of dimethylphenol, C3 alkyl phenols (such as trimethylphenols) and also C4 alkyl phenols.

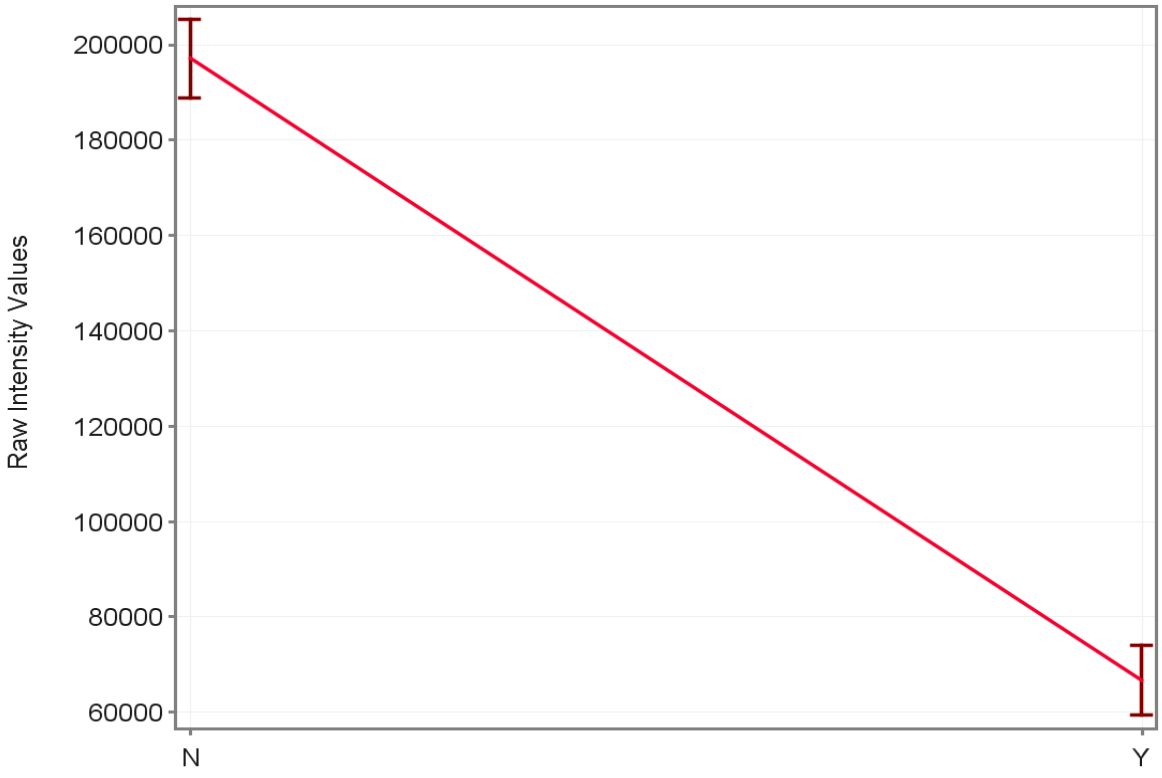

Figure 4.4 Log 2 normalized plot of the average raw intensity values of 2,5-dimethylphenol before and after TOS.

This behavior is also identified for alkyl indoles by this ionization technique. Figure 4.5 shows the raw intensity profile plot for the average intensities of 2,3,7-trimethylindole before and after TOS. Other alkyl indoles are seen to exhibit this behavior as well such as dimethylindole isomers. The alkyl indoles were not detected by the positive ion ESI method, likely due to low ionization efficiency.

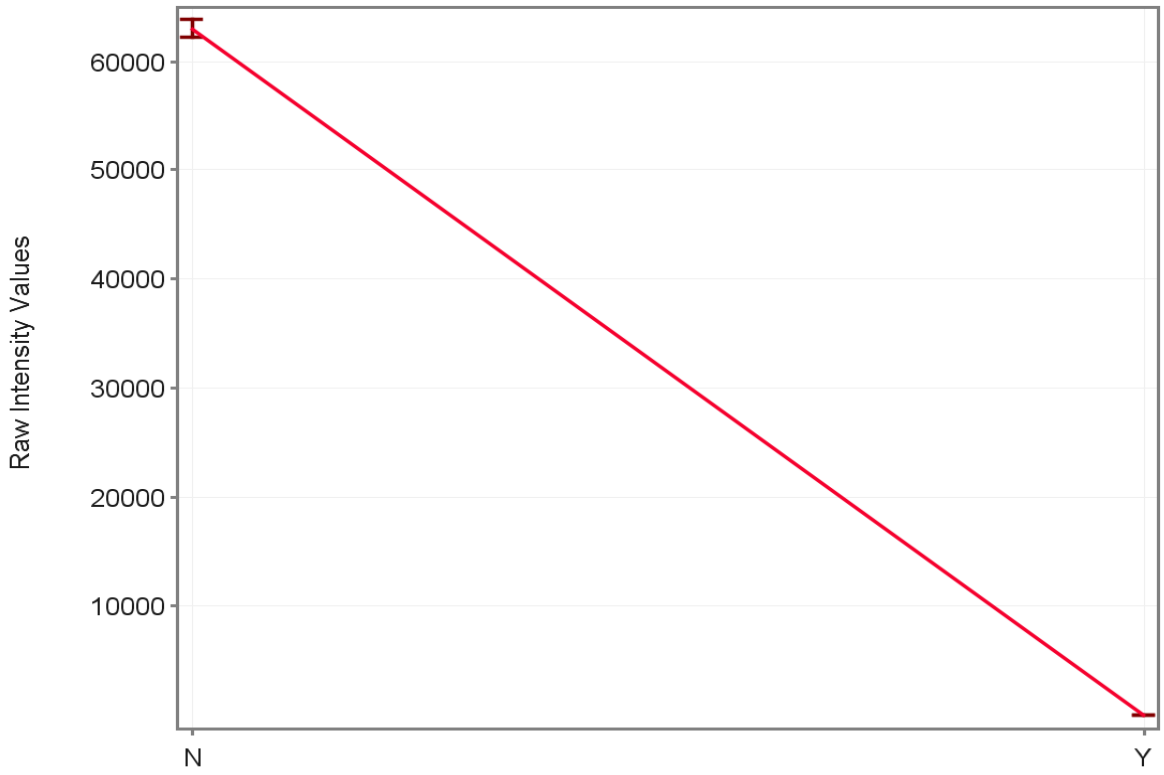

Figure 4.5 Log 2 normalized plot of the average raw intensity values of 2,3,7-trimethylindole before and after TOS.

A number of compounds with general elemental compositions containing 2 or more oxygen atoms were identified to be increasing after TOS. Entities with the general

elemental composition of $C_nH_{2n-8}O_2$ were identified as increasing in abundance after TOS. This general elemental composition could be consistent with either a homologous series of alkyl quinones or benzoic acids. It is possible that either of these types of compounds could lead to TOD. Compounds with the general elemental composition $C_nH_yO_2S$ and $C_nH_yO_3S$ were determined to be increasing after TOS. The expectation for these compounds was that they would have elemental compositions that related to the oxidation of mercaptans or sulfides. However, the elemental compositions for the detected entities tended to have a high degree of unsaturation. For example, entities with the elemental compositions $C_{26}H_{26}O_2S$ and $C_{48}H_{50}O_3S$ were detected. It is possible that the acidic oxides of mercaptans and sulfides are consumed quickly through reaction with basic amines or through other pathways and these large, highly unsaturated compounds are less likely to be consumed quickly through reaction. Other entities that have not been detected before were identified during this analysis. Table 4.2 shows the elemental compositions for the entities detected in this analysis that increase after TOS. Duplicate elemental compositions (isomers) and entities with elemental compositions that cannot be rationalized have been omitted.

Identity	Mass	Score (DB)	Score (MFG)
$C_nH_{2n-8}O_2$			
C7 H6 O2	122.0366	0	47.62
C10 H12 O2	164.0824	0	79.05
C12 H16 O2	192.113	0	73.13
$C_nH_yO_2$			
C13 H12 O2	200.0836	0	76.84
C13 H16 O2	204.1132	0	56.31
$C_nH_yO_2S$			
C14 H24 O2 S	256.1486	0	62.80
C18 H29 O2 S	309.1908	0	41.76
C26 H26 O2 S	402.166	0	67.95
C27 H28 O2 S	416.1829	0	63.78
$C_nH_yO_3S$			
C48 H50 O3 S	706.3521	0	58.54
C_nH_yOS			
C44 H52 O S	628.3761	0	62.84

Table 4.2 Identified compounds and generated elemental compositions for entities detected by negative ion ESI that increase after TOS. Duplicate entities (isomers) and entities with elemental compositions that cannot be rationalized have been omitted.

Table 4.3 shows the elemental compositions for the entities detected in this analysis that decrease after TOS. Duplicate elemental compositions (isomers) and entities with elemental compositions that cannot be rationalized have been omitted. Consistent with what was identified as being statistically significant by negative ion ESI in Chapter 3, alkyl phenols and other C_nH_yO were identified as decreasing in abundance after TOS. Additionally, alkyl indoles were identified as decreasing after TOS.

Identity	Mass	Score (DB)	Score (MFG)
$C_nH_{2n-6}O$ (Phenols)			
2,5-dimethylphenol	122.0712	71.75	0
2,4,6-trimethylphenol	136.087	78.58	0
C11 H16 O	164.1177	0	67.80
C12 H18 O	178.134	0	65.94
C_nH_yO			
C11 H14 O	162.1017	0	67.70
C12 H16 O	176.1179	0	64.94
C13 H18 O	190.133	0	67.14
C12 H12 O	172.0867	0	67.38
$C_nH_{2n-9}N$ (Indoles)			
2,3-dimethylindole	145.0869	68.03	0
2,3,7-trimethylindole	159.103	68.45	0
2-methyl-3-propylindole	173.1184	64.76	0

Table 4.3 Identified compounds and generated elemental compositions for entities detected by negative ion ESI that decrease after TOS. Duplicate entities (isomers) and entities with elemental compositions that cannot be rationalized have been omitted.

Chapter 5 : Py-GC/MS Analysis of Jet Fuel Thermal Oxidative Deposits

In order to study the composition of the thermal oxidative deposits that form in the QCM reactor, two pyrolysis gas chromatography/mass spectrometry (Py-GC/MS) experiments were run. The first was an evolved gas analysis (EGA) in which deposit is placed into the pyrolysis cup, introduced into the pyrolysis oven at 100 °C and the oven is quickly ramped to 850 °C. During this experiment the inlet is connected to the mass spectrometer transfer line with a metal column that does not contain stationary phase which is inside the GC oven at 350 °C. This generates a reconstructed total ion current thermogram from which it is possible to determine when thermal desorption of residual fuel molecules stops and pyrolysis of the non-volatile deposits begins. Figure 5.1 shows a general example of a reconstructed total ion current thermogram for a TOD from the QCM reactor. The same behavior is observed in all of the EGA experiments for these types of deposits. It can be seen that thermal desorption is mostly finished by 350 °C and the deposits begin to pyrolyze at temperatures higher than this. This fits with the boiling range of jet fuel which is approximately 120-300 °C.[3]

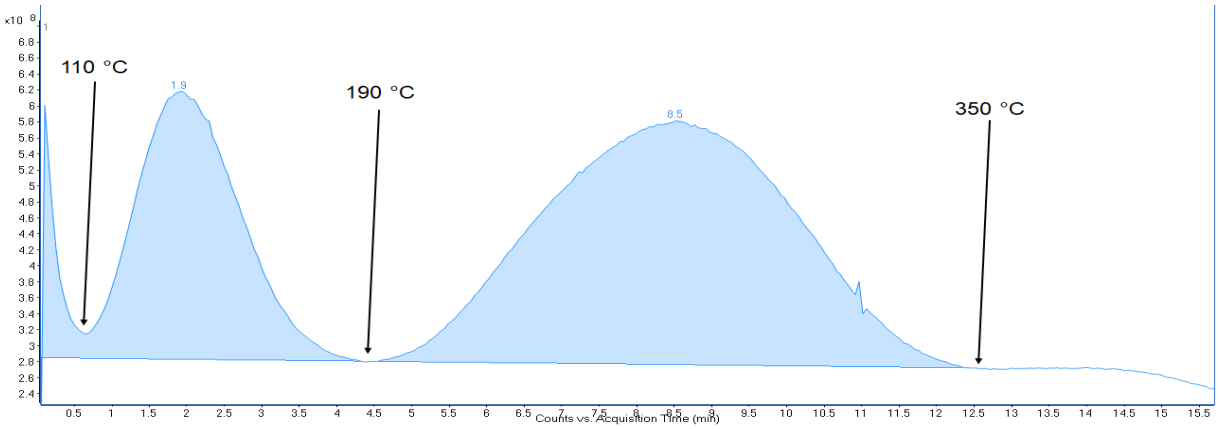

Figure 5.1 Reconstructed total ion thermogram showing the general evolved gas profile for TOD from a QCM reactor.

Given the data generated by the EGA analysis, a heart cut single shot experiment was designed to analyze the pyrolysate products from the deposits. The heart cut was performed at 360 °C allowing all volatile molecules to be thermally desorbed and vented. The temperature was then ramped from 360-850 °C while the pyrolysate products were trapped at the front end of the chromatographic column through cryogenic cooling with liquid nitrogen. A traditional GC/MS analysis was then performed by turning off the cryogen and ramping the GC oven. Detailed description of the methodology can be found in Chapter 2. Deposits from the fuels in Table 4.1 were collected and analyzed for this experiment. Figure 5.2 shows the reconstructed total ion current chromatograms (RTICC) for the deposits that were analyzed. There was not enough deposit collected for J2668 to analyze. An effort was made to try and introduce similar amounts of deposit into the pyrolysis cup for analysis however there was not a balance with sufficient sensitivity to weigh the deposits. Therefore, there is some

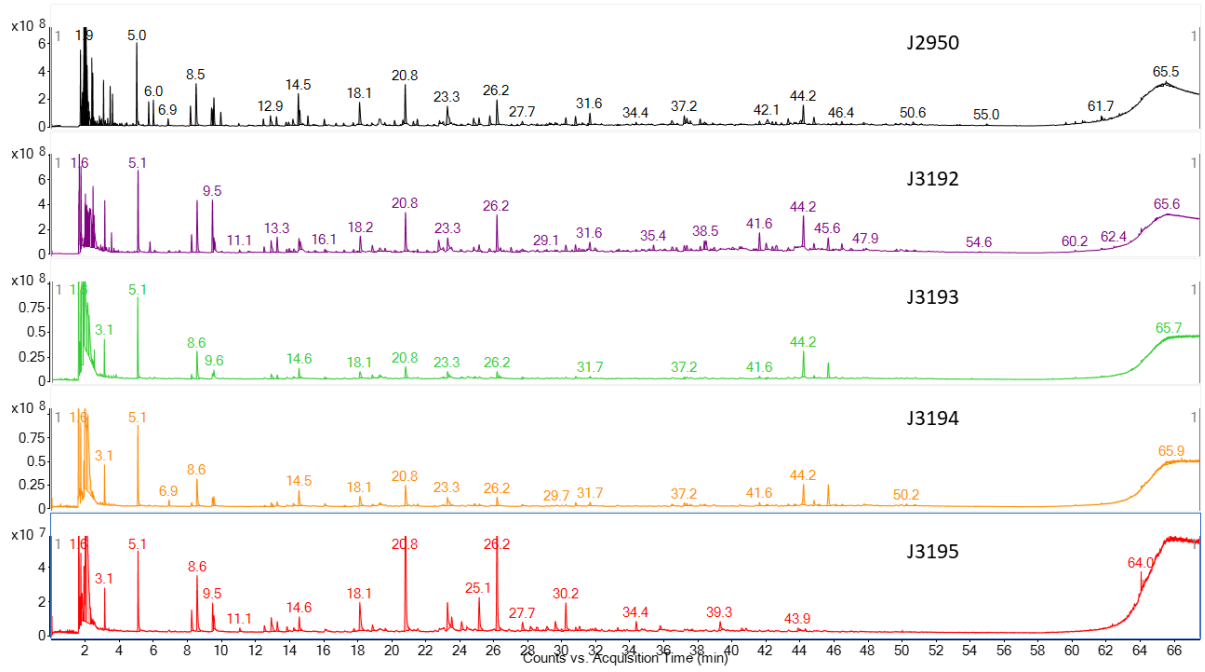

Figure 5.2 Comparison of RTIC chromatograms. Peak intensities are normalized to the peak at 5.1 minutes

variability in the intensities of the peaks and this needs to be taken into consideration when comparing the data. The RTIC chromatograms of the deposits from J2950 and J3192 seem to be similar in intensity meaning that there was likely a similar amount of deposit pyrolyzed. J3193, J3194, and J3195 had lower intensities meaning there was likely less deposit pyrolyzed. The RTIC chromatograms have all been normalized to the peak at 5.1 minutes (NIST 17 library match with toluene).

Table 5.1 shows the retention times and identifications of some of the major peaks in the Py-GC/MS analysis of the TOD. All identifications were made by searching the electron ionization (EI) fragmentation patterns against the NIST 17 library using MS Search V 2.3. No attempt was made to differentiate isomers because this can be generally difficult based on fragmentation patterns. Compounds are named by the

number of carbons attached. In all the RTIC chromatograms, there is a broad peak starting just before 2-minute retention time. The EI fragmentation pattern is consistent with sulfur dioxide (SO_2). This peak is not observed during blank pyrolysis runs suggesting that the SO_2 gas is forming during the pyrolysis of the deposits. There are some sharp peaks that co-elute with the sulfur dioxide. These peaks along with the other main peaks from 2-18 minutes are all consistent with aromatic and aliphatic hydrocarbons. These molecules could be forming as a result of the pyrolysis process and it is unclear whether they are important to the deposit formation process.

Compound, NIST 17 Match	**Retention Time, minutes**	**Present in all pyrolysates?**
Sulfur Dioxide	approx. 1.9-2.5	Yes
Phenol	14.2	Yes
Cresol	18.2	Yes
C2 Phenol	20.8	Yes
C2 Phenol	23.3	Yes
C3 Phenol	26.2	Yes
C3 Phenol	27.7	Yes
C4 Phenol	30.2	No
C3 Aniline	22.1	No
C3 Aniline	22.8	No
C3 Quinoline	41.6	No

Table 5.1 Major peaks detected in Py-GC/MS analysis of TOD from QCM.

There is a small peak observed in all of the samples analyzed at 14.2 minutes that is consistent with phenol. The peak observed at approximately 18.2 minutes is consistent with cresol. The next 3 major peaks at 20.8, 23.3, 26.2 minutes are all consistent with alkyl phenols containing either 2 or 3 saturated carbons attached. The

peaks at 27.7 and 30.2 minutes are consistent with alkyl phenols containing 3 and 4 saturated carbons, respectively. The peak at 30.2 minutes is not present in the TOD from J3193 or J3194. The peaks at 22.1 and 22.8 minutes, which are only detected in the TOD from J2950 and J3192, are consistent with an alkyl aniline containing 3 saturated carbons. There is also a peak at 41.6 minutes that is consistent with alkyl quinoline containing 3 saturated carbons. This peak is present in all samples except the TOD from J3195.

There is no conclusive identification for the peak at 44.2 min which is present in all of the samples except for the TOD from J3195 or the peak at 45.6 min which is present in all the samples except for the TOD from J2950 and J3195 from searching the NIST Library. The EI mass spectra for these two peaks are shown in Figure 5.3. The likely molecular ion peak for the first spectrum (44.2 min) is at *m/z* 231 and the likely molecular ion peak for the second spectrum (45.6 min) is at *m/z* 229. This indicates that there are an odd number of nitrogen atoms in each of these compounds. More interpretation work needs to be done to conclusively identify the structure of these compounds. It is possible to determine prospective elemental compositions based on isotope abundance and work out likely fragmentation pathways but that is outside the scope of this current investigation. Accurate mass data would be helpful in assigning elemental compositions.

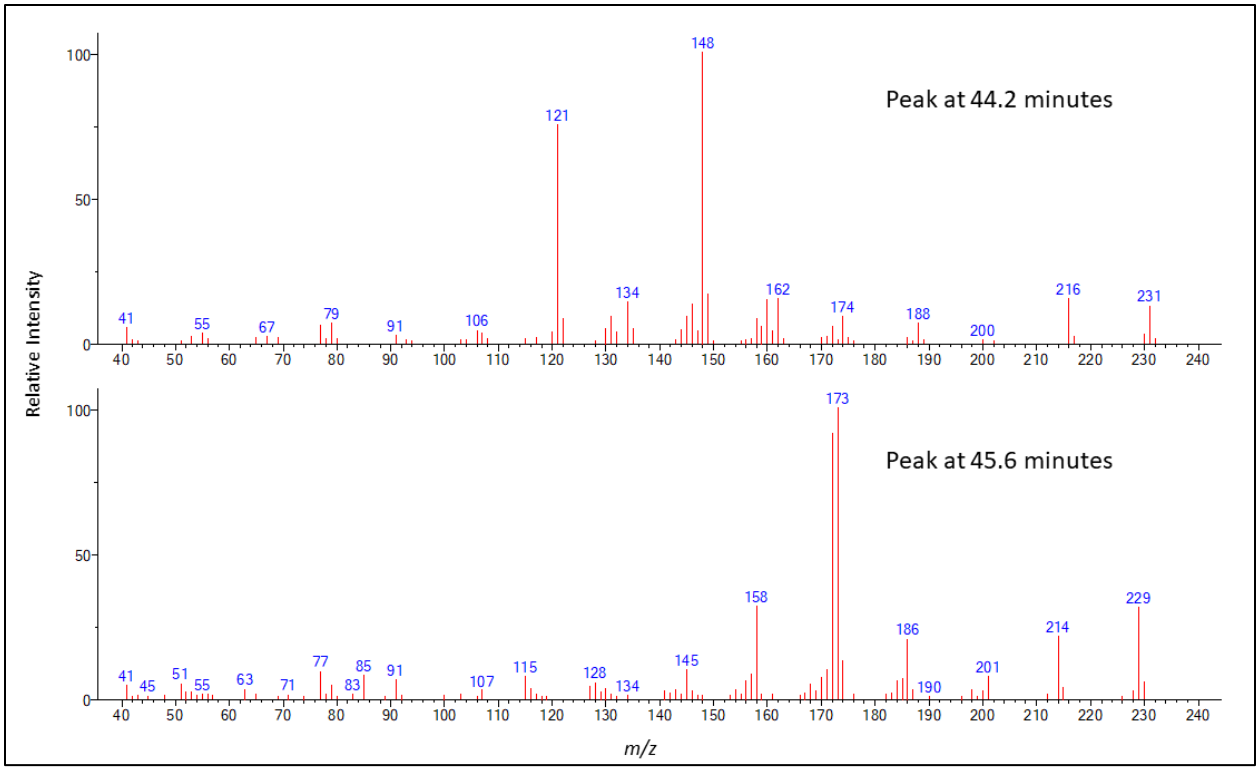

Figure 5.3 Mass Spectra for Unidentified Peaks in Pyrolysates from QCM TOD. Spectra Generated in NIST MS Search v2.3

From a qualitative standpoint, it is informative to look at the relative peak intensities for the RTIC chromatograms for the pyrolysates of the TOD from the different samples. It is important to remember that the chromatograms have been normalized to the peak intensity for toluene and it is unknown whether the same amount of toluene is formed in the pyrolysis of the different thermal oxidative deposits. The peaks for the alkyl phenols are more intense for the TOD from fuels that contain hydrotreated components. The TOD from the two straight run samples, J3193 and J3194, have the lowest relative intensities for the alkyl phenol peaks while having the relative largest peaks for SO_2 evolution and roughly equivalent peaks at 44.2 min and 45.6 min. This could suggest that for these straight run samples sulfur may take a larger role in deposit

formation. These are also the two samples that show an inverse relationship between ASTM D3241 stability and mass accumulation by QCM (Table 4.1).

The presence of alkyl phenols, alkyl anilines, and alkyl quinolines in the pyrolysates is consistent with their presence in fuel with poor thermal oxidative stability as measured by ASTM D3241 (Chapter 3) and the analysis of the samples before and after TOS in the QCM reactor (Chapter 4).[23] It has been reported elsewhere that there can be a negative correlation between basic amines (alkyl anilines) and TOD formation in the QCM.[24] The data reported here suggest that these types of molecules can take part in TOD formation, at least with the given compositions of the samples studied here. Although they take part in the TOD formation in these fuels, they are not necessarily promoting the reactions and it is possible that they could still inhibit them to some degree when compared to other components.

Examining some of the minor peaks, there are alkyl indoles detected. No alkyl carbazoles are detected. Alkyl carbazoles are at the high end of the boiling range of jet fuel and are often not present or are present at very low concentrations. It is possible that alkyl indoles are present in trace amounts in these samples due to the composition of the samples or due to their conversion to alkyl indolines through hydroprocessing. Alkyl indolines are shown to be significant to poor TOS as measured by ASTM D3241 through statistical analysis of LC/MS ESI data, however they are not seen as major components from the Py-GC/MS analysis. It is possible that the composition of the thermal oxidative deposits formed in the QCM are different than the composition of the thermal oxidative deposits that form on the heater tubes during ASTM D3241 analysis. It would be of interest to collect heater tube deposits for Py-GC/MS analysis.

It is notable that alkyl phenols are observed in the pyrolysate from the deposits and there are not appreciable amounts of quinone or hydroquinone compounds detected. In the postulated mechanism for the formation of deposits by the SMORS model, the first step is the oxidation of phenol eventually forming quinone. The quinone then goes on to react with nitrogen heterocycles leading to insoluble compounds which then deposit. The lack of major peaks from quinone and hydroquinone compounds in the pyrolysate could suggest that phenol is incorporated into the deposits though another pathway, at least during TOS in the QCM reactor. It could also be possible that the pyrolytic environment leads to the reformation of the alkyl phenols from the alkyl quinone or alkyl hydroquinone through a reductive process. More work is needed to better understand how the deposits break down during pyrolysis.

Chapter 6 : GCxGC/MS Analysis of Solvent Extracts from Spent Refinery Attapulgus Clay

Attapulgus clay treaters are used in refineries to remove polar compounds from jet fuel which helps to ensure that the product is meets specificationification.[15] The clay is composed of aluminum and silicon oxides and functions similar to silica gel.[15] Clay removes trace polar molecules such as alkyl phenols, nitrogen containing compounds, and other surfactants such as naphthenic acids which often improves the thermal oxidative stability of the fuel.

In order to understand the types of molecules that Attapulgus clay extracts from jet fuel, used clay from a refinery clay treater was extracted with solvents. Solvents of increasing polarity were used to help understand the relative interaction of the different groups of compounds with the clay, similar to extractions performed on silica gel or solid phase extraction cartridges.[56] First the clay was washed with hexane to remove the residual aliphatic molecules. Next the clay was washed with toluene and the extract was concentrated through evaporation of the solvent for analysis. The washing was repeated with methylene chloride and the extract was concentrated for analysis. The washing was repeated again with a 50:50 mixture of methylene chloride and methanol and the extract was concentrated for analysis. Finally, a methanol wash was performed, and the extract was concentrated for analysis. A detailed description of the procedure can be found in Chapter 2.

The washing procedure yielded four extracts of compounds. Each successive extract contains compounds that have stronger affinity for the clay and require a

stronger solvent to remove them. Toluene is the least polar solvent for which the extract is collected and analyzed, followed by methylene chloride, then methylene chloride/methanol, and finally methanol. Each concentrated extract was diluted in methylene chloride prior to comprehensive GCxGC/MS analysis.

Comprehensive GCxGC analyses use 2 orthogonal columns where all of the analytes go through both columns with a modulator in between them.[57] A reverse column set is used for these separations. This means that the first column is polar and the second, shorter column is non-polar. The modulator traps the effluent from the first column with a liquid nitrogen jet at a regular interval, in this case 10 seconds, prior to introducing it to the second column with a hot jet that re-volatilizes the trapped molecules. This allows for the separation of compounds that co-elute from the first column. Because the compounds are represented in 3-dimensions, they are referred to as blobs instead of peaks.

The mass spectral analyses were performed utilizing both electron ionization and photoionization. It was necessary to analyze each sample twice, once by each different ionization technique. Photoionization offers the advantage of yielding mostly molecular ions in the mass spectra at the expense of sensitivity and structural information.[42-43] Electron ionization has the advantage of higher sensitivity and fragmentation which allows for structural determination, usually through searching against mass spectral libraries however direct interpretation of the spectra can be performed as well. However, electron ionization does not always allow for the detection of molecular ion peaks. Only about 80% of the spectra in NIST Mass Spectral Database exhibit molecular ion peaks.[42] Therefore, photoionization and electron ionization can be good complementary

techniques for the identification of unknowns when they are not in mass spectral databases.

The RTICC for the hexane fraction can be found in Appendix A2 (Supplemental Figure 6.1). The compounds detected are the aromatic and aliphatic compounds that comprise jet fuel.

Toluene Extract

Figure 6.1 is the RTICC for the toluene fraction analyzed with electron ionization mode. A reverse column set was used in these analyses with the first column being more polar than the second column.[57-58] This type of column configuration has been shown to be best for the analysis of polar heteroatom-containing compounds in petroleum products.[59] The x-axis represents the retention time of compounds on the first column in minutes. The y-axis represents the retention time of the compounds on the second column in seconds. In general, the polarity and size of the compounds increases as the retention time on the first column increases.[60] The polarity of the compounds decreases as the retention time of the second column increases.[60] The color of the blob represents its intensity. Red is the most intense and blue is the least intense with green in between. A cryogenic thermal modulator was used and operated at 10 second intervals. This means that every 10 seconds a hot jet activates blowing nitrogen at the temperature set in the method for the time duration set in the method. At all other times, the liquid nitrogen is trapping compounds eluting off the first column. The flow rate of the nitrogen is controlled by a manual bubble flow meter. It was experimentally determined that for jet fuel 5-6 mL/min of liquid nitrogen was sufficient to

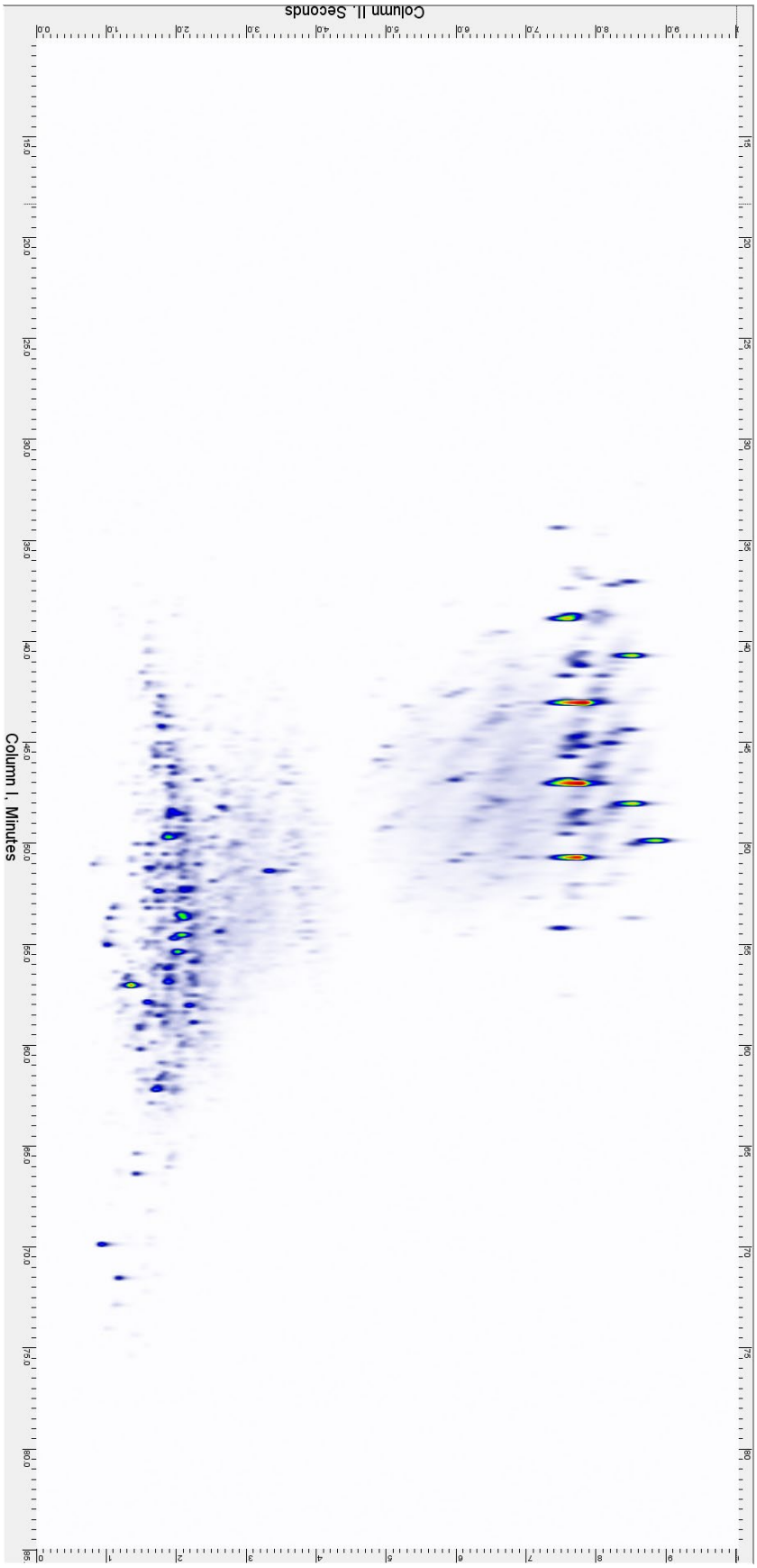

Figure 6.1 GCxGC/MS Electron ionization RTICC for the Toluene Extracted Fraction of Attapulgus Clay Used for Treating Jet Fuel

trap the most volatile compounds without causing insufficient volatilization of the least volatile compounds. Detailed experimental parameters can be found in Chapter 2.

The time-of-flight mass spectrometer used in these analyses provides high-resolution accurate-mass data. Therefore, it is possible to determine elemental compositions for the ions in the mass spectra based on their measured *m/z* values and isotope abundance. Additionally, it is possible to search the EI mass spectra against the NIST library using MS Search v2.3. Searching the mass spectra for some of the major peaks in the RTICC, it appears that the primary compounds in this fraction are alkyl phenol compounds, alkyl indole compounds, alkyl carbazole compounds, and normal and isoparaffins. Figure 6.2 shows the mass spectrum for the blob at 44.116 minutes, 1.757 seconds and its match in the NIST library, 2-methyl-6-propylphenol.

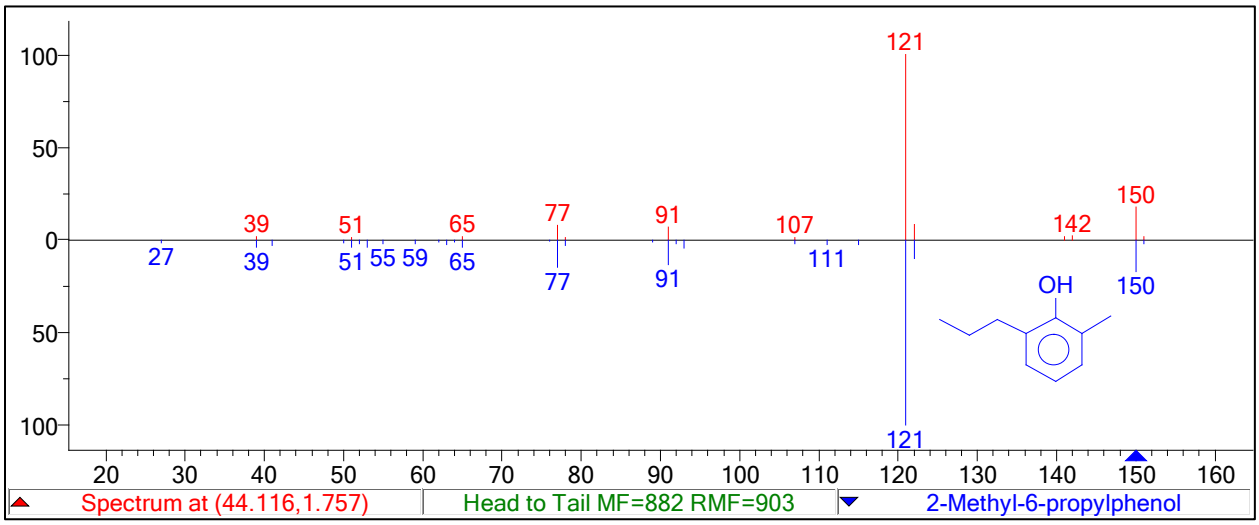

Figure 6.2 Mass Spectrum (Top) and NIST Library Match (Bottom) for 2-Methyl-6-propylphenol. Plot Generated in NIST MS Search v2.3

Figure 6.3 shows the mass spectrum for the blob at 54.949 minutes, 1.004 seconds and its match in the NIST library, 2,3-dimethylindole.

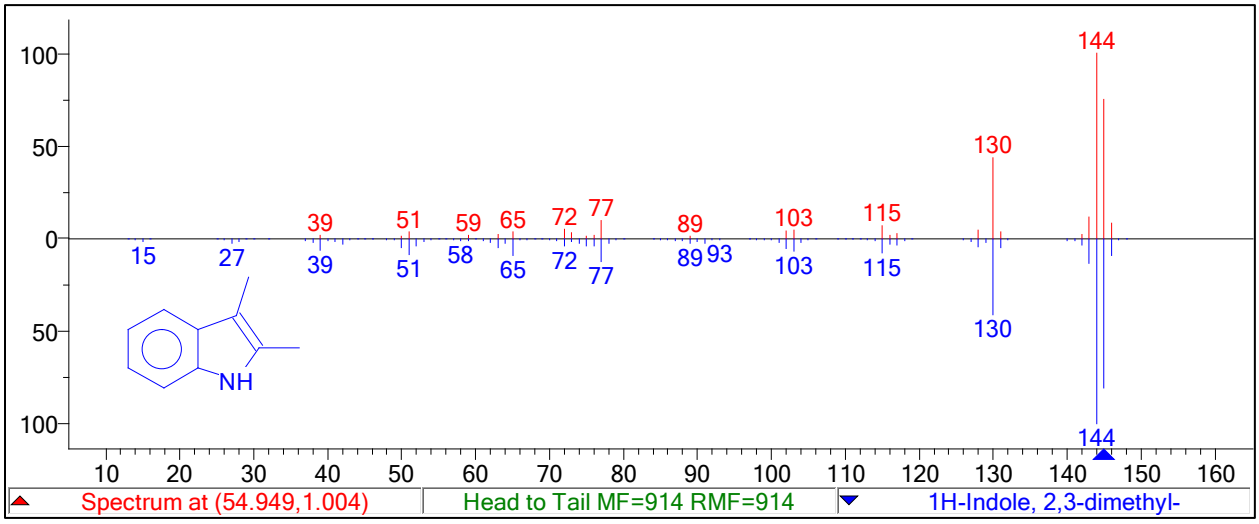

Figure 6.3 Mass Spectrum (Top) and NIST Library Match (Bottom) for 2,3-dimethylindole. Plot Generated in NIST MS Search v2.3

Figure 6.4 shows the mass spectrum for the blob at 71.449 minutes, 1.213 seconds and its match in the NIST library, 2-methylcarbazole.

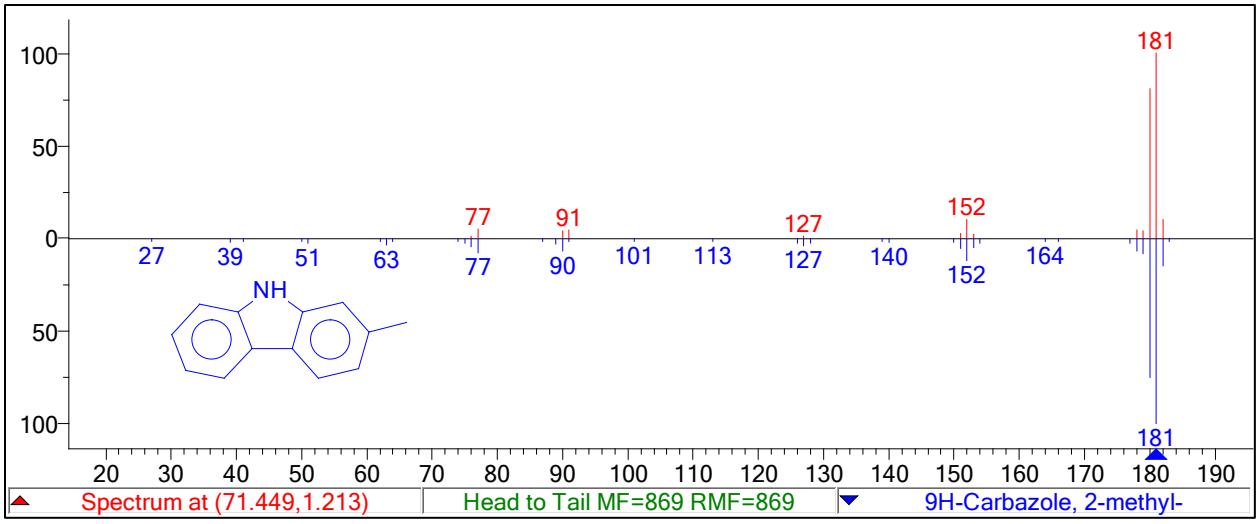

Figure 6.4 Mass Spectrum (Top) and NIST Library Match (Bottom) for 2-Methylcarbazole. Plot Generated in NIST MS Search v2.3

Figure 6.5 shows the mass spectrum for the blob at 46.949 minutes, 7.612 seconds and its match in the NIST library, pentadecane.

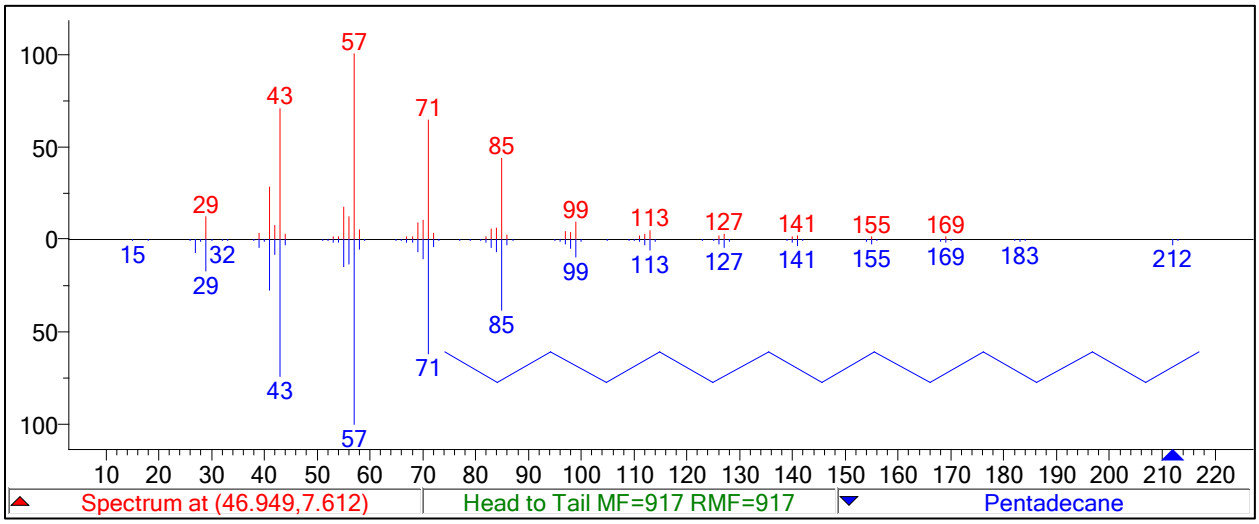

Figure 6.5 Mass Spectrum (Top) and NIST Library Match (Bottom) for Pentadecane. Plot Generated in NIST MS Search v2.3

There is no molecular ion displayed in the spectrum shown in Figure 6.5. It is often the case that when the molecular ion is absent the identification of the compound

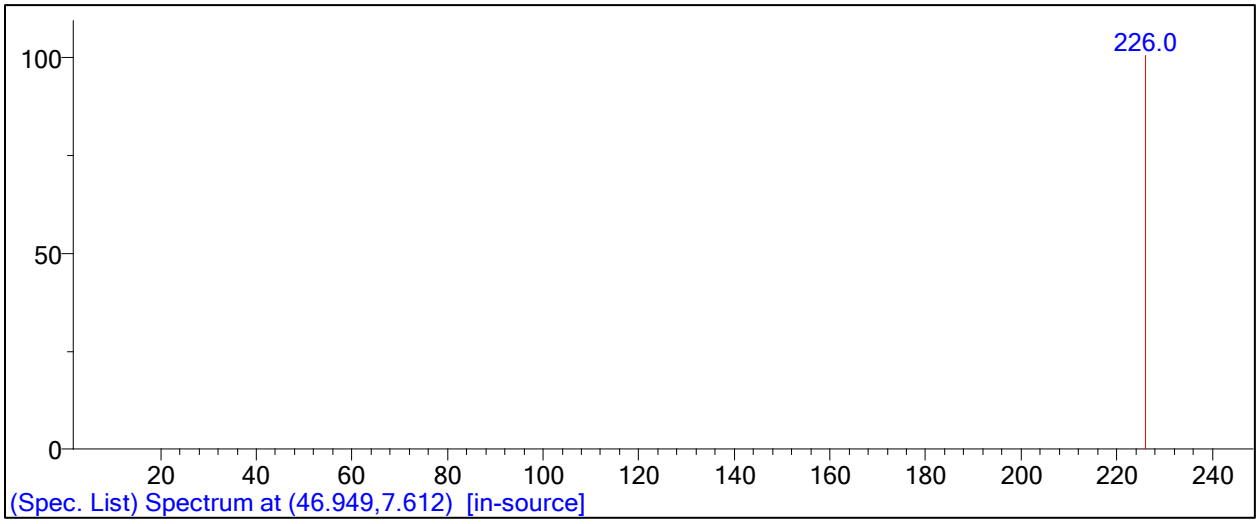

Figure 6.6 Photoionization Mass Spectrum for Blob at 46.949 minutes, 7.612 seconds. Plot Generated in NIST MS Search v2.3

from its mass spectrum can be incorrect. Figure 6.6 shows the mass spectrum for the same blob using photoionization instead of EI. There are no isotope peaks in this spectrum due to the low abundance of ions generated utilizing photoionization. From the PI spectrum it is clear that the molecular ion for the blob at 46.949 minutes, 7.612 seconds has a nominal *m/z* value of 226 Da. The GC Image software shows the accurate-mass value for this ion to be 226.2667 Da. The Formula Generator in the GC Image software shows the closest matching elemental composition to be $C_{16}H_{34}$, which has an exact mass of 226.2661 Da. The difference between the measured accurate-mass value and the calculated exact-mass value is 0.6 mDa. It is likely that the blob at

46.949 minutes, 7.612 seconds is actually hexadecane and not pentadecane as suggested by the library match. This illustrates the fact that it is necessary to examine every mass spectrum and library search result in order to verify its validity. Using complimentary data can be invaluable.

It is possible to use the GC Image software to create extracted ion chromatograms (EIC) based on general elemental compositions of homologous series. Figure 6.7 shows the EIC for the general elemental composition $C_nH_{2n-6}O$ from n = 6 to n = 12 with a mass tolerance of +/- 0.01 Da. This illustrates that the one of the primary polar sets of compounds found in this extract are a homologous series of alkyl phenols.

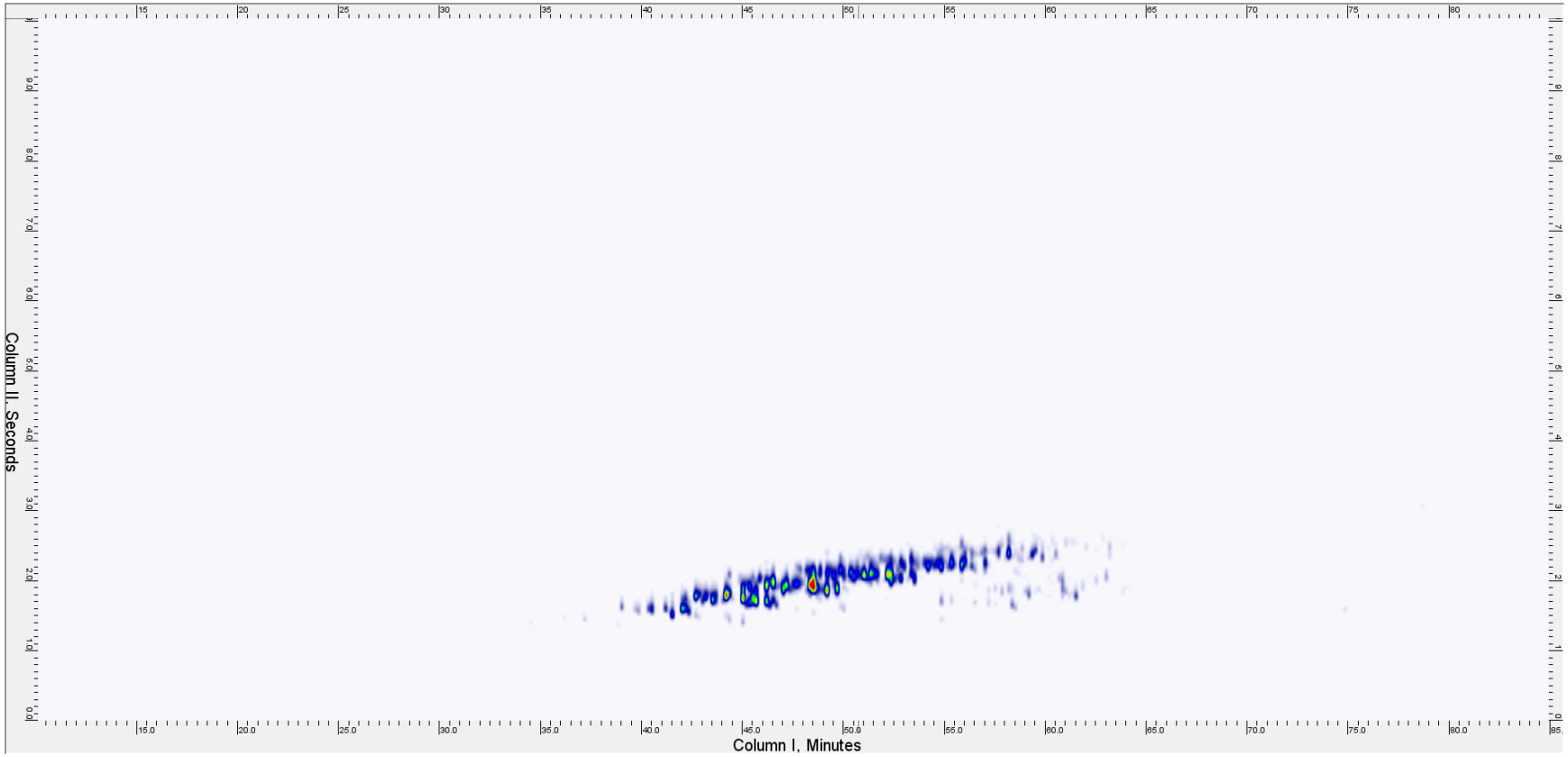

Figure 6.7 Extracted Ion Chromatogram for the General Elemental Composition $C_nH_{2n-6}O$ in the Toluene Extracted Fraction of Attapulgus Clay used for Treating Jet Fuel

The same procedure was performed for the alkyl indole homologous series using the general elemental composition $C_nH_{2n-9}N$ from n = 8 to n = 14 with a mass tolerance of +/- 0.01 Da., the alkyl carbazole homologous series using the general elemental composition $C_nH_{2n-15}N$ from n = 12 to n = 14 with a mass tolerance of +/- 0.01 Da., and the normal and isoparaffin homologous series using the general elemental composition C_nH_{2n+2} from n = 6 to n = 18 with a mass tolerance of +/- 0.01 Da. The images of these individual EICs can be found in Appendix B (Supplemental Figures 6.1-3) By drawing a polygon around each extracted homologous series, the polygon is also added to the RTICC. This allows for visualization of the different homologous series on the RTICC. Figure 6.8 shows the RTICC with the polygons added for the major homologous series detected in the toluene fraction. The normal and isoparaffinic homologous series is shown with a red polygon. The alkyl phenol homologous series is shown with a dark blue polygon. The alkyl indole homologous series is shown with a green polygon. The alkyl carbazole homologous series is shown with a light blue polygon.

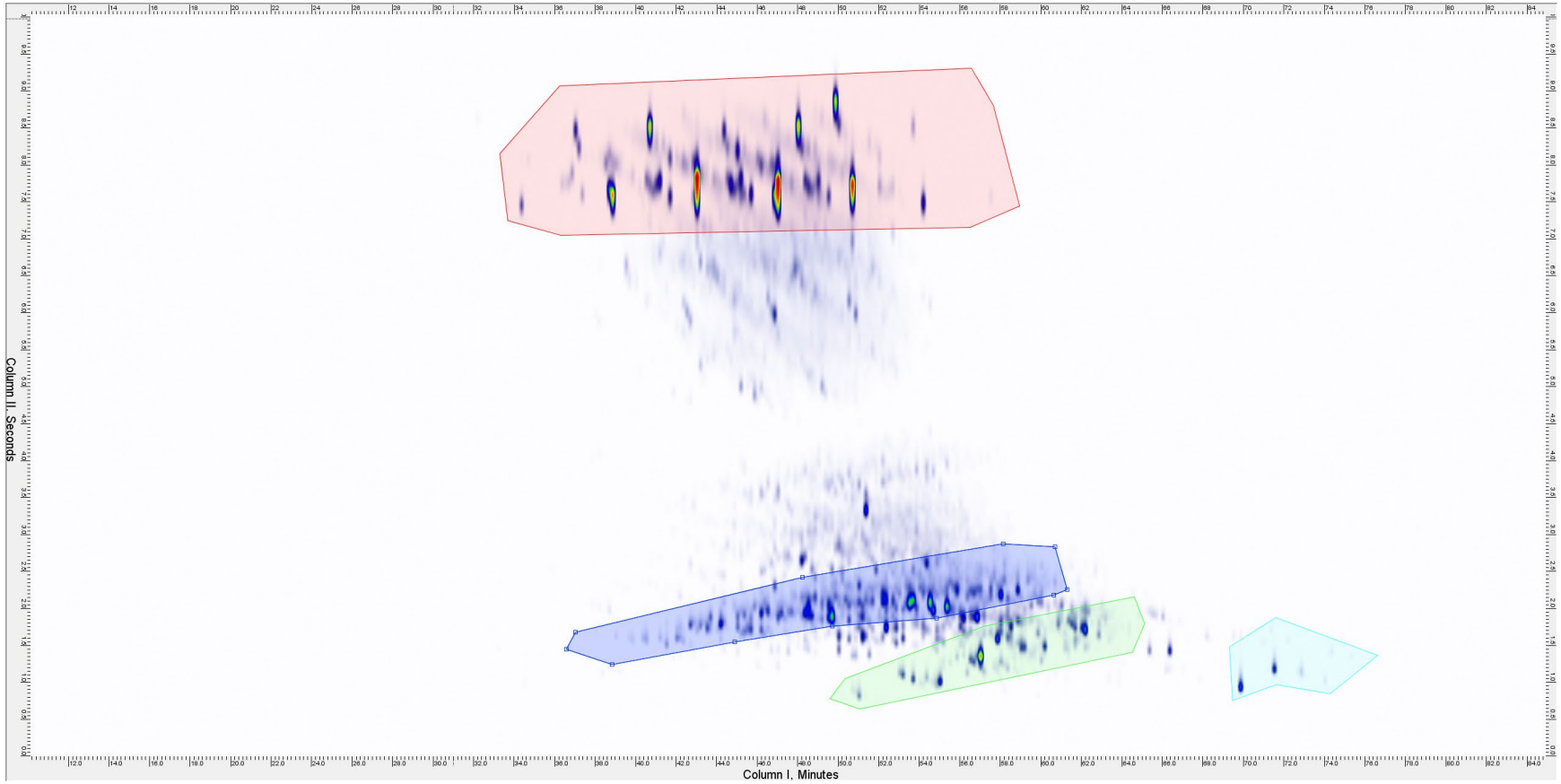

Figure 6.8 GCxGC/MS Electron ionization RTICC for the Toluene Extracted Fraction of Attapulgus Clay Used for Treating Jet Fuel. Red Polygons Highlights Paraffinic Compounds, Blue Polygon Highlights Alkyl Phenols, Green Polygon Highlights Alkyl Indoles, Blue Polygon Highlights Alkyl Carbazoles

Examining the RTICC with the polygons added, it becomes apparent that there is a series of compounds that co-elute with the alkyl phenol homologous series. These compounds are off-set slightly from the main series and have a higher abundance distributed over fewer compounds. Searching their EI mass spectra in the NIST 17 library shows them to be a homologous series of alkyl naphthalenes that are co-eluting with the alkyl phenols. Figure 6.9 shows the mass spectrum for the blob at 53.449 minutes, 2.091 seconds and its match in the NIST library, 1,6,7-trimethylnaphthalene.

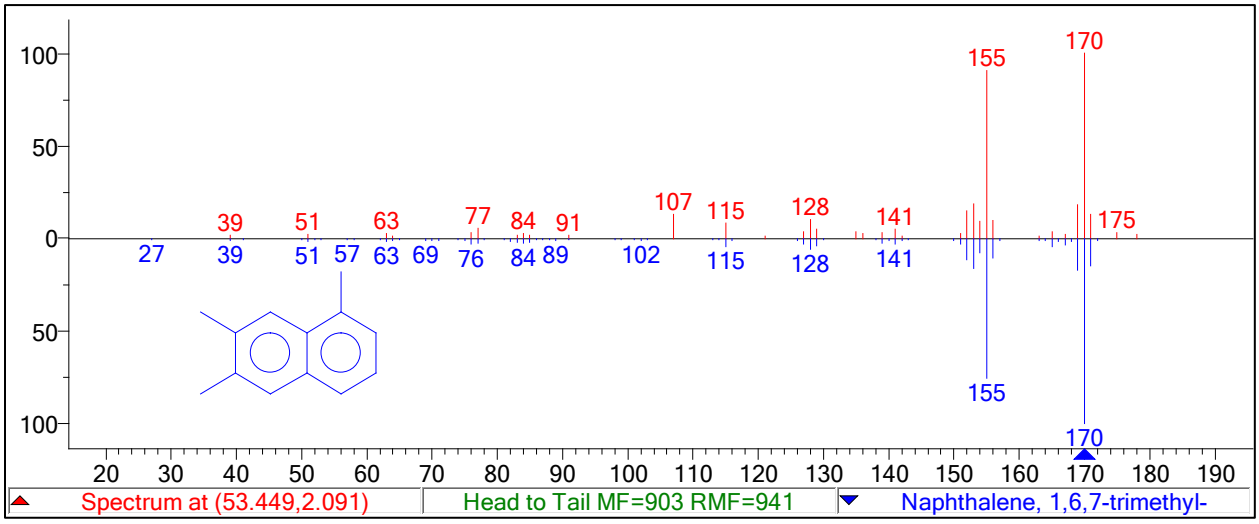

Figure 6.9 Mass Spectrum (Top) and NIST Library Match (Bottom) for 1,6,7-Trimethylindole. Plot Generated in NIST MS Search v2.3

There are also a number of blobs that sit outside of the polygons that were added to the RTICC. Most of the blobs had mass spectra that were consistent with aromatic hydrocarbon compounds. However, there were two blobs that had mass spectra of particular interest. First is the EI mass spectrum for the blob at 51.282 minutes, 3.304

seconds. This spectrum does not have a satisfactory match in the NIST library. However, this spectrum matches the spectrum shown in Figure 5.3 for the peak at 44.2 minutes. Figure 6.10 shows this mass spectrum and its comparison to the spectrum from Figure 5.3. It is notable that the compound with this mass spectrum was found as a result of the pyrolysis of TOD and also in the toluene extract from Attapulgus clay. This suggests that the molecule with this mass spectrum can be present in jet fuel, removed by Attapulgus clay, and can be incorporated into TOD when it is present in the fuel.

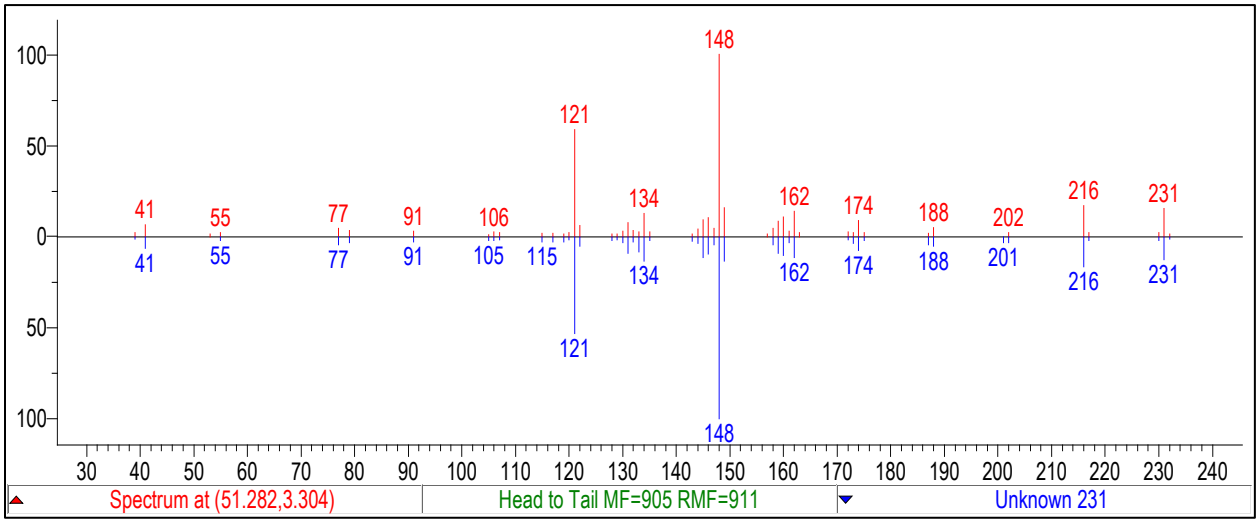

Figure 6.10 Mass Spectrum (Top) and NIST Library Match (Bottom) for the Blob at 51.282 minutes, 3.304 seconds and a Library Entry Created from the Unknown Spectrum for the Peak at 44.2 minutes in the Py-GC/MS of TOD (Figure 5.3). Plot Generated in NIST MS Search v2.3

One of the advantages for interpreting this spectrum from the GCxGC/MS analysis over the Py-GC/MS analysis is that the time-of-flight mass spectrometer utilized has high-resolving power accurate-mass measurement capabilities and the single quadrupole mass spectrometer in the Py-GC/MS does not have either. The

accurate mass measurement of the ions allows for the generation of elemental compositions for the ions in the mass spectra. Examining the mass spectrum, the likely molecular ion peak is at *m/z* 231. The accurate-mass measurement for this ion gives a value of 231.1963 Da. Using the Formula Calculator in the GC Image software the closes matching elemental composition is $C_{16}H_{25}N$ which has an exact mass of 231.1987 Da which is a difference of -2.4 mDa or 10.4 ppm. This is reasonable given the JEOL AccuTOF GCv 4g instrument has an allowable error of +/- 5 mDa. A compound containing basic nitrogen with the elemental composition of $C_{16}H_{25}N$ was found to be present in large quantities in the Edeleanu extract of the kerosene fraction from a California crude oil.[61-62] The Edeleanu process is a method for removing sulfur and nitrogen containing compounds from petroleum distillates through extraction with liquid sulfur dioxide.[63] Detailed structural characterization was done for this particular compound.[61] The reported structure for this basic nitrogen containing compound was 2-(2,2,6-trimethylcyclohexyl)-4,6-dimethylpyridine. In order to investigate if the mass spectrum in Figure 6.10 could represent the EI fragmentation of 2-(2,2,6-trimethylcyclohexyl)-4,6-dimethylpyridine, the mass spectrum and structure were analyzed using MS Interpreter which is available from NIST. The annotated mass spectrum is shown in Figure 6.11 (the molecular ion peak is selected showing that it is consistent with the structure).

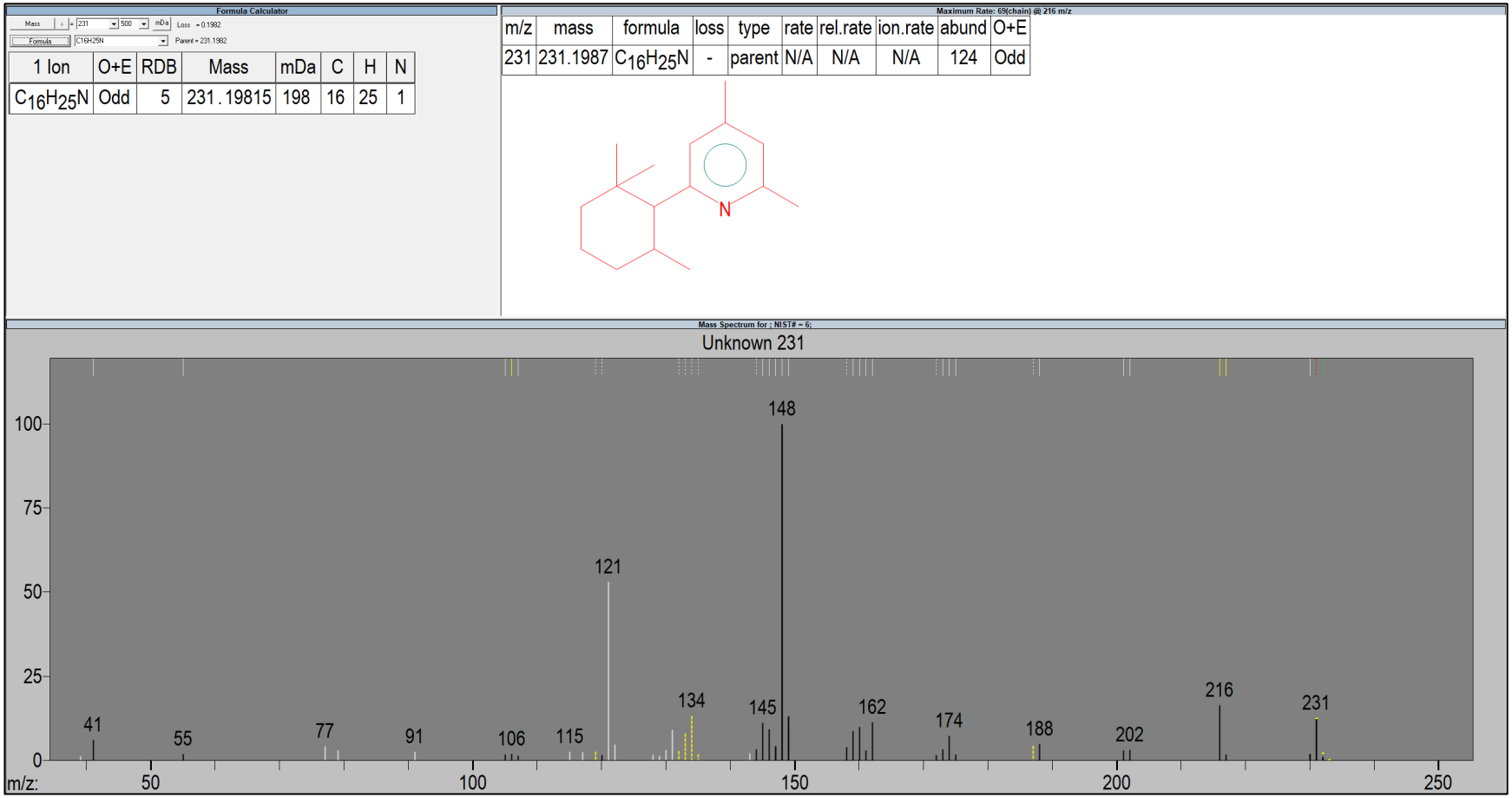

Figure 6.11 MS Interpreter (Version 3.4.3l) Analysis comparing the mass spectrum for the Blob at 51.282 minutes, 3.304 seconds and the Structure for 2-(2,2,6-trimethylcyclohexyl)-4,6-dimethylpyridine. The Black Peaks Denote Fragments that are Easily Explained.

The annotations are based on likely fragmentation pathways from the structure of the submitted molecule. The black peaks denote fragment ions that the software can explain. Most of the peaks in the spectrum can be explained through simple fragmentation pathways from the molecular ion. The gray peaks denote fragment ions that cannot be predicted by the software and likely are the result of more complex fragmentation or could be indicative that the structure and spectrum do not match. The main fragment that is not explained by the software is the peak at *m/z* 121. The accurate-mass for this ion is 121.0893 Da. The Formula Calculator in the GC Image software suggests that the fragment has an elemental composition of $C_8H_{11}N$. The exact mass for the suggested elemental composition is 121.0891 Da which has a 0.2 mDA difference. This would represent an odd electron ion that is formed from the loss of a neutral molecule. The likely fragmentation occurs from a rearrangement that results in the loss of C_8H_{14} from the molecular ion. A reasonable fragmentation mechanism that could occur to produce the ion with *m/z* 121 is shown in Figure 6.12.

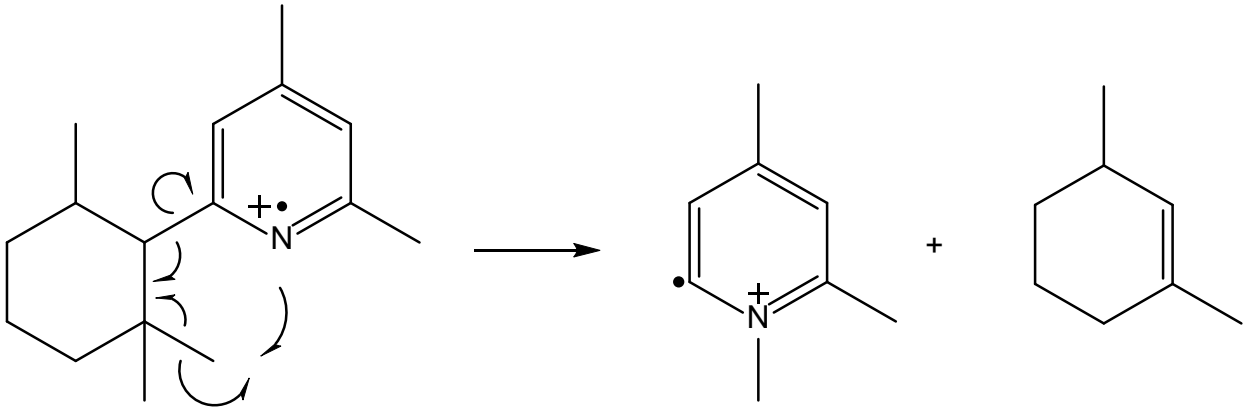

m/z 231 *m/z* 121

Figure 6.12 Possible Fragmentation Mechanism to Explain the Formation of the Odd Electron Ion with *m/z* 121.

The second EI mass spectrum of interest is for the blob at 54.282 minutes, 2.593 seconds. Similar to the previous blob of interest, this blob's mass spectrum matches a mass spectrum from Figure 5.3 but this time it is the second spectrum for the peak at 45.6 minutes in the Py-GC/MS chromatograms of TOD. Figure 6.13 shows the mass spectrum for the blob at 54.282 minutes, 2.593 seconds compared to the mass spectrum from 45.6 minutes in the Py-GC/MS chromatogram of J3192 (Figure 5.3).

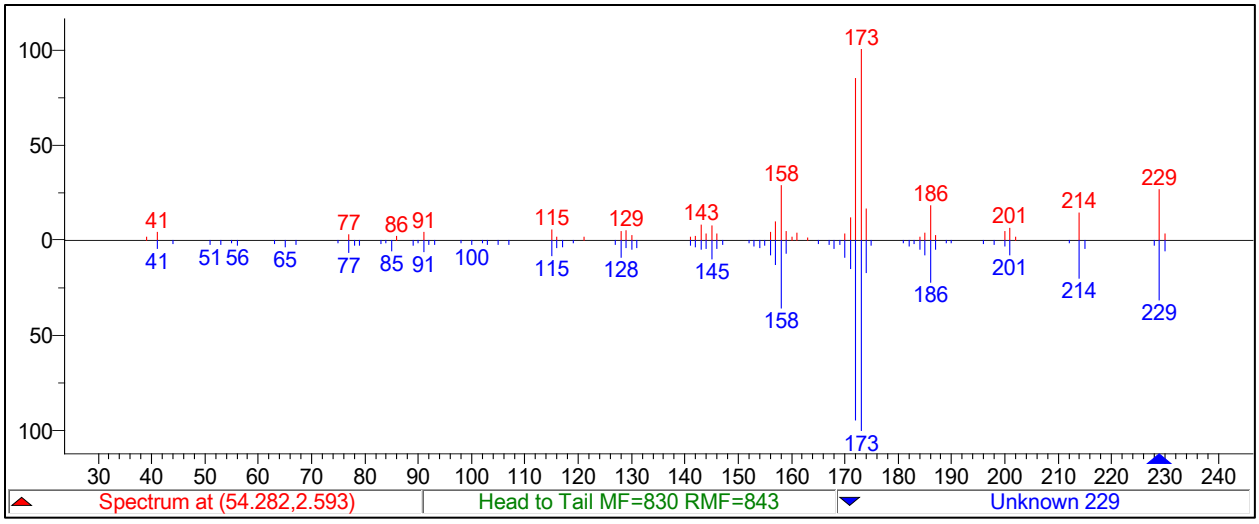

Figure 6.13 Mass Spectrum (Top) and NIST Library Match (Bottom) for the Blob at 54.282 minutes, 2.593 seconds and a Library Entry Created from the Unknown Spectrum for the Peak at 45.6 minutes in the Py-GC/MS of TOD (Figure 5.3). Plot Generated in NIST MS Search v2.3

The likely molecular ion peak for this mass spectrum is represented by the peak at *m/z* 229. Its accurate-mass value is 229.1811 Da. Using the Formula Calculator in the GC Image Software, the elemental composition $C_{16}H_{23}N$ is the closest match. The exact mass value for this elemental composition is 229.1830 Da which is -1.9 mDa different from the measured accurate-mass value. The suggested elemental composition is one double bond equivalent (DBE) greater than the elemental composition previously discussed. Using the previous structure as a starting point, it would be reasonable to expect that the compound with the molecular ion peak at *m/z* 229 has an added ring or double bond. To explore this theory, the mass spectrum along with the postulated structure shown in Figure 6.14 were submitted to MS Interpreter.

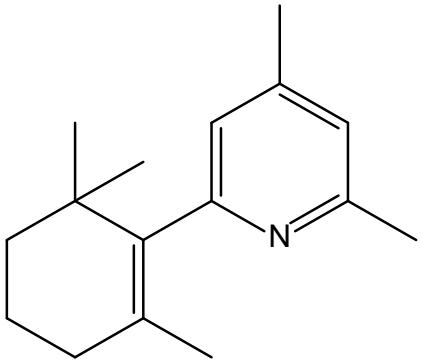

Figure 6.14 Postulated Structure for the Mass Spectrum Shown in Figure 6.13.

The annotated mass spectrum based on this structure is shown in Figure 6.15. All of the major peaks in the mass spectrum are explained by MS Interpreter, including the base peak at *m/z* 173, which is an odd electron ion. The accurate-mass measurement for this ion is 173.1195 Da. Using the Formula Calculator in the GC Image software, the closest matching elemental composition is $C_{12}H_{15}N$. The exact mass value for this elemental composition is 173.1204 Da which is -0.9 mDa different from the measured accurate-mass value. This is consistent with the elemental composition of the fragment ion suggested by MS Interpreter which results from an H-loss-in-ring with the loss of a neutral molecule with the elemental composition C_4H_8 (the base peak ion is selected to illustrate MS Interpreter's suggested fragmentation for this peak). There are a number of lower *m/z* value peaks for which MS Interpreter does not suggest fragmentation mechanisms. However, the fact that most of the major peaks can be explained from this structure make it a good candidate.

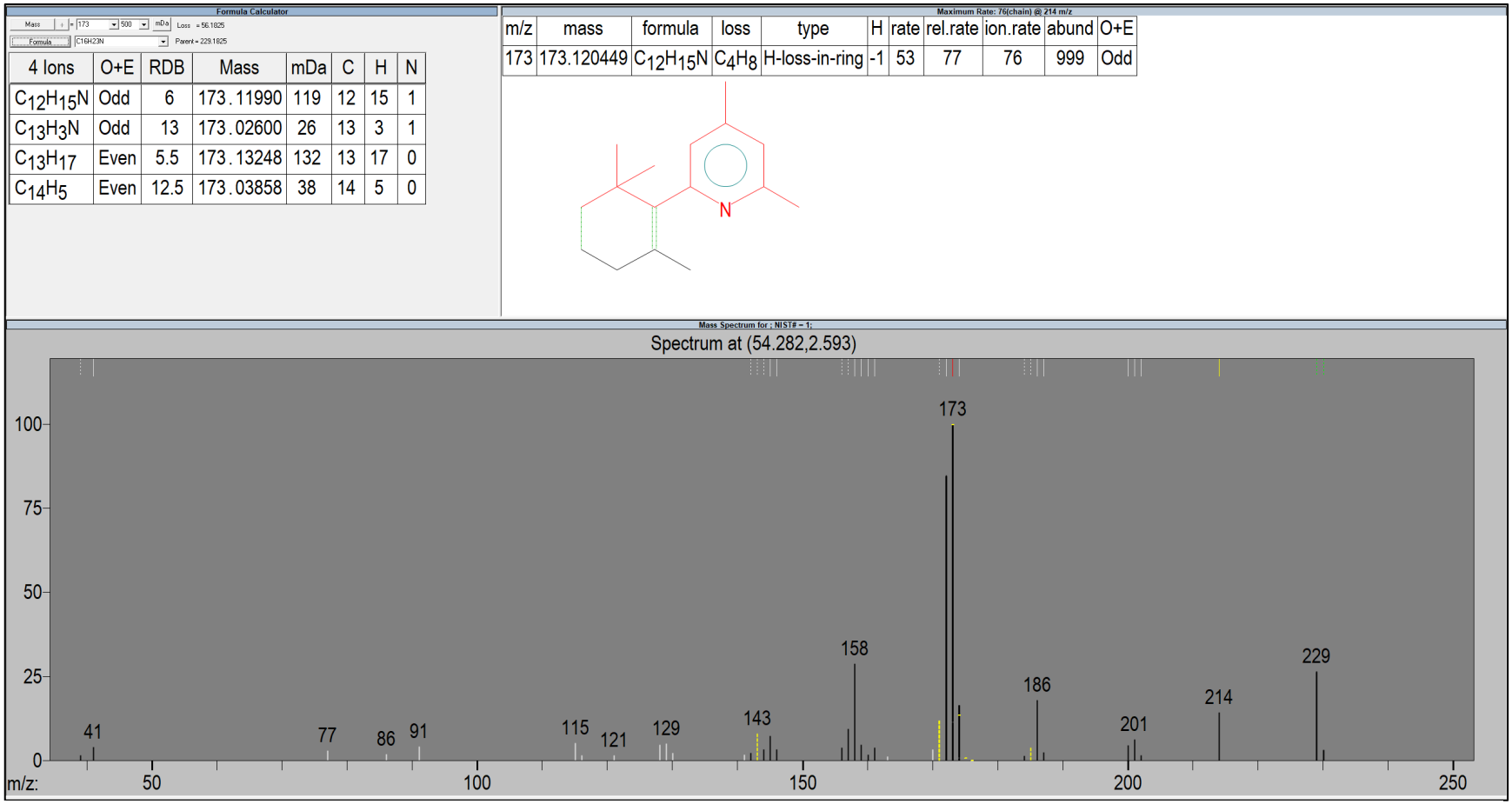

Figure 6.15 MS Interpreter (Version 3.4.3l) Analysis comparing the mass spectrum for the Blob at 54.282 minutes, 2.593 seconds and the Structure Shown in Figure 6.14. The Black Peaks Denote Fragments that are Easily Explained.

DCM Extract

Figure 6.16 is the RTICC for the GCxGC/MS analysis of the DCM fraction utilizing electron ionization mode. The same process of identifying the compounds that are present in this extract as the toluene extract was used. First mass spectra were explored to get an understanding of the compounds present. The types of molecules in this extract is similar to what was seen in the toluene extract although their distribution was slightly different.

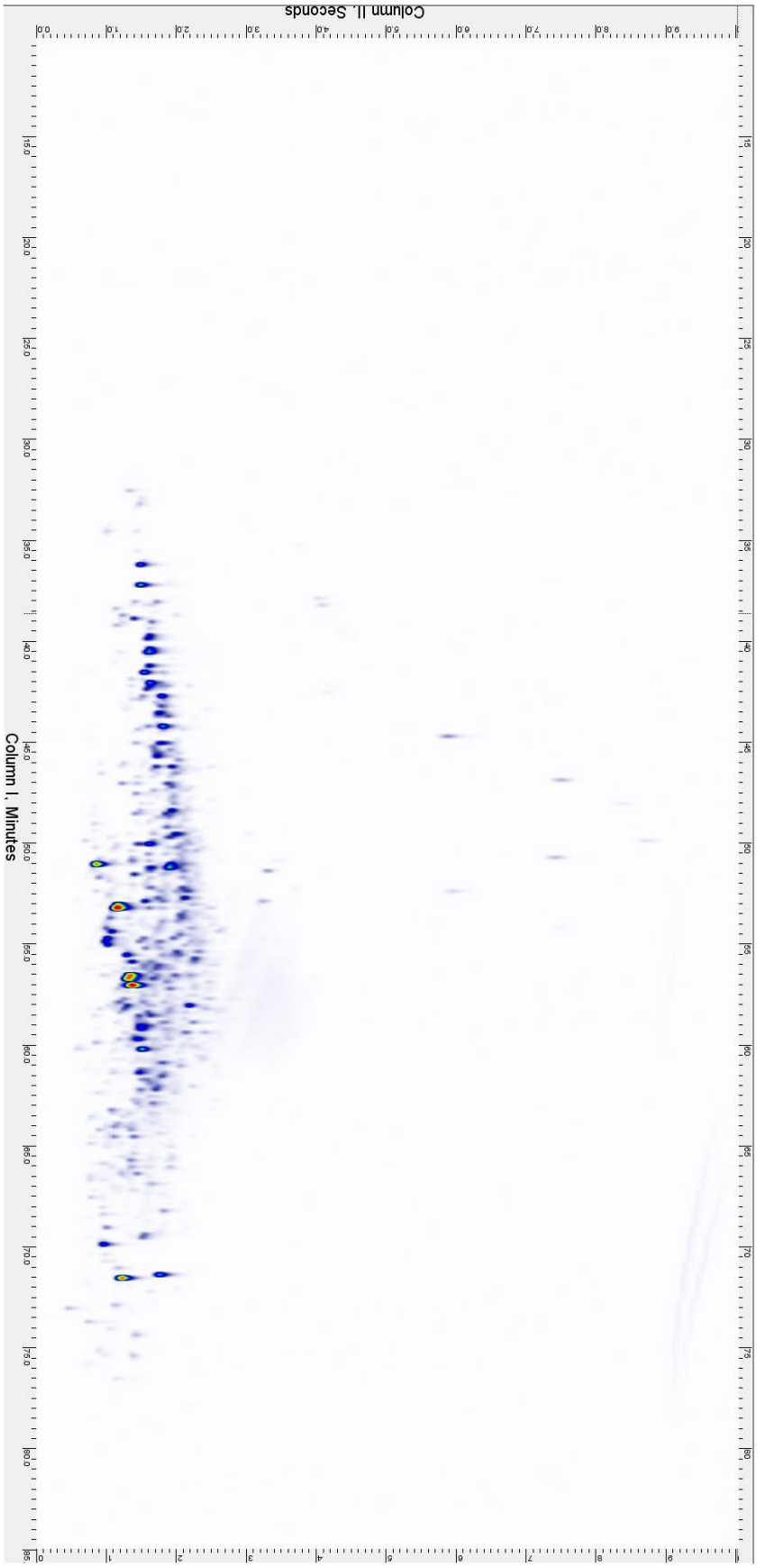

Figure 6.16 GCxGC/MS Electron ionization RTICC for the DCM Extracted Fraction of Attapulgus Clay Used for Treating Jet Fuel

Alkyl phenols were detected in this fraction as well. The distribution of the homologous series started at a lower carbon number which is likely due to the fact that these alkyl phenols are more polar and bind to the clay more strongly requiring a stronger solvent to remove them. Figure 6.17 shows the mass spectrum for the blob at 37.122 minutes, 1.548 seconds and its NIST Library match 2,5-dimethylphenol. This is one of the earliest eluting alky phenols in the homologous series and was not detected in the toluene extract.

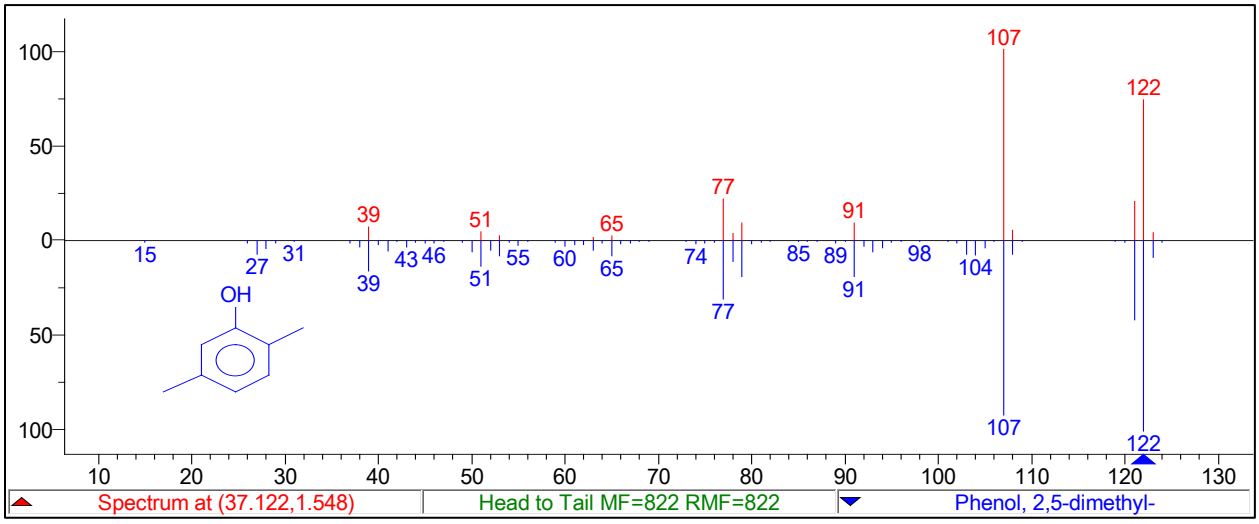

Figure 6.17 Mass Spectrum (Top) and NIST Library Match (Bottom) for 2,5-Dimethylphenol. Plot Generated in NIST MS Search v2.3

Alkyl indoles were also detected in this fraction as well. Upon visual inspection, the intensity of the blobs was higher for this series in the DCM extract than in the toluene extract suggesting they are removed more efficiently by the stronger solvent. The higher intensity is relative to the other compounds present across the sample set

because the concentration of the extract and injection volumes was the same for every sample. Figure 6.18 shows the mass spectrum for the blob at 50.956 minutes, 0.753 and its NIST Library match 4-methyl indole. This is one of the earliest eluting alkyl indoles in the homologous series and is present at a higher intensity than it was in the toluene extract.

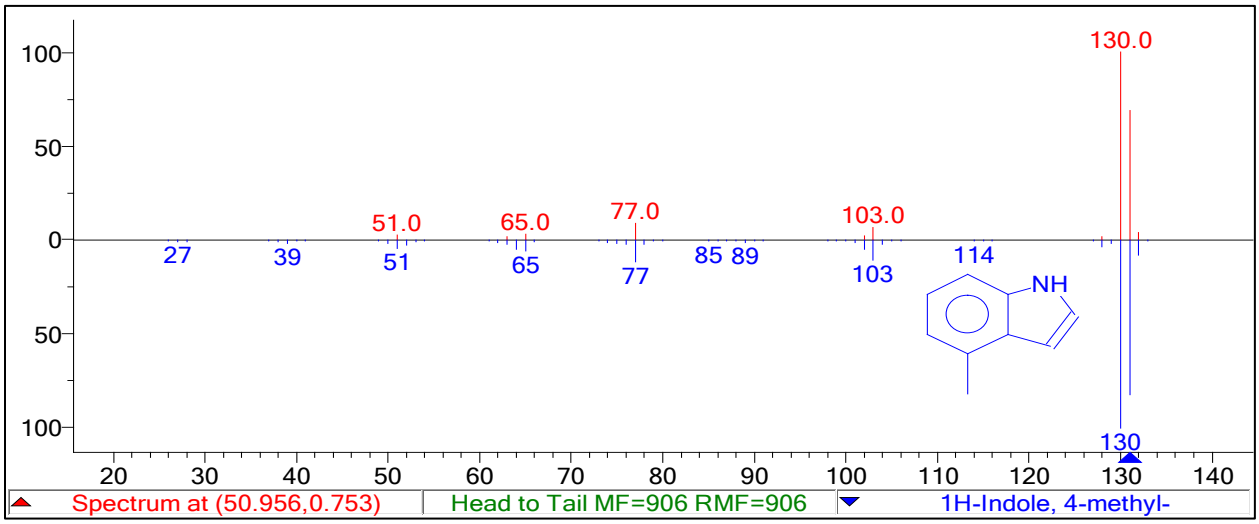

Figure 6.18 Mass Spectrum (Top) and NIST Library Match (Bottom) for 4-Methylindole. Plot Generated in NIST MS Search v2.3

Similar to the alkyl indole homologous series, alkyl carbazoles are detected in this fraction at higher intensities than in the toluene fraction. Figure 6.19 shows the mass spectrum for the blob at 69.789 minutes, 0.962 seconds and its NIST Library match carbazole.

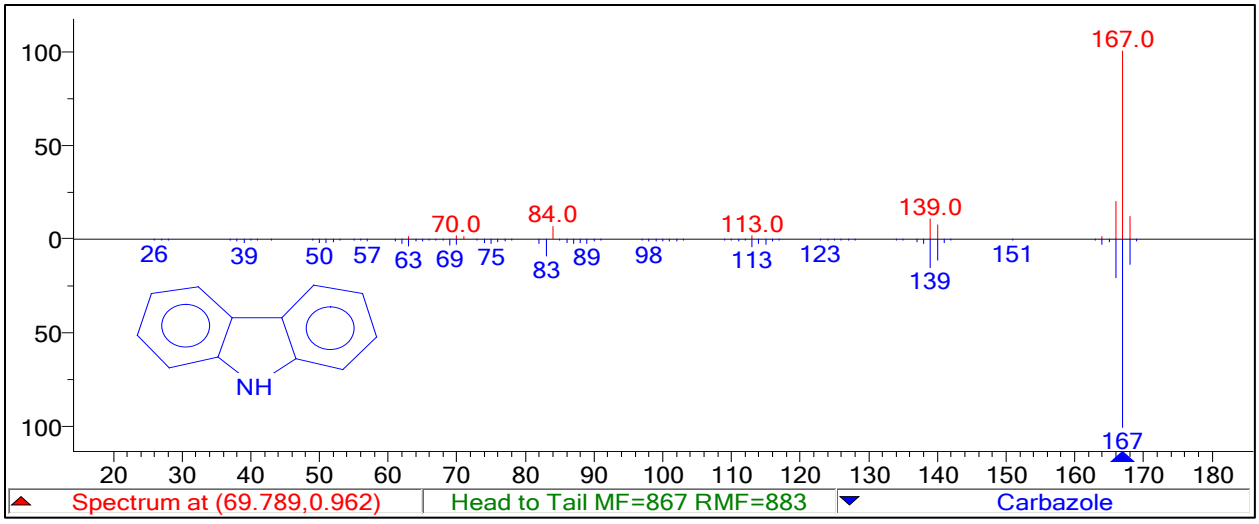

Figure 6.19 Mass Spectrum (Top) and NIST Library Match (Bottom) for Carbazole. Plot Generated in NIST MS Search v2.3

In addition to the homologous series detected in the DCM extract that were also present in the toluene extract, a new homologous series was detected. Figure 6.20 shows the mass spectrum for the blob at 49.956 minutes, 1.631 seconds and its NIST Library match.

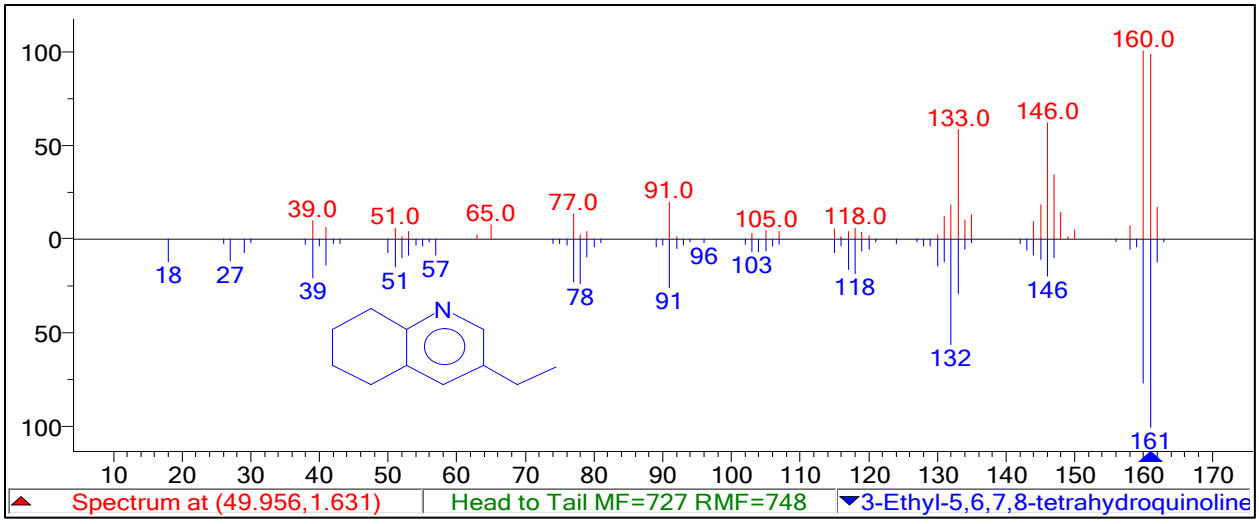

Figure 6.20 Mass Spectrum (Top) and NIST Library Match (Bottom) for 3-Ethyl-5,6,7,8-tetrahydroquinoline. Plot Generated in NIST MS Search v2.3

Each of the homologous series was extracted in order to draw polygons to help visualize their presence. Figure 6.21 shows the RTICC containing polygons for each homologous series. This was created by extracting the alkyl phenol homologous series using the general elemental composition $C_nH_{2n-6}O$ from n = 6 to n = 12 with a mass tolerance of +/- 0.01 Da, the alkyl indole homologous series using the general elemental composition $C_nH_{2n-9}N$ from n = 8 to n = 14 with a mass tolerance of +/- 0.01 Da., the alkyl carbazole homologous series using the general elemental composition $C_nH_{2n-15}N$ from n = 12 to n = 14 with a mass tolerance of +/- 0.01 Da., and the tetrahydroquinoline homologous series using the general elemental composition $C_nH_{2n-7}N$ from n = 9 to n = 14 with a mass tolerance of +/- 0.01 Da.

The images of the individual EICs can be found in Appendix B (Supplemental Figures 6.4-8). By drawing a polygon around each extracted homologous series, the polygon is also added to the RTICC. The RTICC with polygons added is shown in

Figure 6.21. The alkyl phenol homologous series is shown with a dark blue polygon. The alkyl indole homologous series is shown with a green polygon. The alkyl carbazole homologous series is shown with a light blue polygon. The alkyl tetrahydroquinoline series is shown with a red polygon. As can be seen, there is significant co-elution between the alkyl tetrahydroquinoline series and the alkyl indole homologous series even with the excellent chromatographic resolution provided by the comprehensive GCxGC analysis. While it is still possible to identify the different homologous series present, it would be difficult to accurately quantitate the individual compounds or the relative amounts of each homologous series due to co-elution if that was a desired outcome of this analysis. However, this analysis is being done for qualitative purposes to understand the types of polar molecules present.

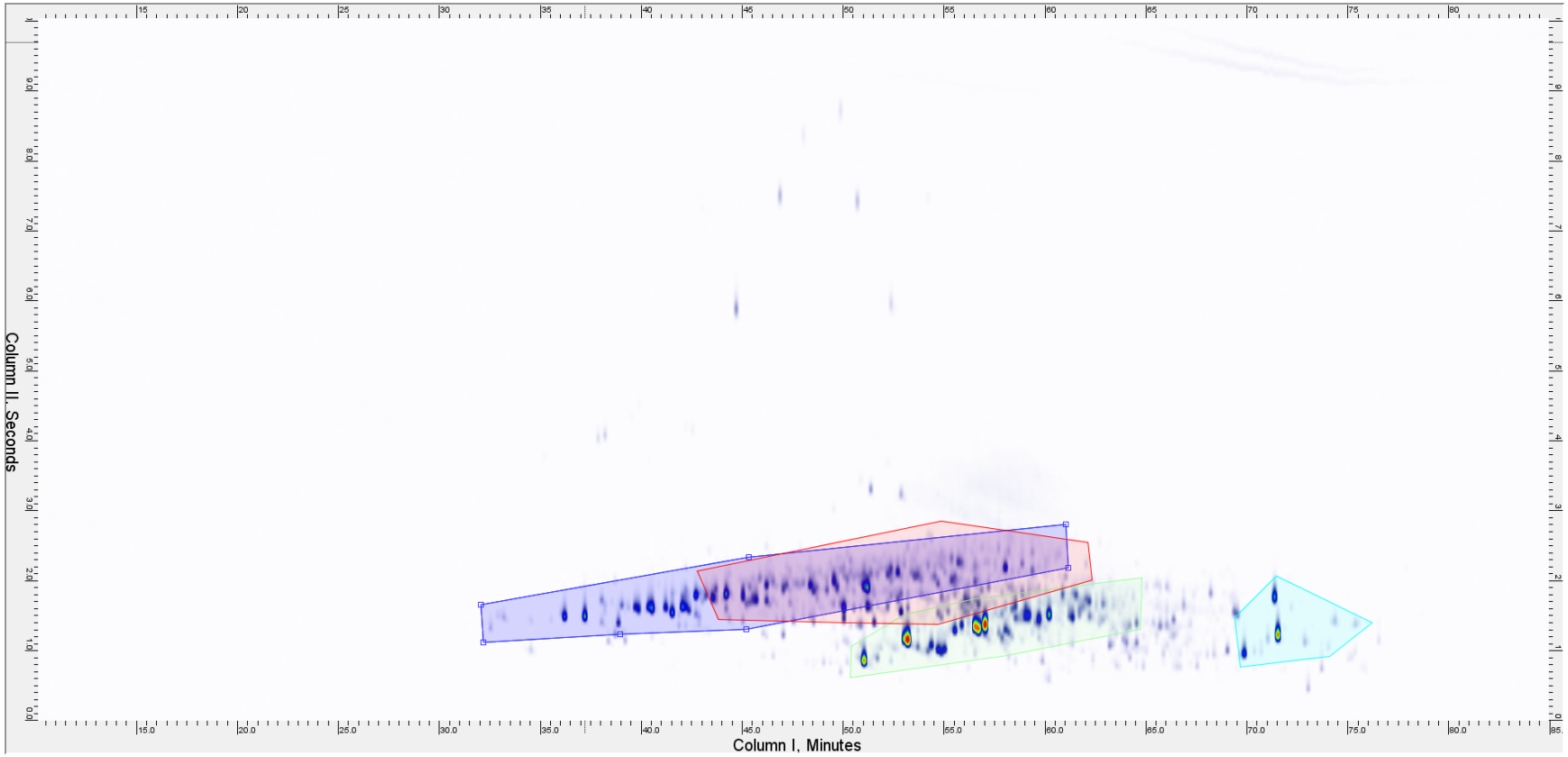

Figure 6.21 GCxGC/MS Electron ionization RTICC for the DCM Extracted Fraction of Attapulgus Clay Used for Treating Jet Fuel. Red Polygons Highlights Alkyl Tetrahydroquinoline Compounds, Dark Blue Polygon Highlights Alkyl Phenols, Green Polygon Highlights Alkyl Indoles, Light Blue Polygon Highlights Alkyl Carbazoles.

In addition to the primary series of homologous compounds that have polygons added. There are some less abundant species present in the sample. The series of blobs in between the alkyl indole and alkyl carbazole homologous series are consistent with polynuclear aromatic compounds. Figure 6.22 shows the mass spectrum for the blob at 66.289 minutes, 1.422 seconds and its match in the NIST Library anthracene.

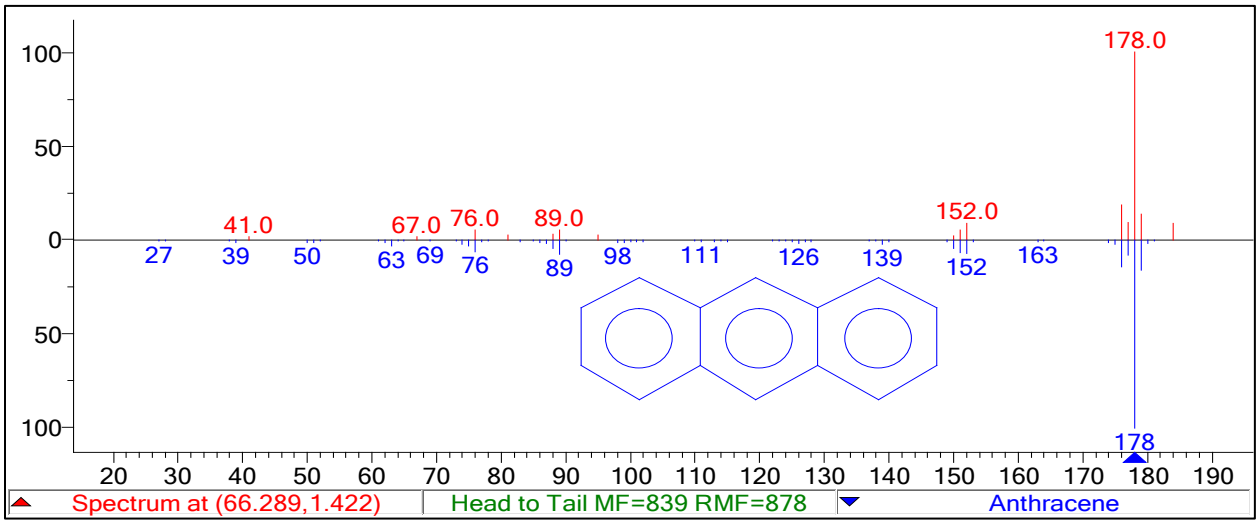

Figure 6.22 Mass Spectrum (Top) and NIST Library Match (Bottom) for Anthracene. Plot Generated in NIST MS Search v2.3

There are some low abundance compounds that elute right below (earlier on the second column) the alkyl carbazole polygon. Figure 6.23 shows the mass spectrum for the blob at 72.956 minutes, 0.460 seconds and its match in the NIST Library 2-methylindole-3-carboxaldehyde. This series of compounds could result from the oxidation of indole compounds with a 2-methyl group. The 2-methyl position is prone to oxidation due to resonance stabilization after the loss of a hydrogen radical.

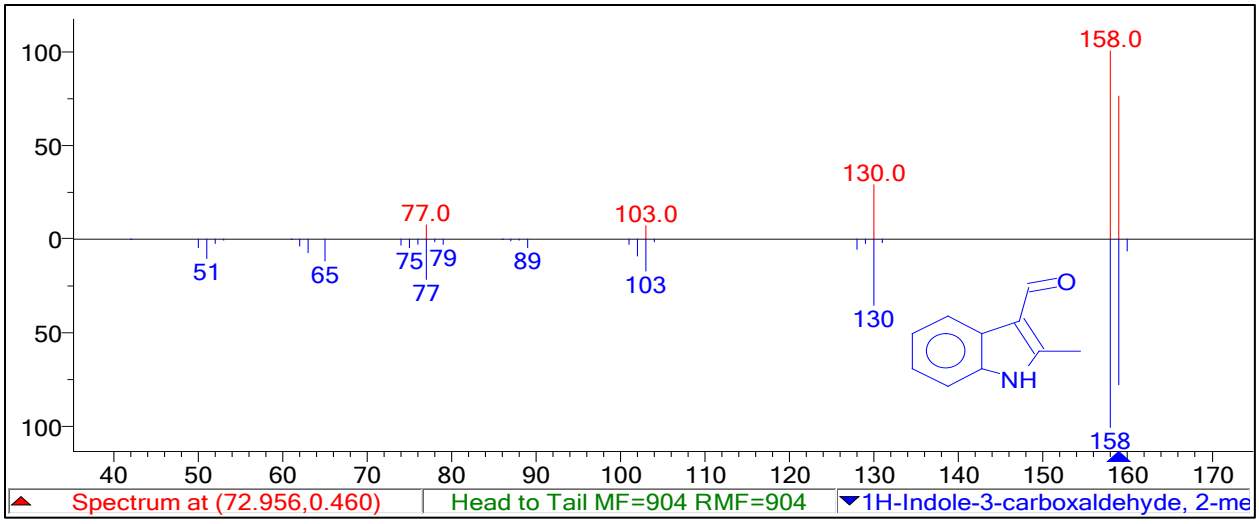

Figure 6.23 Mass Spectrum (Top) and NIST Library Match (Bottom) for 2-methylindole-3-carboxaldehyde. Plot Generated in NIST MS Search v2.3

DCM/MeOH Extract

Figure 6.24 is the RTICC for the GCxGC/MS analysis of the DCM/MeOH fraction utilizing electron ionization mode. The same process of identifying the compounds that are present in this extract as the toluene extract was used. First mass spectra were explored to get an understanding of the compounds present.

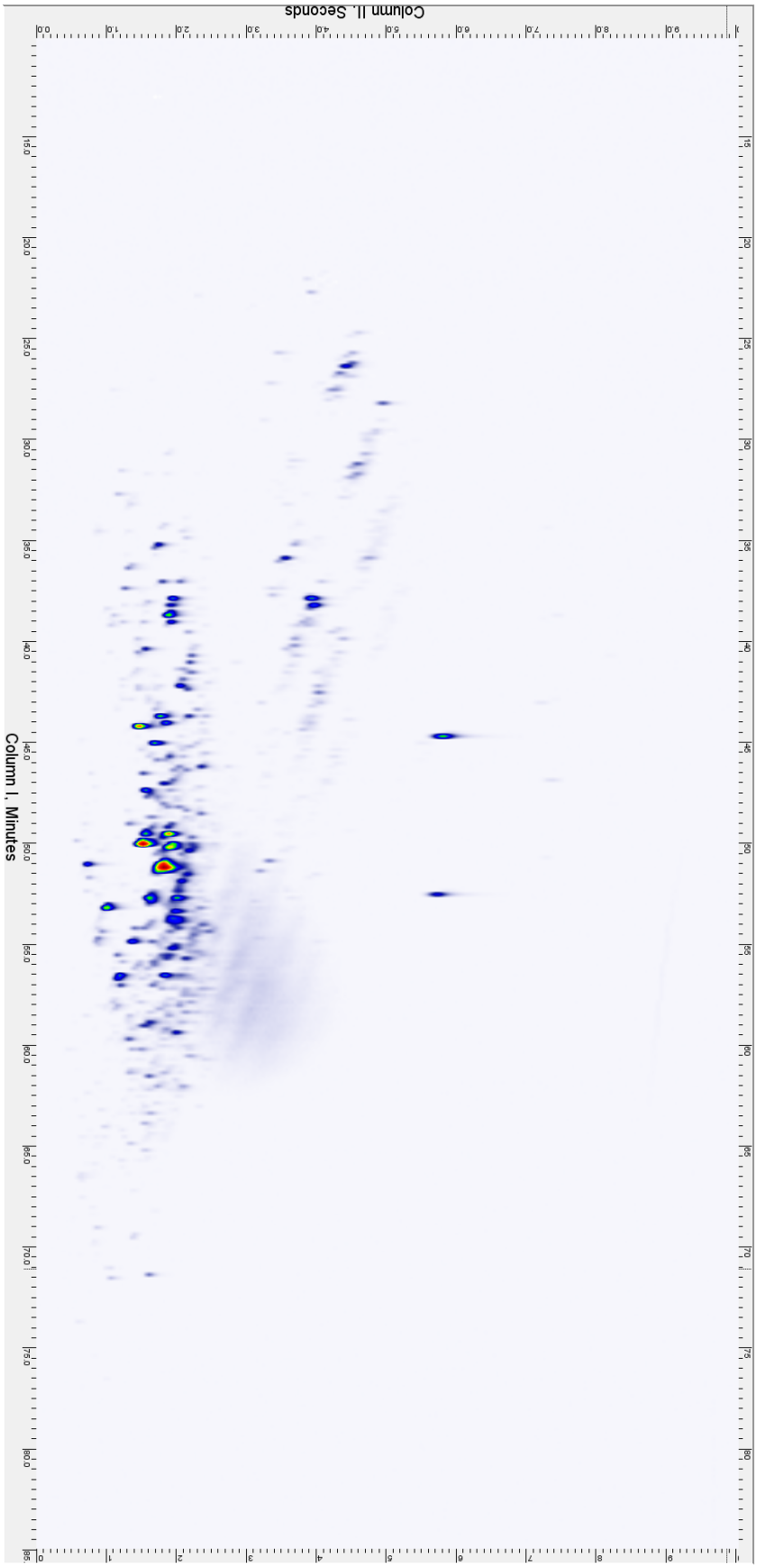

Figure 6.24 GCxGC/MS Electron ionization RTICC for the DCM/MeOH Extracted Fraction of Attapulgus Clay Used for Treating Jet Fuel

The most abundant compounds in this fraction appear to be isomers of two homologous series with the same general elemental compositions of $C_nH_{2n-7}N$. Alkyl tetrahydroquinolines were detected in the previous fraction and are also detected in this fraction. Figure 6.25 shows the mass spectrum for the blob at 49.949 minutes, 1.506 seconds and its NIST Library match 3-ethyl-5,6,7,8-tetrahydroquinoline.

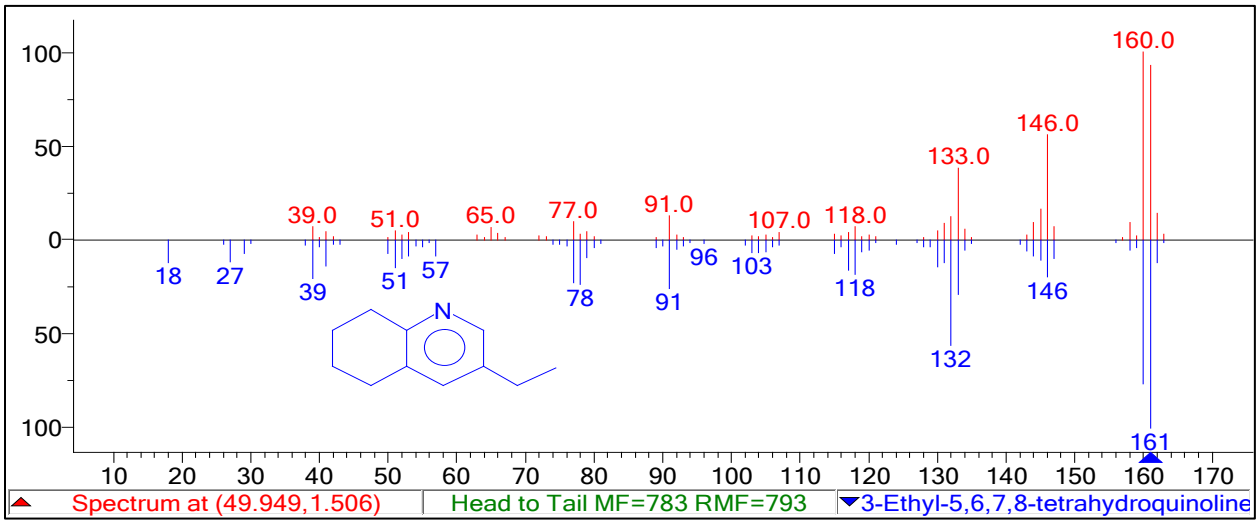

Figure 6.25 Mass Spectrum (Top) and NIST Library Match (Bottom) for 3-Ethyl-5,6,7,8-tetrahydroquinoline. Plot Generated in NIST MS Search v2.3

The other homologous series with the general elemental composition of $C_nH_{2n-7}N$ was alkyl tetrahydroisoquinolines. Figure 6.26 shows the mass spectrum for the blob at 50.116 minutes, 1.882 seconds and its NIST Library match 2,4,8-trimethyl-1,2,3,4-tetrahydroisoquinoline. Because both of these homologous series have the same general elemental composition, they will be indistinguishable when the polygons are

built. This could also be the case for other isomers of homologous series although this is the first case where it is directly observed.

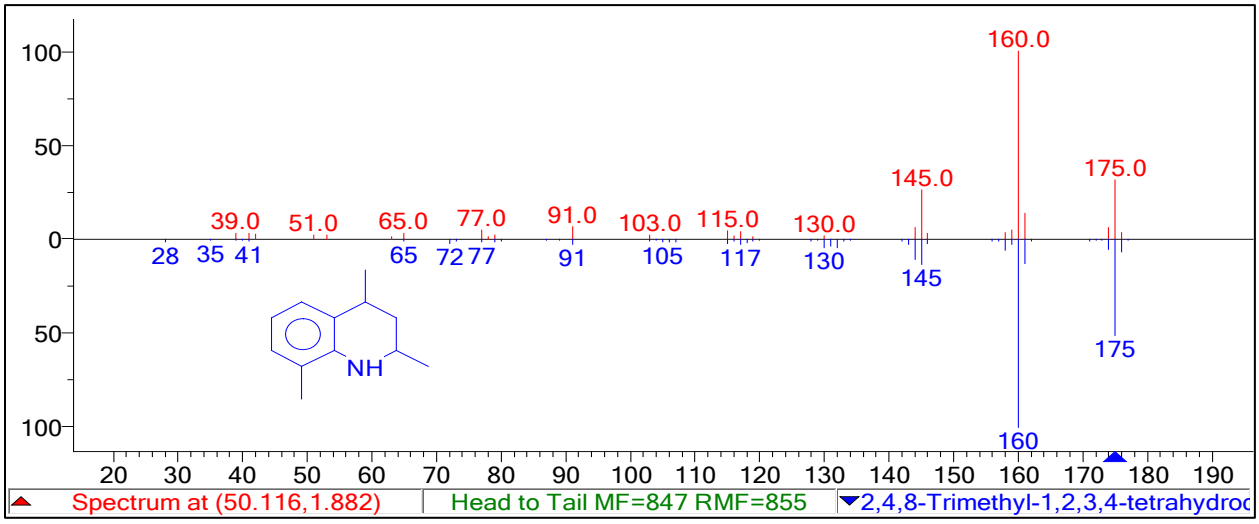

Figure 6.26 Mass Spectrum (Top) and NIST Library Match (Bottom) for 2,4,8-Trimethyl-1,2,3,4-tetrahydroisoquinoline. Plot Generated in NIST MS Search v2.3

A homologous series of alkyl aniline compounds is also detected in this fraction. Figure 6.27 shows the mass spectrum for the blob at 35.116 minutes, 1.757 seconds and its NIST Library match 2,4,6-trimethylaniline.

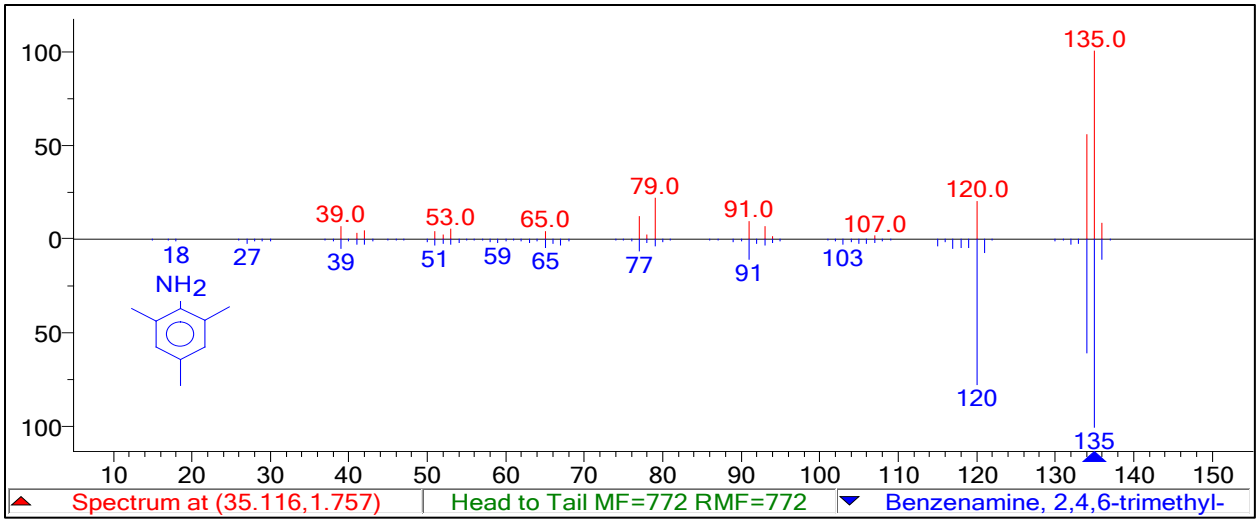

Figure 6.27 Mass Spectrum (Top) and NIST Library Match (Bottom) for 2,4,6-Trimethylaniline. Plot Generated in NIST MS Search v2.3

Alkyl indole compounds were also detected in this fraction. Figure 6.28 shows the mass spectrum for the blob at 53.116 minutes,1.004 seconds and its NIST Library match 2,6-dimethylindole.

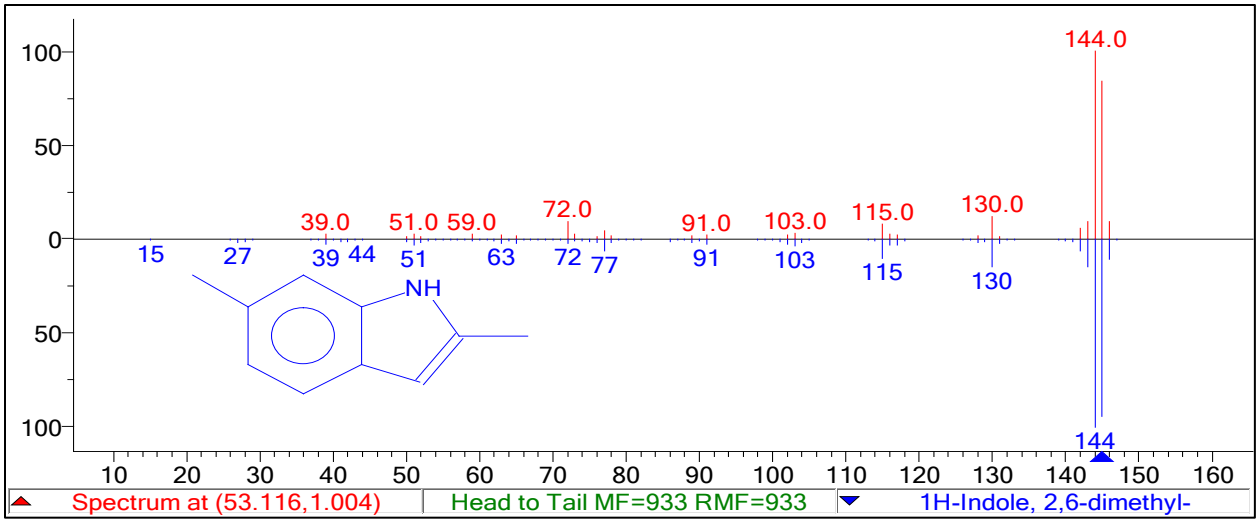

Figure 6.28 Mass Spectrum (Top) and NIST Library Match (Bottom) for 2,6-Dimethylindole. Plot Generated in NIST MS Search v2.3

There are two homologous series that have not been previously observed. Figure 6.29 shows the mass spectrum for the blob at 37.782 minutes, 3.973 seconds and its NIST Library match 3-butylindolizidine. A homologous series indolizidines have the general elemental composition of $C_nH_{2n-1}N$. The blobs for what appear to be the second homologous series have mass spectra that do not appear to have molecular ion peaks present, likely due to low abundance. The position of the homologous series fits a pattern that suggest the homologous series would have one less DBE which would make the general elemental composition $C_nH_{2n+1}N$.

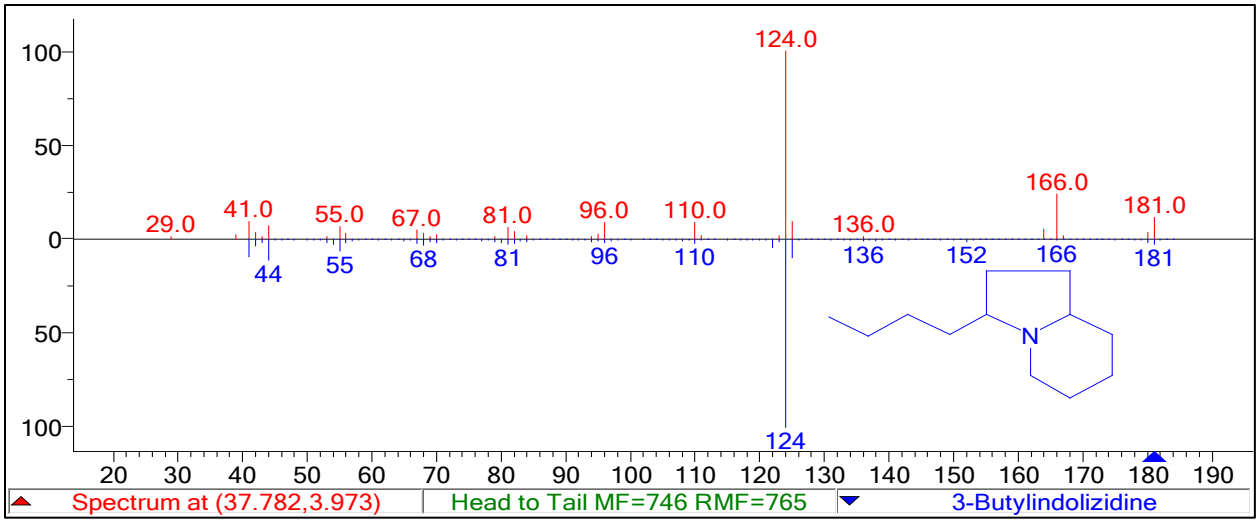

Figure 6.29 Mass Spectrum (Top) and NIST Library Match (Bottom) for 3-Butylindolizidine. Plot Generated in NIST MS Search v2.3

There are two distinct blobs have retention times of around 5.6 seconds on the second column. Figure 6.30 shows the mass spectrum for the blob at 44.616 minutes, 5.772 seconds and its NIST Library Match N,N-dimethyl-1-dodecanamine. The other is consistent with N,N-dimethyl-1-tetradecanamine.

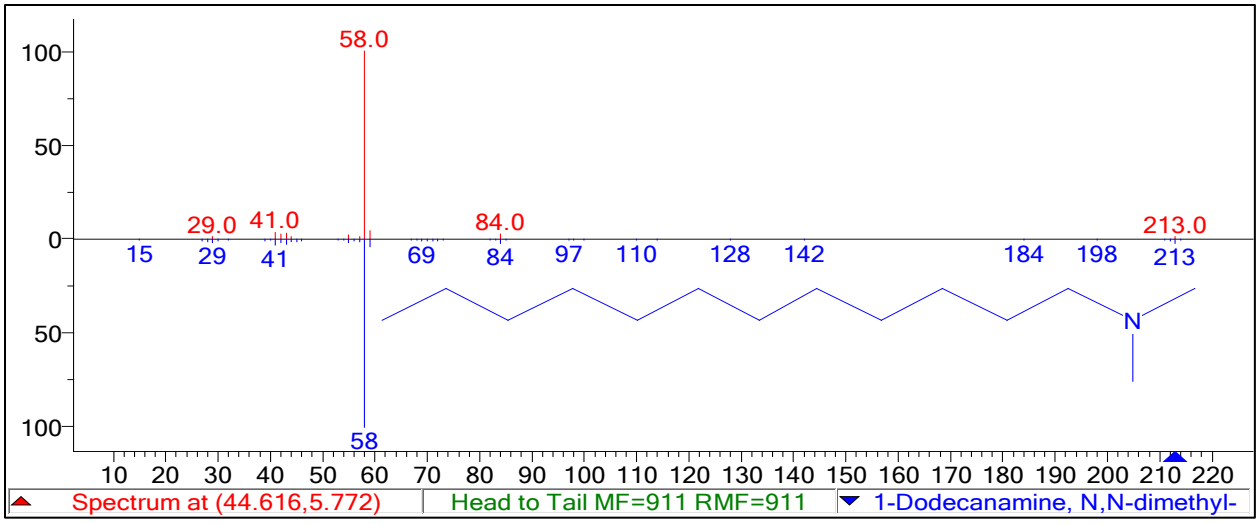

Figure 6.30 Mass Spectrum (Top) and NIST Library Match (Bottom) for N,N-Dimethyldodecanamine. Plot Generated in NIST MS Search v2.3

Figure 6.31 shows the RTICC with polygons added for the homologous series that have been previously discussed for this fraction.

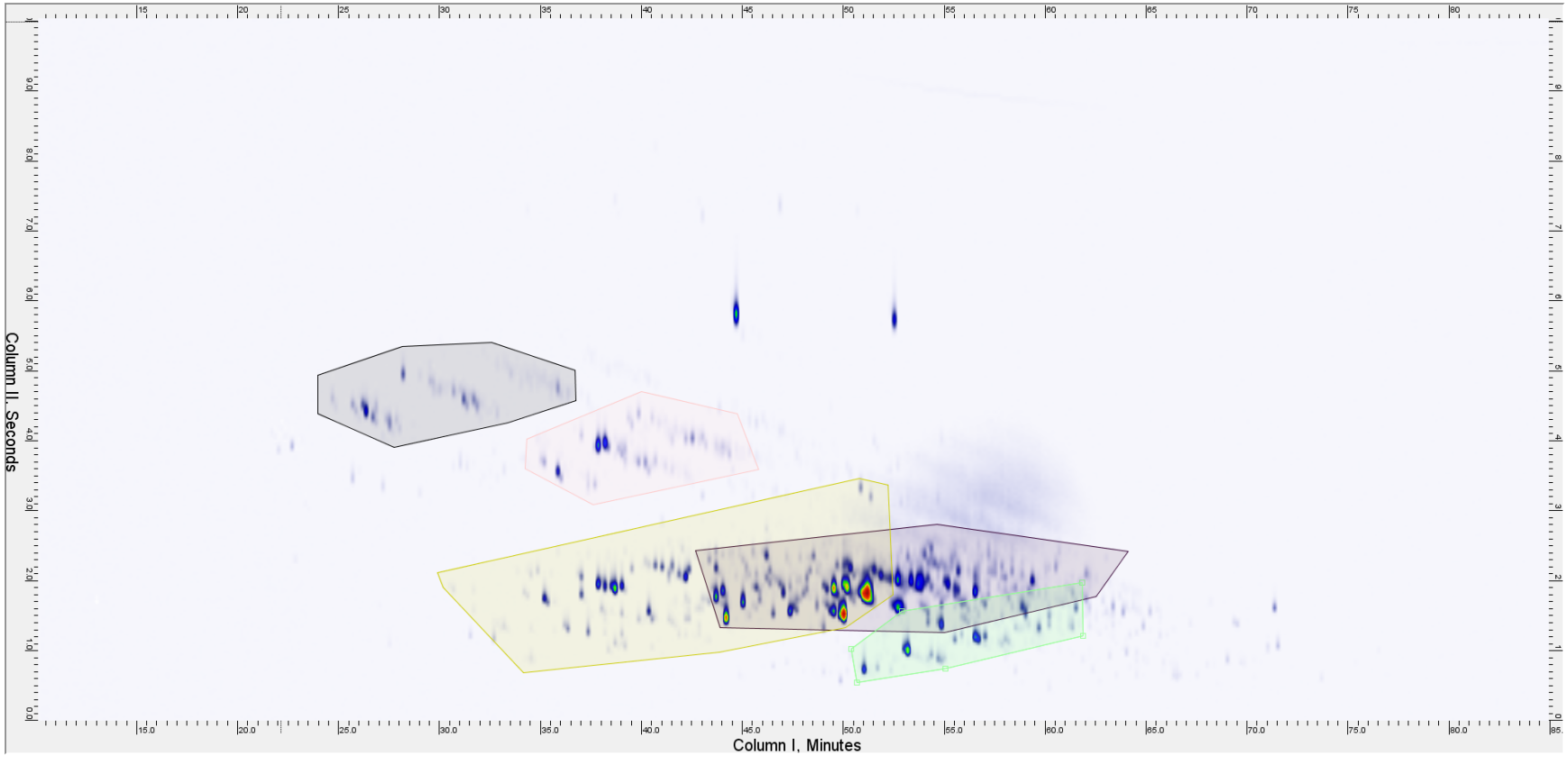

Figure 6.31 GCxGC/MS Electron ionization RTICC for the DCM/MeOH Extracted Fraction of Attapulgus Clay Used for Treating Jet Fuel. Yellow Polygons Highlight Alkyl Tetrahydroquinoline and Tetrahydroisoquinoline Compounds, Purple Highlights Alkyl Aniline Compounds, Green Polygon Highlights Alkyl Indoles, Peach Highlights Alkyl Indolizine Compounds and Black Highlights the Unknown Homologous Series

Figure 6.31 was created by drawing polygons around the EICs generated by extracting the tetrahydroquinoline and tetrahydroisoquinoline homologous series using the general elemental composition $C_nH_{2n-7}N$ from n = 6 to n = 12 with a mass tolerance of +/- 0.01 Da (shown in yellow), the alkyl indole homologous series using the general elemental composition $C_nH_{2n-9}N$ from n = 8 to n = 14 with a mass tolerance of +/- 0.01 Da (shown in green), the alkyl aniline homologous series using the general elemental composition $C_nH_{2n-5}N$ from n = 12 to n = 14 with a mass tolerance of +/- 0.01 Da (shown in purple), and homologous series consistent with the 3-butylindolizine compound detected using the general elemental composition $C_nH_{2n-1}N$ from n = 9 to n = 14 with a mass tolerance of +/- 0.01 Da (shown in peach). The images of the individual EICs can be found in Appendix B (Supplemental Figures 6.9-12). A polygon was drawn around the remaining homologous series that could not be extracted due to the lack of the molecular ion peak (shown in black). These blobs were not observed in the PI analysis due to low abundance therefore no additional information could be gained through that analysis. The two blobs at 44.616 minutes, 5.772 seconds minutes and 51.982 minutes, 5.632 seconds that are not annotated are the N,N-dimethylamine compounds.

As can be seen, there is some co-elution between the alkyl quinoline/alkyl isoquinoline, alkyl aniline, and alkyl indole homologous series. While it would be difficult to accurately quantitate the individual compounds or the homologous series a very good qualitative picture of the compounds present in this fraction is gained from this analysis.

MeOH Extract

Figure 6.32 is the RTICC for the GCxGC/MS analysis of the DCM/MeOH fraction utilizing electron ionization mode. All of the major peaks in this fraction are consistent with what was observed in the previous fraction. No new compounds or compound classes were observed in this analysis. It is likely that the DCM/MeOH solvent was strong enough to begin eluting the compounds that interacted with the clay the most strongly. There are slight variations in the relative intensities of the blobs compared to the previous fraction.

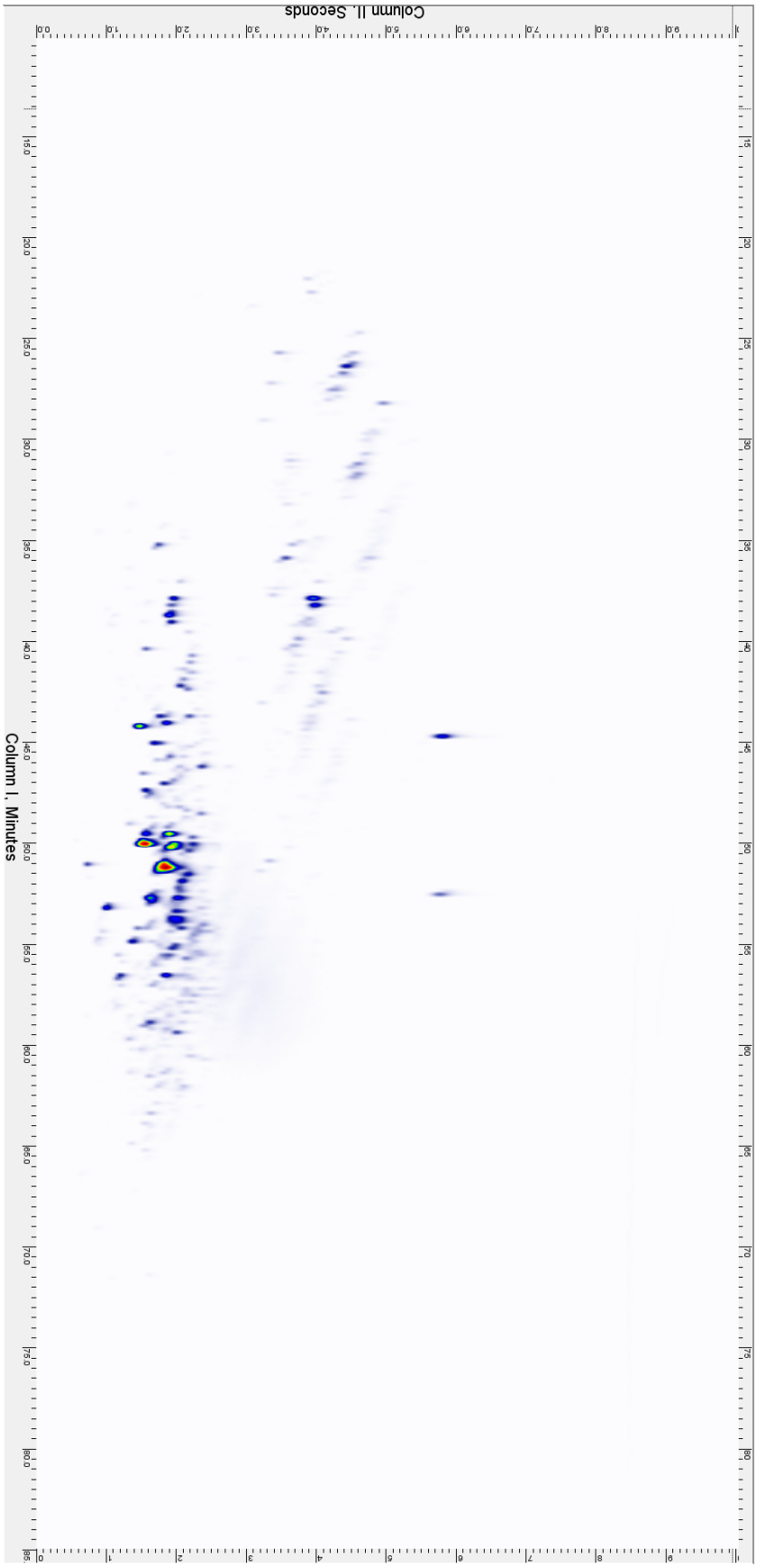

Figure 6.32 GCxGC/MS Electron ionization RTICC for the MeOH Extracted Fraction of Attapulgus Clay Used for Treating Jet Fuel

Figure 6.33 shows the RTICC with polygons added for the major homologous series identified in this fraction and is nearly identical to Figure 6.29. All the details for the generation of Figure 6.29 are the same for Figure 6.31.

The match factors for the compounds identified searching the EI spectra in the NIST17 library range from the mid-700s to the low-900s. In general, the higher the match factor, the more similar the spectra are. Visual inspection of the spectra coupled with the chemical identities of the matches, along with calculated elemental compositions from accurate masses leading to elemental composition matches, show the suggested matches to be reasonable. There are a number of different reasons for the variability in the match factors.[42, 64] The JEOL instrument's ion source configuration is more open than many other instruments. The ion body is not closed due to the use of the photoionization source which requires a window to allow the photons to enter. This along with differences in tuning parameters between instruments may affect the ratios of ion intensities which will in turn could lower the match factors.[42, 64]

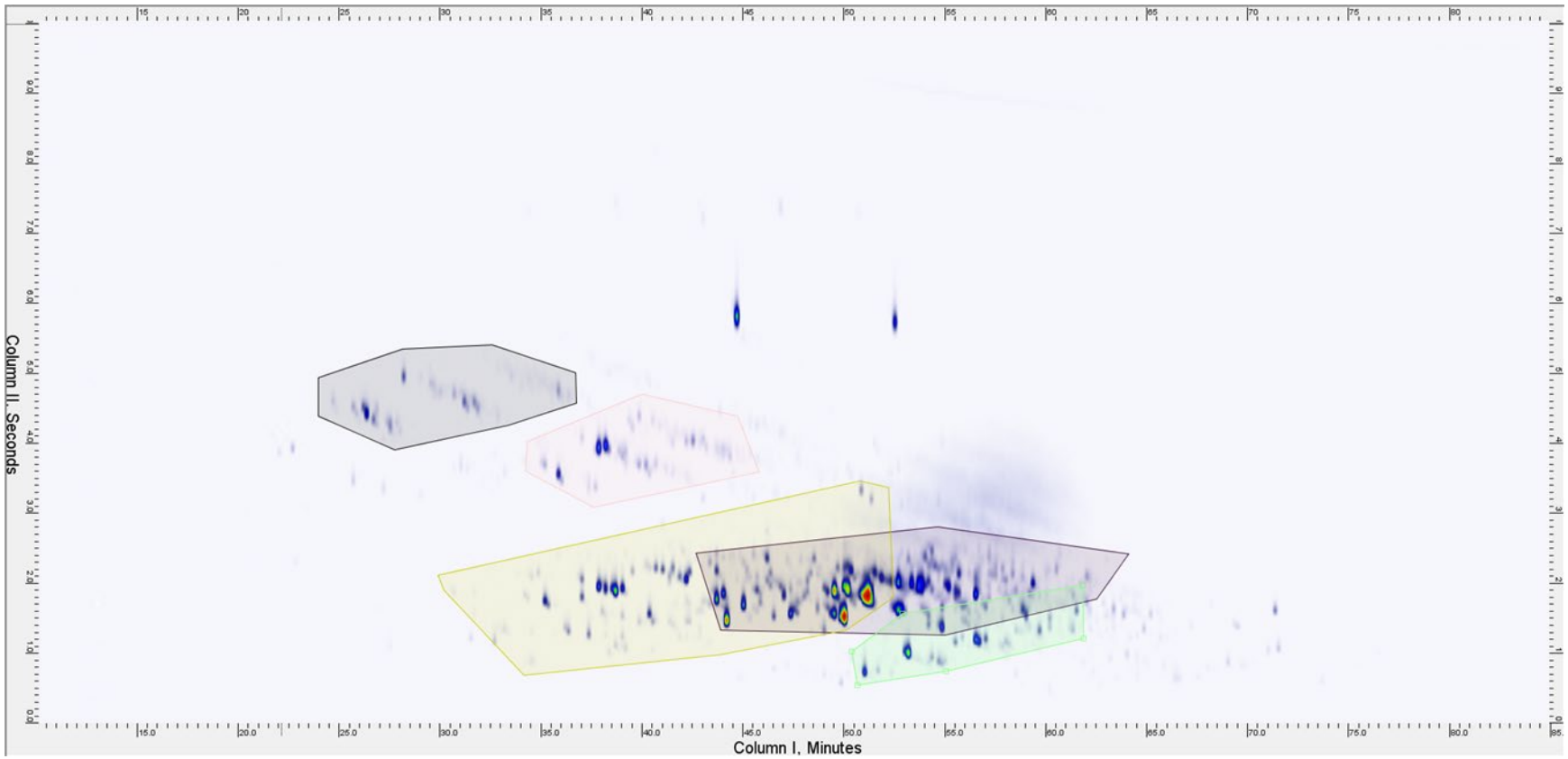

Figure 6.33 GCxGC/MS Electron ionization RTICC for the MeOH Extracted Fraction of Attapulgus Clay Used for Treating Jet Fuel. Yellow Polygons Highlight Alkyl Tetrahydroquinoline and Tetrahydroisoquinoline Compounds, Purple Highlights Alkyl Aniline Compounds, Green Polygon Highlights Alkyl Indoles, Peach Highlights Alkyl Indolizine Compounds and Black Highlights the Unknown Homologous Series

Chapter 7 : Summary and Conclusions from Results

Molecules containing sulfur, nitrogen, and oxygen have been shown to negatively impact the thermal oxidative stability of jet fuels. It was the goal of the research presented here to develop and apply new analytical methodologies for the analysis of jet fuels and related samples in order to further the understanding of the molecules involved in thermal oxidative deposition and ASTM D3241 failures. Positive ion and negative ion mode ESI LC/MS methods were developed. In the first set of experiments, jet fuels with varying thermal oxidative stabilities as measured by ASTM D3241 were analyzed by the LC/MS methods. The resulting data underwent statistical analysis to allow for the determination of compounds significant to poor thermal oxidative stability. In the next set of experiments, the LC/MS methods were applied to the analysis of jet fuels before and after thermal oxidative stressing in a QCM reactor. The data were analyzed once again using statistics for differential analysis to identify the significant changes in the fuels. It was observed that appreciable deposits formed in the QCM reactor for a number of fuels and it was possible to collect the deposits for further analysis. A pyrolysis GC/MS method was developed to allow for the analysis of the molecular composition of thermal oxidative deposits which provides insight into the molecules involved in forming deposits. Finally, to understand the types of polar molecules that are removed by Attapulgus clay, which often improves the thermal oxidative stability of jet fuels during refining, a GCxGC/MS method was developed and applied to the analysis of extracts from Attapulgus clay that had been used in a refinery.

The statistical analysis of mass spectral data generated from the LC/MS analysis of jet fuels with varying thermal oxidative stabilities yielded insights into compounds that are significant to poor thermal oxidative stability as measured by ASTM D3241. Utilizing data from LC/MS with ESI in positive ion mode, the statistical analysis identified a number of different significant series of compounds. Alkyl phenols, alkyl indoles, basic nitrogen compounds (alkyl anilines/pyridines, alkyl indolines, and alkyl quinolines), and oxides of sulfur and nitrogen containing compounds were shown to be significantly higher in fuels that performed poorly by ASTM D3241. Statistical analysis of data from LC/MS with ESI in negative ion mode once again identified alkyl phenols but also identified compounds with two oxygens that could be consistent with acidic oxidation products.

Applying statistical analysis to the data from the LC/MS methods for fuel samples before and after thermal oxidative stressing in the QCM reactor provided further evidence for the involvement of the compounds previously identified to be significant to poor thermal oxidative stability. It was observed that alkyl phenols, alkyl indoles, and basic nitrogen compounds decrease in abundance after thermal oxidative stressing in the QCM reactor. This suggests that they are consumed during oxidation/deposition and reinforces the fact that they are significant precursors to poor thermal oxidative stability and thermal oxidative deposition. Compounds consistent with the oxidation of sulfur and nitrogen containing compounds were shown to increase after thermal oxidative stressing in the QCM reactor. Although this does not directly imply that these compounds are involved in forming thermal oxidative deposits, because they were identified as significant in the previous set of experiments, it shows that they are

somehow related to the oxidation of the fuels which is related to its thermal oxidative stability.

Pyrolysis GC/MS of thermal oxidative deposits that formed in the QCM reactor allowed for the determination of molecular components that are incorporated into the deposits. Consistent with the previous analyses, major peaks in the reconstructed total ion current chromatograms of the pyrolysate were identified as alkyl phenols and basic nitrogen compounds (pyridines, anilines, and quinolines). There were trace peaks identified as alkyl indoles. Additionally, there was a peak consistent with the evolution of sulfur dioxide gas suggesting that oxidized sulfur molecules were incorporated into the deposits. There were two significant peaks in most of the deposit pyrolysate RTICCs that were not present in the NIST17 library. From the mass spectra, it appears that the compounds contain an odd number of nitrogen atoms.

Extraction of Attapulgus clay used to treat jet fuel in a refinery and analysis of the fractions by GCXGC/MS offered a different perspective on the types of polar heteroatom-containing molecules present in jet fuel. A series of solvents of increasing polarity were used to extract the clay; hexane, toluene, DCM, DCM:MeOH, and methanol. The hexane fraction was mostly composed of hydrocarbon molecules. The toluene fraction had some hydrocarbons but was composed primarily of alkyl phenols, alkyl indoles, and alkyl carbazoles. Additionally, there were compounds in this fraction that had EI mass spectra consistent with the unidentified peaks in the RTICCs from the pyrolysates of the deposits. Given the accurate mass capability of the mass spectrometer in this analysis, it was possible to generate elemental compositions for the molecular ions which eventually led to the identification of likely structures for the two

compounds which appear to be basic amines. The DCM fraction also contained alkyl phenols, alkyl indoles, and alkyl carbazoles. Additionally, there were tetrahydroquinolines present in this sample. The DCM:MeOH and methanol fractions were nearly identical to each other. They contained alkyl indole, alkyl tetrahydroquinoline, alkyl tetrahydroisoquinoline, a homologous series consistent with alkyl indolizidines, and aliphatic amines.

Many compounds are identified across a number of the different analyses reported here. For example, 2,5-dimethylphenol was shown to be significantly higher in abundance in fuels with poor ASTM D3241 thermal oxidative stability. It was also identified as decreasing in abundance after thermal oxidative stressing in a QCM reactor. Pyrolysis GC/MS identified it as a major component of the QCM thermal oxidative deposits (denoted as C2 phenol). It was also identified in the homologous series of alkyl phenols. This exercise can be done for basic nitrogen compounds, indoles, and carbazoles. Some of the compounds are only identified in two or three of the different experiments. However, identifying these compounds across multiple different analyses adds confidence to the significance of their involvement in causing poor thermal oxidative stability.

It would be advantageous to have more information on the sulfur compounds involved in the formation of deposits. There has been evidence for the SMORS model which does not need sulfur compounds reported in Chapter 3. However, the pyrolysis GC/MS data suggest that in many cases sulfur is involved, and the deposition process is likely going through a different pathway, similar to what is shown in Figure 1.4. It has been reported that reactive sulfur species such as mercaptans, sulfides, and disulfides

are involved in thermal oxidative deposition. The analyses utilized here were not able to identify these compounds directly in the fuels. Having data on these compounds would offer additional insight into their effect on thermal oxidative stability.

References

1. ASTM International, ASTM D1655-18, Standard Specification for Aviation Turbine Fuels. West Conshohocken, PA, 2018.

2. Defence Standard, 91-91. *Turbine Fuel, Aviation Kerosene Type, Jet A-1 NATO Code: F-35 Joint Service Designation: AVTUR (18 2011)* **2015**.

3. Hemighaus, G.; Boval, T.; Bacha, J.; Barnes, F.; Franklin, M.; Gibbs, L.; Hogue, N.; Jones, J.; Lesnini, D.; Lind, J., Aviation fuels technical review. *Chevron Corporation* **2006**.

4. ASTM International, ASTM D3241-18, Standard Test Method for Thermal Oxidation Stability of Aviation Turbine Fuels. West Conshohocken, PA, 2018.

5. Hazlett, R. N., *Thermal oxidation stability of aviation turbine fuels*. ASTM International: West Conshohocken, PA, 1991.

6. Mushrush, G. W.; Beal, E. J.; Slone, E.; Hardy, D. R., Reaction of Organosulfur Compounds with Naturally Occurring Peroxides in Jet Fuel. *Energy & Fuels* **1996,** *10* (2), 504-508.

7. West, Z., Linda Shafer, Rich Striebich, Steve Zabarnic In *Investigations of Poor Thermal Stability Behavior Exhibited in US Jet Fuels*, DLA Worldwide Energy Conference, National Harbor, MD, National Harbor, MD, 2017.

8. Balster, L. M.; Zabarnick, S.; Striebich, R. C.; Shafer, L. M.; West, Z. J., Analysis of Polar Species in Jet Fuel and Determination of Their Role in Autoxidative Deposit Formation. *Energy & Fuels* **2006,** *20* (6), 2564-2571.

9. Sobkowiak, M.; Griffith, J. M.; Wang, B.; Beaver, B., Insight into the Mechanisms of Middle Distillate Fuel Oxidative Degradation. Part 1: On the Role of Phenol, Indole,

and Carbazole Derivatives in the Thermal Oxidative Stability of Fischer−Tropsch/Petroleum Jet Fuel Blends. *Energy & Fuels* **2009,** *23* (4), 2041-2046.

10. Zabarnick, S.; West, Z.; Kuprowicz, N.; Balster, L.; Ervin, J.; Minus, D.; Striebich, R. In *Measurement of key species and development of a chemical kinetic model toward the prediction of jet fuel thermal stability*, International Association for Stability, Handling and Use of Liquid Fuels, Inc.: 2006; pp 215-229.

11. Kabana, C. G.; Botha, S.; Schmucker, C.; Woolard, C.; Beaver, B., Oxidative stability of middle distillate fuels. Part 1: Exploring the soluble macromolecular oxidatively reactive species (SMORS) mechanism with jet fuels. *Energy & Fuels* **2011,** *25* (11), 5145-5157.

12. Mushrush, G. W., Fuel instability. 1. Organo-sulfur hydroperoxide reactions. *Fuel Sci. Technol. Int.* **1992,** *10* (9), 1523-60.

13. Rawson, P. M.; Webster, R. L.; Evans, D.; Abanteriba, S., Contribution of sulfur compounds to deposit formation in jet fuels at 140 °C using a quartz crystal microbalance technique. *Fuel* **2018,** *231*, 1-7.

14. Coordinating Research, C., *Handbook of aviation fuel properties*. 2014.

15. Pillon, L. Z., Effect of clays and adsorbents on the nitrogen content and the stability of jet fuels. *Pet. Sci. Technol.* **2001,** *19* (7 & 8), 961-970.

16. Morris, R. E.; Turner, N. H., Influences exerted by metal deactivator on the thermal stability of aviation fuel in the presence of copper. *Fuel Sci. Technol. Int.* **1990,** *8* (4), 327-50.

17. Abdallah, D. J.; Kreno, L. E.; Thompson, K. E.; Gaughan, R. G.; Hoskin, D. H. In *Impact of additives on jet fuel thermal stability*, International Association for Stability, Handling and Use of Liquid Fuels, Inc.: 2013; pp 1-6.

18. Shafer, L.; Striebich, R.; Zabarnick, S.; West, Z. In *Identification and quantitation of polar species in liquid transportation fuels by GCxGC*, The 14th International Symposium on Stability, Handling, and Use of Liquid Fuels, Charleston, South Carolina, Charleston, South Carolina, 2015.

19. Webster, R. L.; Rawson, P. M.; Kulsing, C.; Evans, D. J.; Marriott, P. J., Investigation of the Thermal Oxidation of Conventional and Alternate Aviation Fuels with Comprehensive Two-Dimensional Gas Chromatography Accurate Mass Quadrupole Time-of-Flight Mass Spectrometry. *Energy & Fuels* **2017,** *31* (5), 4886-4894.

20. ASTM International, ASTM D7739-11, Standard Practice for Thermal Oxidative Stability Measurement via Quartz Crystal Microbalance. West Conshohocken, PA, 2016.

21. Hardy, D. R.; Wechter, M. A., Characterization of soluble macromolecular oxidatively reactive species (SMORS) from middle distillate diesel fuels: Their origin and role in instability. *PREPRINTS OF PAPERS-AMERICAN CHEMICAL SOCIETY DIVISION FUEL CHEMISTRY* **1994,** *39*, 912-912.

22. Beaver, B.; Gao, L.; Burgess-Clifford, C.; Sobkowiak, M., On the mechanisms of formation of thermal oxidative deposits in jet fuels. Are unified mechanisms possible for both storage and thermal oxidative deposit formation for middle distillate fuels? *Energy & Fuels* **2005,** *19* (4), 1574-1579.

23. Christison, K. M.; Lorenz, R. M.; Xue, L.; Sparkman, O. D., Exploring the Molecular Origin of Jet Fuel Thermal Oxidative Instability through Statistical Analysis of Mass Spectral Data. *Energy & Fuels* **2019,** *33* (2), 830-836.

24. Balster, L. M.; Zabarnick, S.; Striebich, R. C., Division of polar species in jet fuel by their relative polarity and molecule types, and possible implications of these sub-classes on jet fuel thermal stability. *Prepr. - Am. Chem. Soc., Div. Pet. Chem.* **2004,** *49* (4), 477-480.

25. Kuprowicz, N. J.; Zabarnick, S.; West, Z. J.; Ervin, J. S., Use of measured species class concentrations with chemical kinetic modeling for the prediction of autoxidation and deposition of jet fuels. *Energy & fuels* **2007,** *21* (2), 530-544.

26. Kauffman, R. E., The effects of different sulfur compounds on jet fuel oxidation and deposition. *J. Eng. Gas Turbines Power* **1997,** *119* (2), 322-327.

27. Ben Amara, A.; Kaoubi, S.; Starck, L., Toward an optimal formulation of alternative jet fuels: Enhanced oxidation and thermal stability by the addition of cyclic molecules. *Fuel* **2016,** *173* (Supplement C), 98-105.

28. ASTM International, ASTM D7566-19 Standard Specification for Aviation Turbine Fuel Containing Synthesized Hydrocarbons. ASTM International: West Conshohocken, PA, 2019.

29. DeWitt, M. J.; West, Z.; Zabarnick, S.; Shafer, L.; Striebich, R.; Higgins, A.; Edwards, T., Effect of Aromatics on the Thermal-Oxidative Stability of Synthetic Paraffinic Kerosene. *Energy & Fuels* **2014,** *28* (6), 3696-3703.

30. Mushrush, G. W.; Beal, E. J.; Hughes, J. M.; Bonde, S. E.; Gore, W. L.; Dolbear, G. E., Stability studies of a jet fuel containing no organo-sulfur compounds. *Pet. Sci. Technol.* **2002,** *20* (5 & 6), 561-570.

31. Hartough, H. D.; Meisel, S. L., *Compounds with Condensed Thiophene Rings*. Interscience Pubs.: 1954; p 632 pp.

32. Kulsing, C.; Rawson, P.; Webster, R. L.; Evans, D. J.; Marriott, P. J., Group-Type Analysis of Hydrocarbons and Sulfur Compounds in Thermally Stressed Merox Jet Fuel Samples. *Energy & Fuels* **2017,** *31* (9), 8978-8984.

33. Hock, H.; Lang, S., Autoxydation von Kohlenwasserstoffen, IX. Mitteil.: Über Peroxyde von Benzol-Derivaten. *Berichte der deutschen chemischen Gesellschaft (A and B Series)* **1944,** *77* (3-4), 257-264.

34. van Bergen, L. A. H.; Roos, G.; De Proft, F., From Thiol to Sulfonic Acid: Modeling the Oxidation Pathway of Protein Thiols by Hydrogen Peroxide. *The Journal of Physical Chemistry A* **2014,** *118* (31), 6078-6084.

35. Brown, W. H.; Iverson, B. L.; Anslyn, E.; Foote, C. S., *Organic Chemistry*. Cengage Learning: 2013.

36. ASTM International, ASTM D4294-16e1, Standard Test Method for Sulfur in Petroleum and Petroleum Products by Energy Dispersive X-ray Fluorescence Spectrometry. West Conshohocken, PA, 2016.

37. ASTM International, UOP163-10, Hydrogen Sulfide and Mercaptan Sulfur in Liquid Hydrocarbons by Potentiometric Titration. West Conshohocken, PA, 2010.

38. ASTM International, ASTM D4629-17, Standard Test Method for Trace Nitrogen in Liquid Hydrocarbons by Syringe/Inlet Oxidative Combustion and Chemiluminescence Detection. West Conshohocken, PA, 2017.

39. ASTM International, UOP269-10, Nitrogen Bases in Hydrocarbons by Potentiometric Titration. West Conshohocken, PA, 2010.

40. ASTM International, UOP1005-14, Trace Metals in Organics by ICP-MS. West Conshohocken, PA, 2014.

41. Budzikiewicz, H.; Djerassi, C.; Williams, D. H., Mass spectrometry of organic compounds. **1964**.

42. Watson, J. T.; Sparkman, O. D., *Introduction to mass spectrometry: instrumentation, applications, and strategies for data interpretation*. John Wiley & Sons: 2007.

43. Worton, D. R.; Zhang, H.; Isaacman-VanWertz, G.; Chan, A. W. H.; Wilson, K. R.; Goldstein, A. H., Comprehensive Chemical Characterization of Hydrocarbons in NIST Standard Reference Material 2779 Gulf of Mexico Crude Oil. *Environmental Science & Technology* **2015,** *49* (22), 13130-13138.

44. Lorentz, C.; Laurenti, D.; Zotin, J. L.; Geantet, C., Comprehensive GC×GC chromatography for the characterization of sulfur compound in fuels: A review. *Catalysis Today* **2017,** *292*, 26-37.

45. Coordinating Research Council, I. *Review of Existing Test Methods Used for Aviation Jet Fuel and Additive Property Evaluations with Respect to Alternative Fuel Compositions*; May 2018, 2018.

46. Zabarnick, S., Studies of jet fuel thermal stability and oxidation using a quartz crystal microbalance and pressure measurements. *Industrial & engineering chemistry research* **1994,** *33* (5), 1348-1354.

47. Martin, S. J.; Granstaff, V. E.; Frye, G. C., Characterization of a quartz crystal microbalance with simultaneous mass and liquid loading. *Analytical chemistry* **1991,** *63* (20), 2272-2281.

48. Adams, R. K.; Zabarnick, S.; West, Z. J.; Striebich, R. C.; Johnson, D. W., Chemical Analysis of Jet Fuel Polar, Heteroatomic Species via High-Performance Liquid Chromatography with Electrospray Ionization–Mass Spectrometric Detection. *Energy & Fuels* **2013,** *27* (5), 2390-2398.

49. Jansen, R.; Lachatre, G.; Marquet, P., LC-MS/MS systematic toxicological analysis: Comparison of MS/MS spectra obtained with different instruments and settings. *Clin. Biochem.* **2005,** *38* (4), 362-372.

50. Lane, D., Online statistics education: a multimedia course of study (http://onlinestatbook. com/). *Rice University* **2006**.

51. Sander, Z. H.; West, Z. J.; Ervin, J. S.; Zabarnick, S., Experimental and Modeling Studies of Heat Transfer, Fluid Dynamics, and Autoxidation Chemistry in the Jet Fuel Thermal Oxidation Tester (JFTOT). *Energy & Fuels* **2015,** *29* (11), 7036-7047.

52. Gandarias, I.; Barrio, V. L.; Requies, J.; Arias, P. L.; Cambra, J. F.; Güemez, M. B., From biomass to fuels: Hydrotreating of oxygenated compounds. *International Journal of Hydrogen Energy* **2008,** *33* (13), 3485-3488.

53. Dahl, I. M.; Tangstad, E.; Mostad, H. B.; Andersen, K., Effect of Hydrotreating on Catalytic Cracking of a VGO. *Energy & Fuels* **1996,** *10* (1), 85-90.

54. Kiontke, A.; Oliveira-Birkmeier, A.; Opitz, A.; Birkemeyer, C., Electrospray Ionization Efficiency Is Dependent on Different Molecular Descriptors with Respect to Solvent pH and Instrumental Configuration. *PLoS One* **2016,** *11* (12), e0167502-e0167502.

55. Link, D. D.; Baltrus, J. P.; Rothenberger, K. S.; Zandhuis, P.; Minus, D. K.; Striebich, R. C., Class- and Structure-Specific Separation, Analysis, and Identification Techniques for the Characterization of the Sulfur Components of JP-8 Aviation Fuel. *Energy & Fuels* **2003,** *17* (5), 1292-1302.

56. Thurman, E. M., Solid-phase extraction: principles and practice. *Chemical analysis; 147* **1998**.

57. Pollo, B. J.; Alexandrino, G. L.; Augusto, F.; Hantao, L. W., The impact of comprehensive two-dimensional gas chromatography on oil & gas analysis: Recent advances and applications in petroleum industry. *TrAC, Trends Anal. Chem.* **2018,** *105*, 202-217.

58. van der Westhuizen, R.; Ajam, M.; De Coning, P.; Beens, J.; de Villiers, A.; Sandra, P., Comprehensive two-dimensional gas chromatography for the analysis of synthetic and crude-derived jet fuels. *J. Chromatogr. A* **2011,** *1218* (28), 4478-4486.

59. Potgieter, H.; Bekker, R.; Beigley, J.; Rohwer, E., Analysis of oxidised heavy paraffininc products by high temperature comprehensive two-dimensional gas chromatography. *J Chromatogr A* **2017,** *1509*, 123-131.

60. Olivero, J.; Gracia, T.; Payares, P.; Vivas, R.; Diaz, D.; Daza, E.; Geerlings, P., Molecular structure and gas chromatographic retention behavior of the components of ylang-ylang oil. *J. Pharm. Sci.* **1997,** *86* (5), 625-630.

61. Shive, B.; Roberts, S. M.; Mahan, R. I.; Bailey, J. R., The Nitrogen Compounds in Petroleum Distillates. XXIII. The Structure of a C16H25N Base from California Petroleum1. *Journal of the American Chemical Society* **1942,** *64* (4), 909-912.

62. Poth, E.; Schulze, W.; King, W.; Thompson, W.; Slagle, W.; Floyd, W.; Bailey, J., AN INVESTIGATION OF THE BASES IN THE KEROSENE DISTILLATE OF CALIFORNIA PETROLEUM1. *Journal of the American Chemical Society* **1930,** *52* (3), 1239-1250.

63. Brandt, R. L., The Edeleanu Process for Refining Petroleum1. *Industrial & Engineering Chemistry* **1930,** *22* (3), 218-223.

64. Stein, S., Mass spectral reference libraries: an ever-expanding resource for chemical identification. ACS Publications: 2012.

APPENDIX A: Extra Charts from Mass Profiling

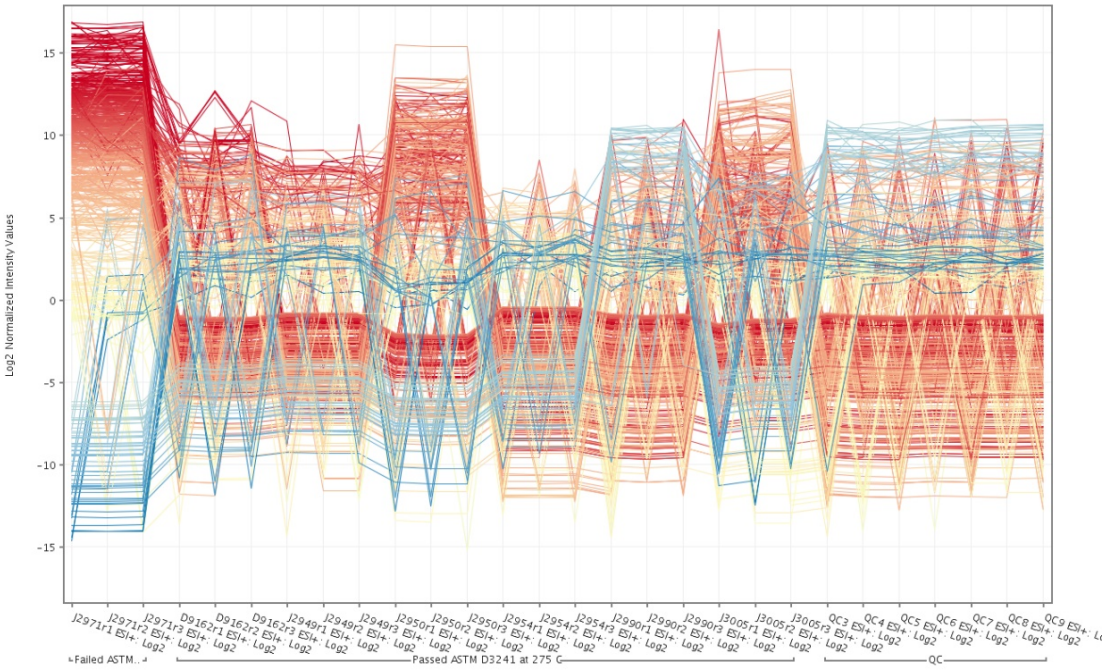

Supplemental Figure 3.1. Log 2 normalized intensity values of remaining entities after Filter by Frequency (entities must occur in 100% of samples in at least 1 condition) for positive ion ESI.

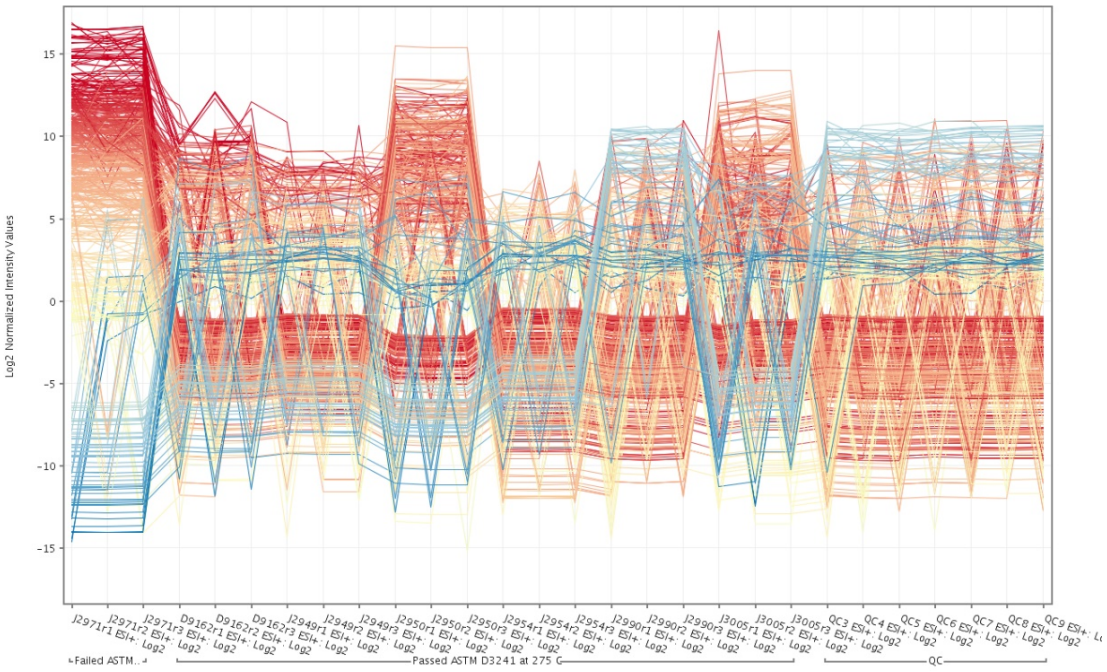

Supplemental Figure 3.2. Log 2 normalized intensity values of remaining entities after Filter by Variability (coefficient of variation ≥ 25%) for positive ion ESI.

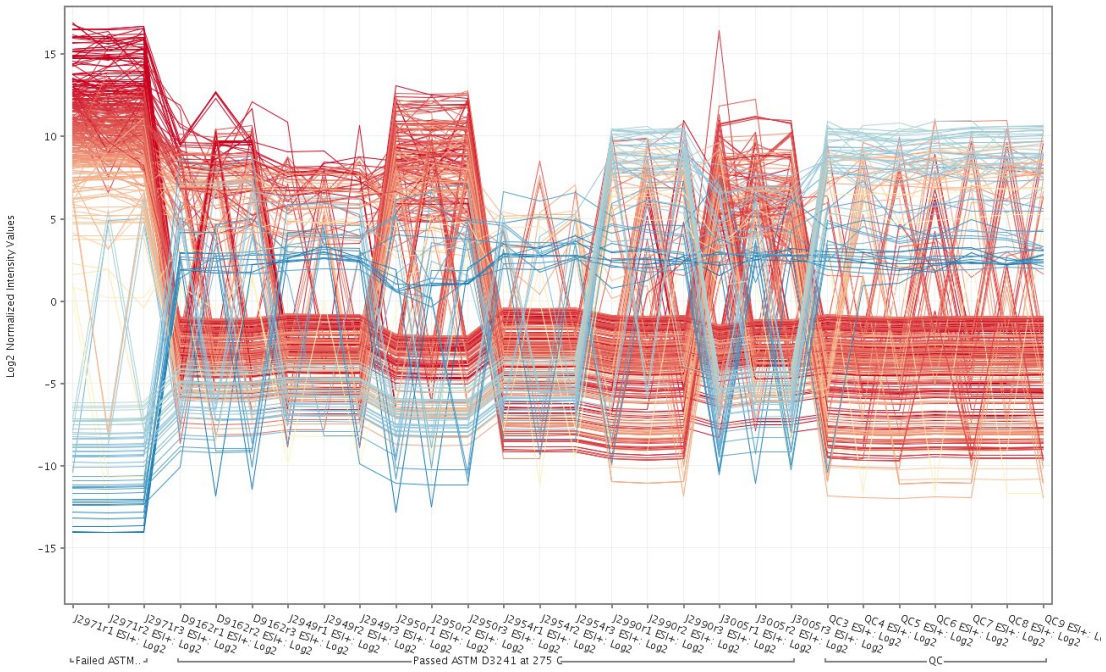

Supplemental Figure 3.2. Log 2 normalized intensity values of remaining entities after Filter by Variability (coefficient of variation ≥ 25%) for positive ion ESI.

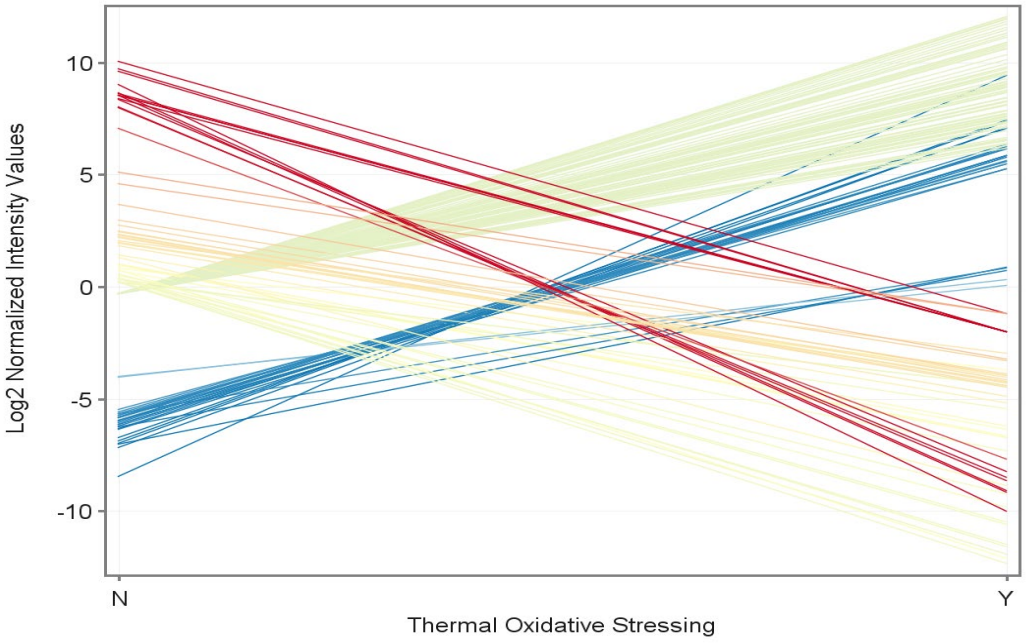

Supplemental Figure 4.1. Log 2 normalized intensity value of entities remaining after moderated T-test in J3192 comparing before and after TOS with positive ion ESI.

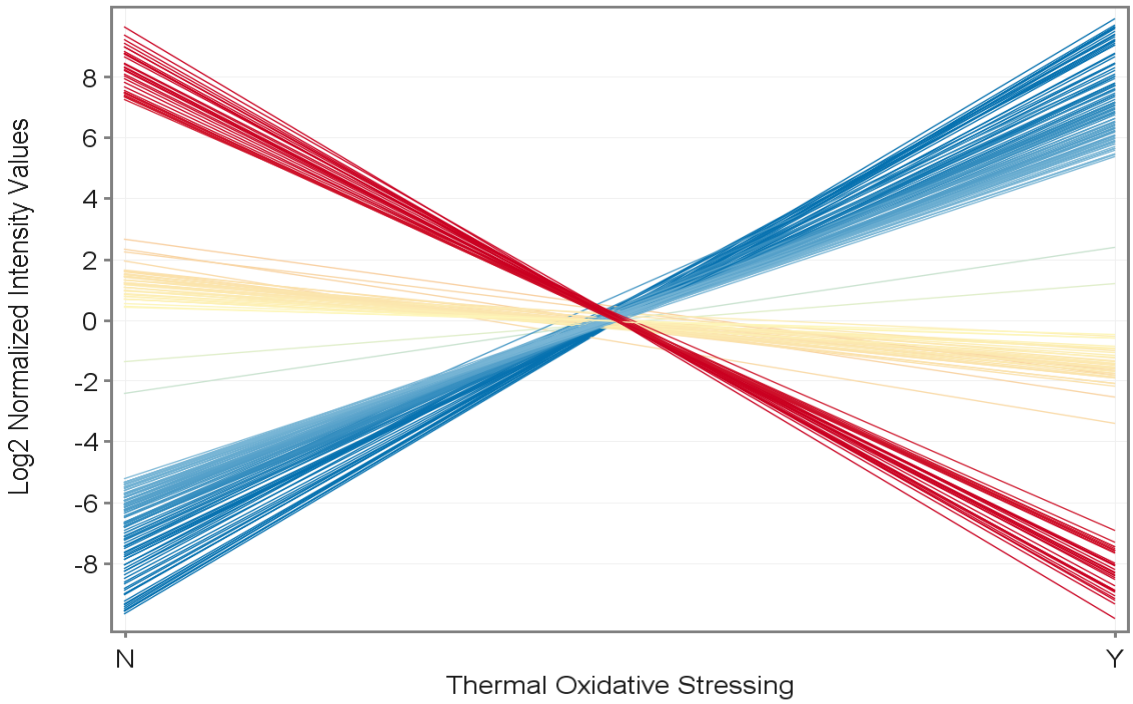

Supplemental Figure 4.2. Log 2 normalized intensity value of entities remaining after moderated T-test in J3192 comparing before and after TOS with negative ion ESI.

APPENDIX B: Extra Chromatograms from GCxGC/MS Analysis of Attapulgus Clay

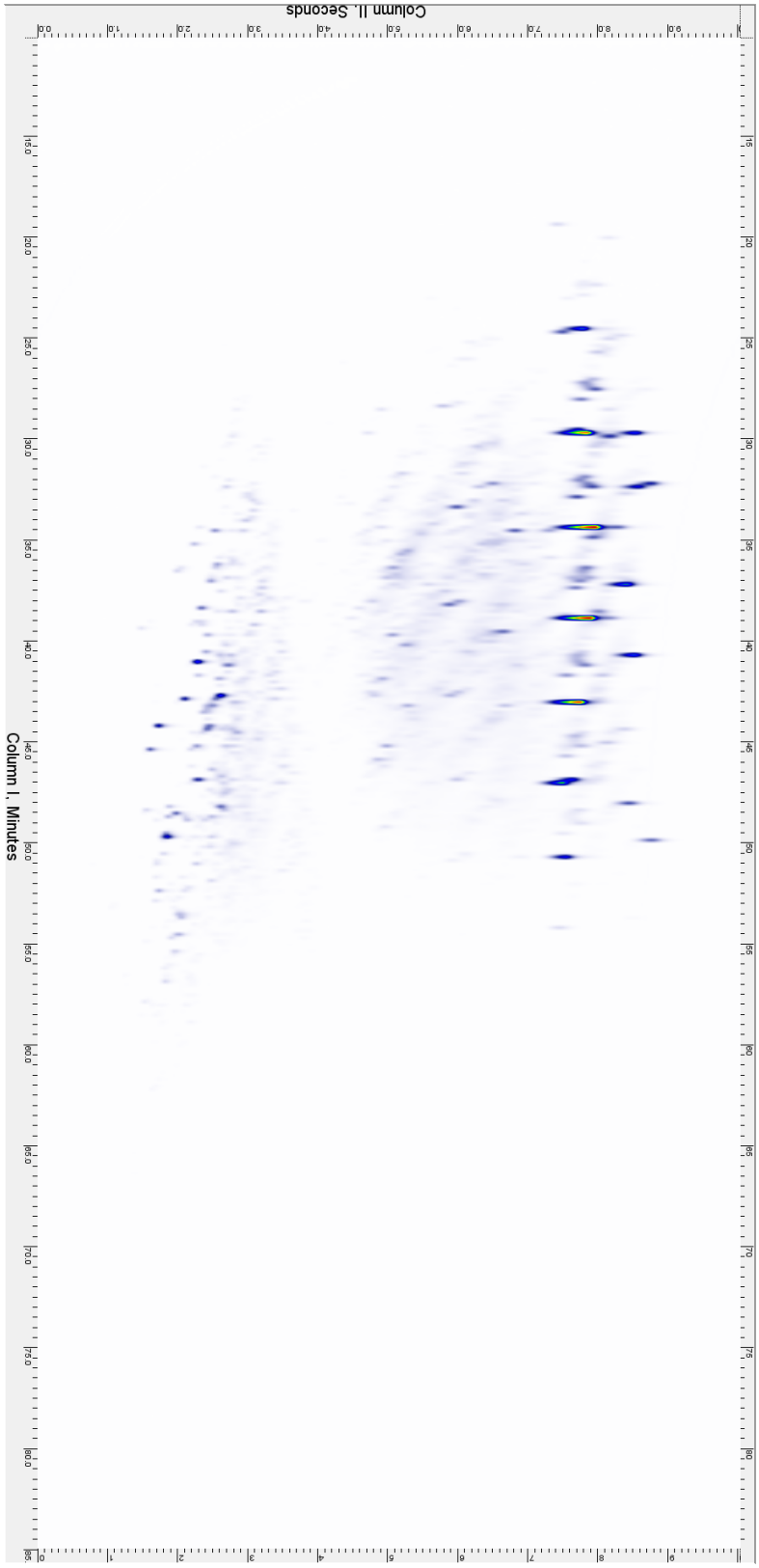

Supplemental Figure 6.1 GCxGC/MS Electron ionization RTICC for the Hexane Extracted Fraction of Attapulgus Clay Used for Treating Jet Fuel

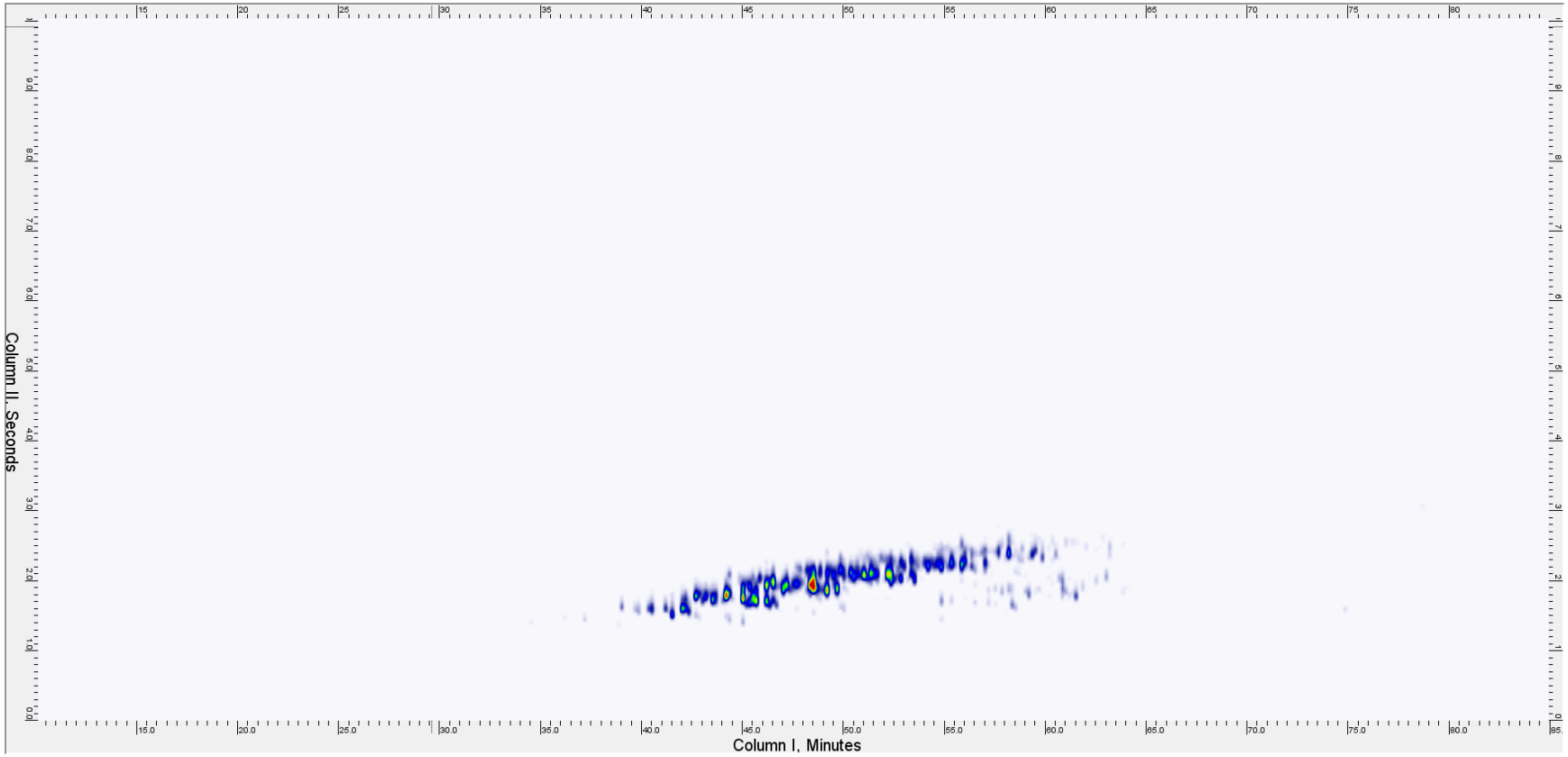

Supplemental Figure 6.2 GCxGC/MS Electron ionization EIC for $C_nH_{2n-6}O$ (consistent with alkyl phenols) for the Toluene Extracted Fraction of Attapulgus Clay Used for Treating Jet Fuel

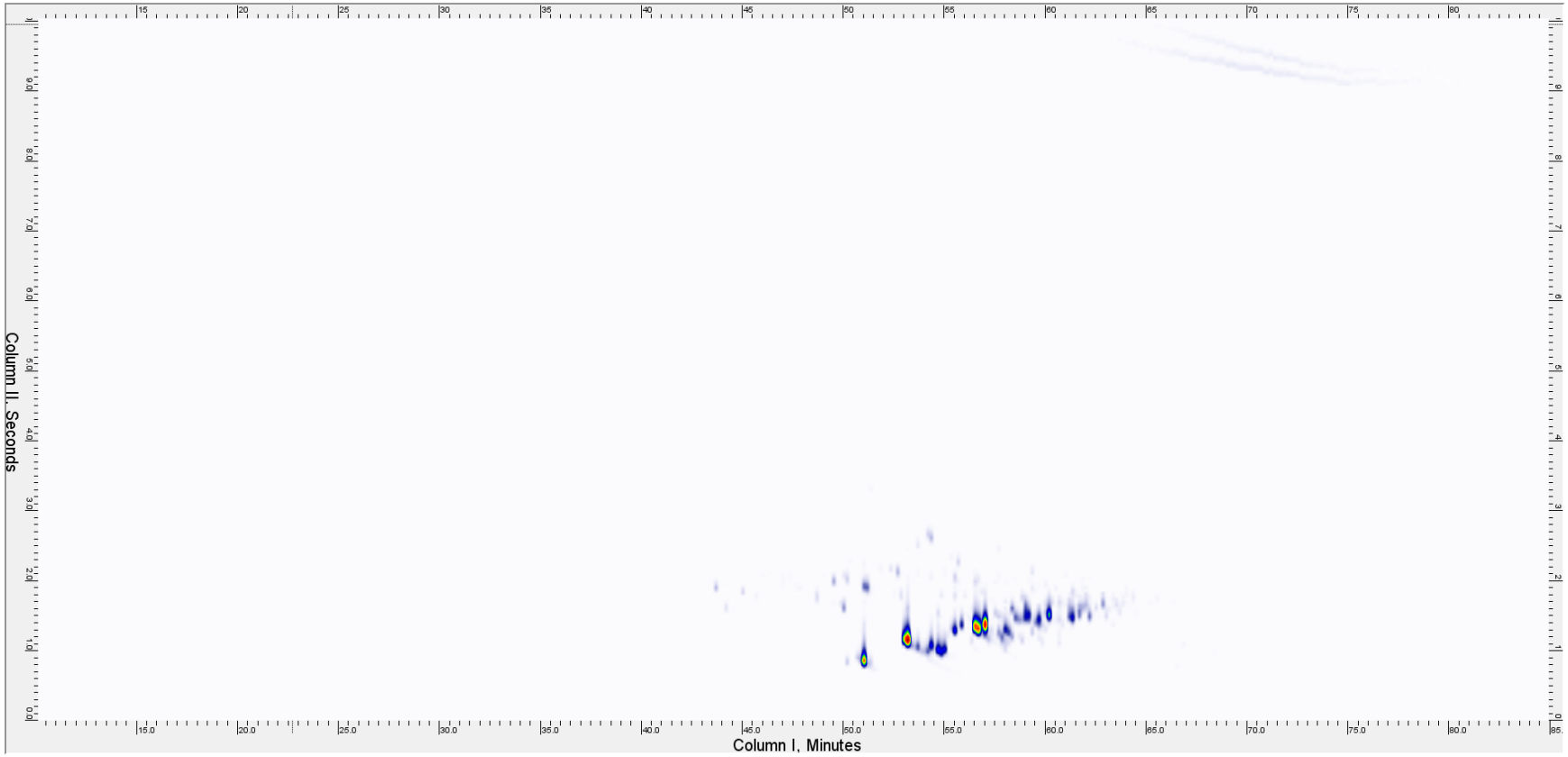

Supplemental Figure 6.3 GCxGC/MS Electron ionization EIC for $C_nH_{2n-9}N$ (consistent with alkyl indoles) for the Toluene Extracted Fraction of Attapulgus Clay Used for Treating Jet Fuel

Supplemental Figure 6.4 GCxGC/MS Electron ionization EIC for $C_nH_{2n-15}N$ (consistent with alkyl carbazoles) for the Toluene Extracted Fraction of Attapulgus Clay Used for Treating Jet Fuel

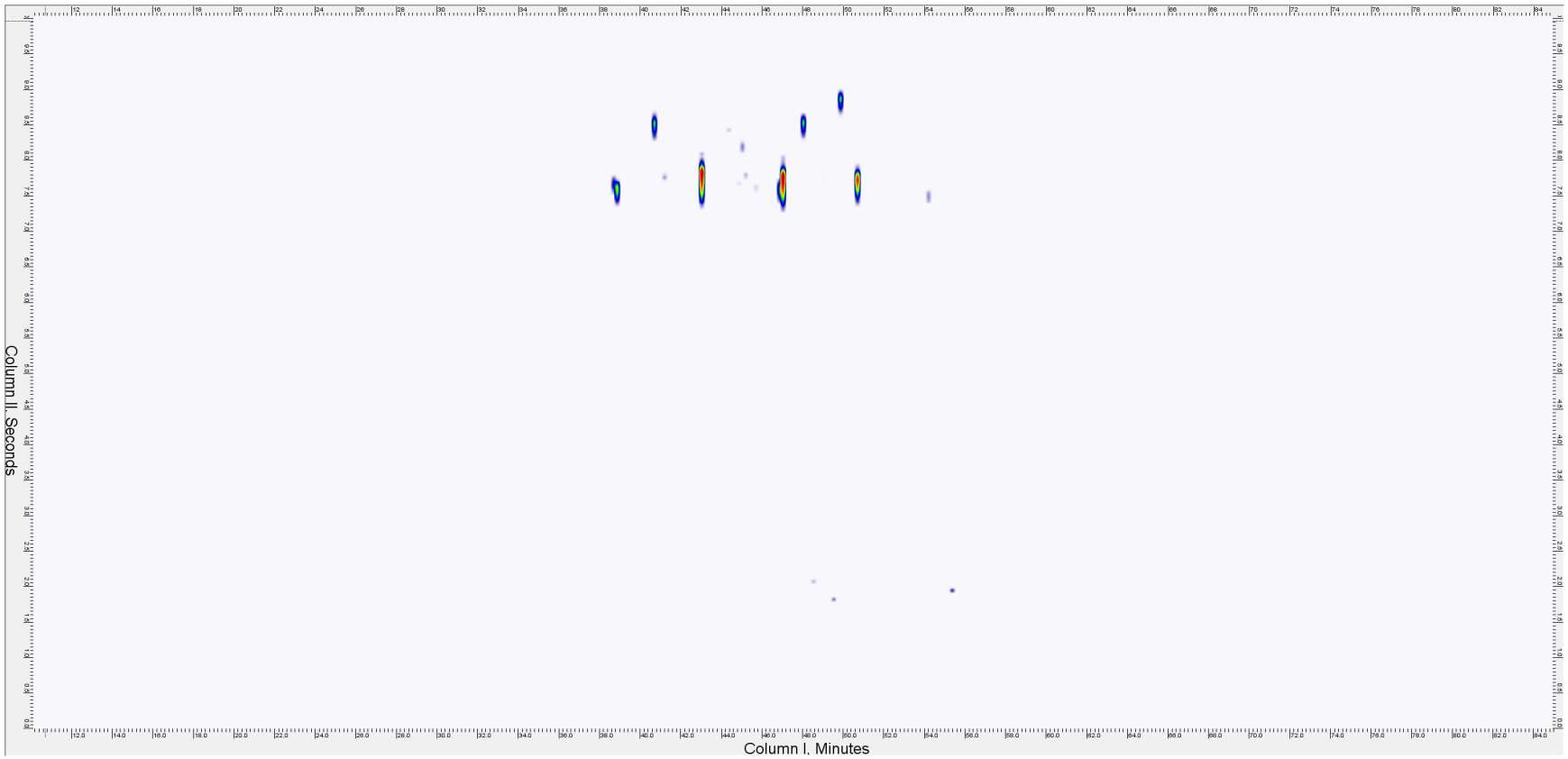

Supplemental Figure 6.5 GCxGC/MS Electron ionization EIC for C_nH_{2n+2} (consistent with normal and isoparaffins) for the Toluene Extracted Fraction of Attapulgus Clay Used for Treating Jet Fuel

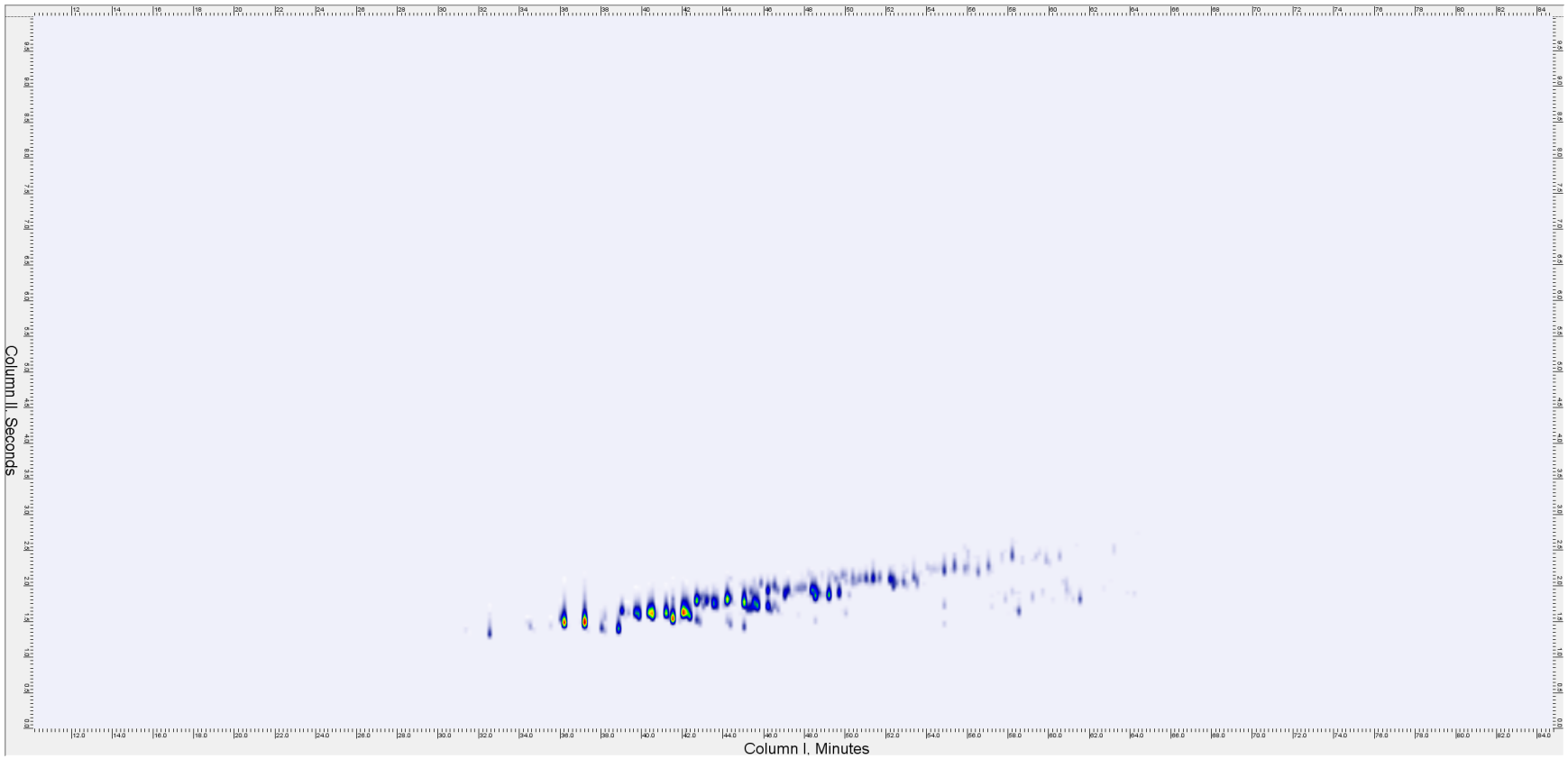

Supplemental Figure 6.6 GCxGC/MS Electron ionization EIC for $C_nH_{2n-6}O$ (consistent with alkyl phenols) for the DCM Extracted Fraction of Attapulgus Clay Used for Treating Jet Fuel

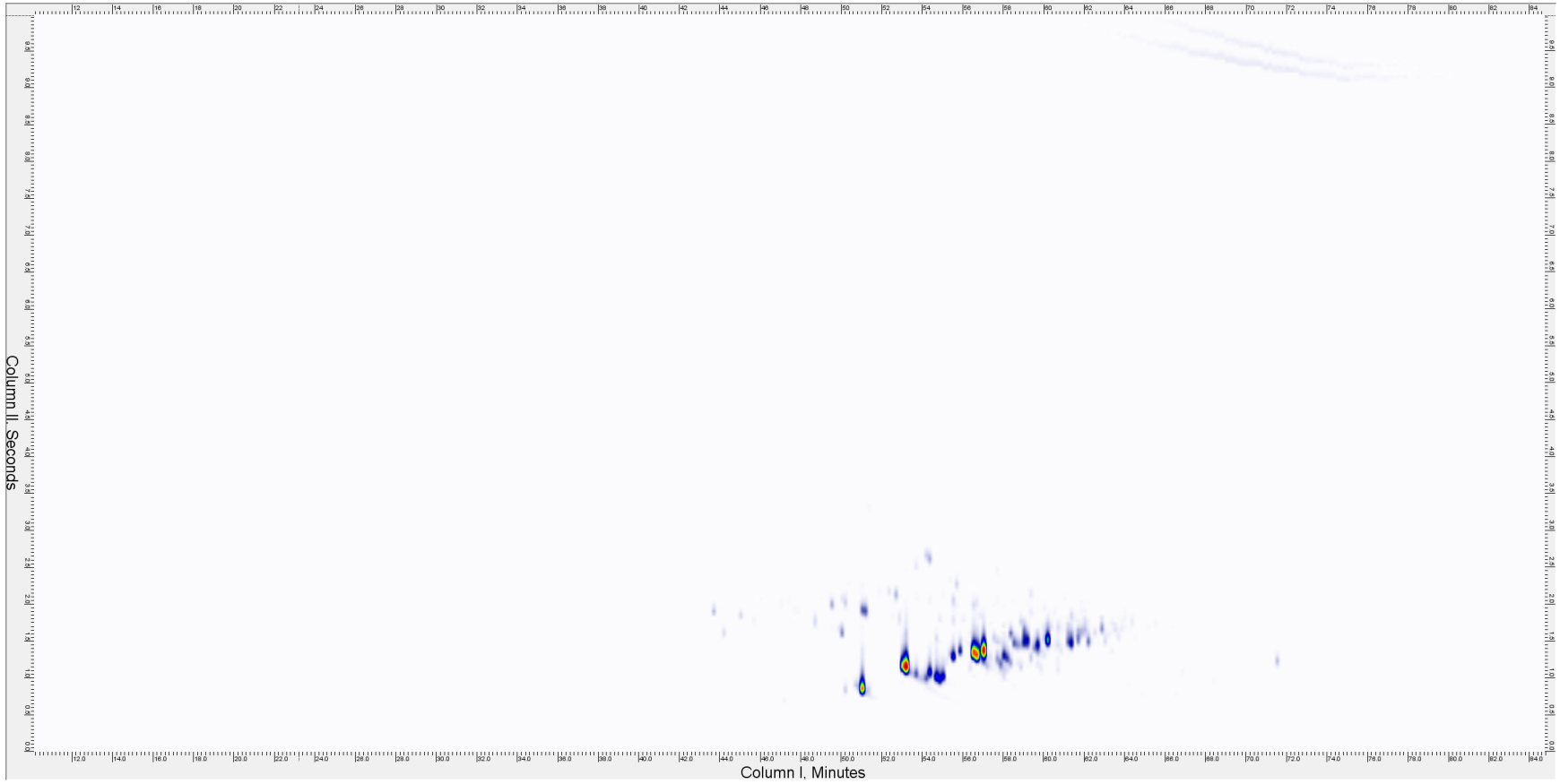

Supplemental Figure 6.7 GCxGC/MS Electron ionization EIC for $C_nH_{2n-9}N$ (consistent with alkyl indoles) for the DCM Extracted Fraction of Attapulgus Clay Used for Treating Jet Fuel

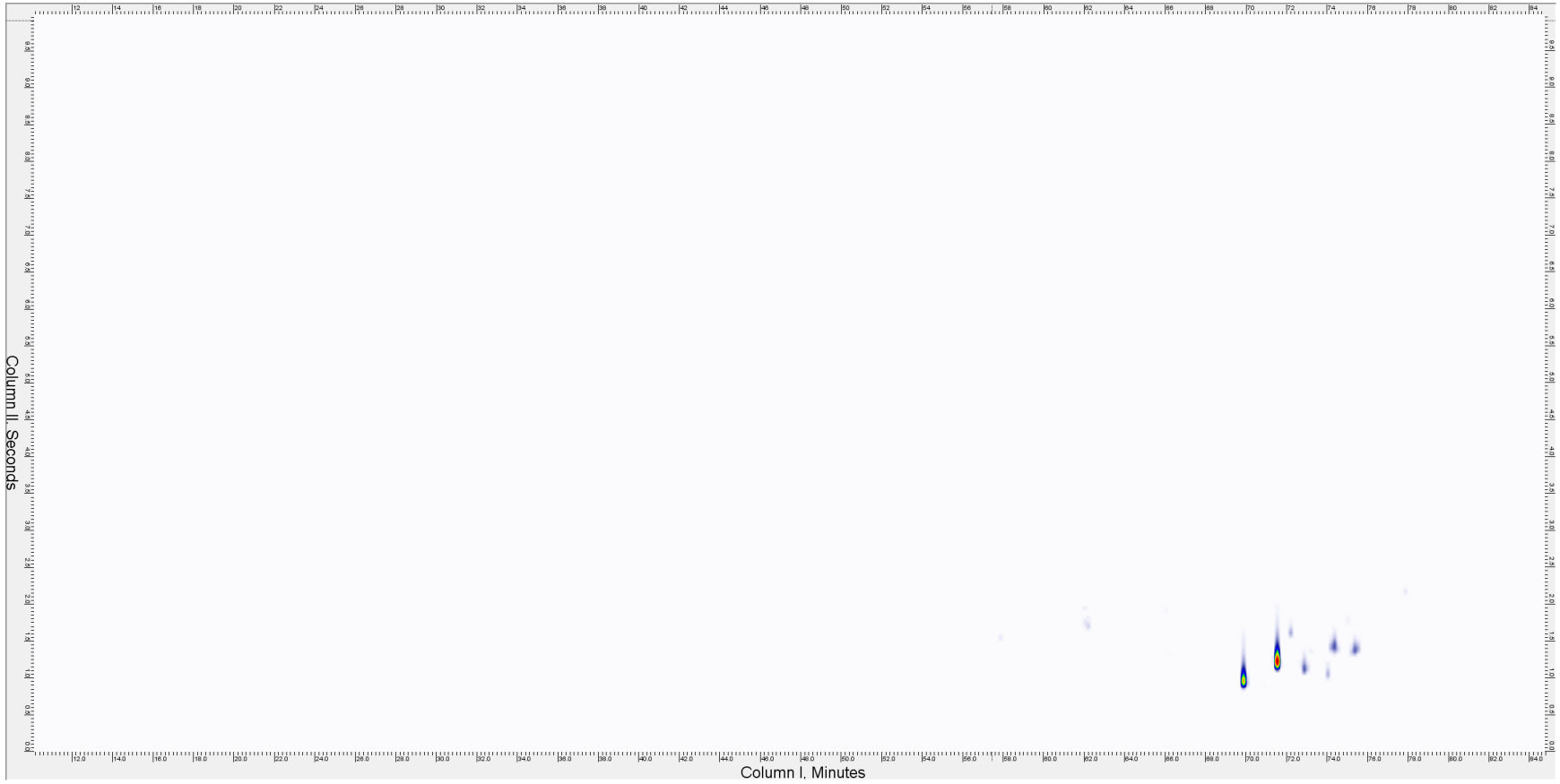

Supplemental Figure 6.8 GCxGC/MS Electron ionization EIC for $C_nH_{2n-15}N$ (consistent with alkyl carbazoles) for the DCM Extracted Fraction of Attapulgus Clay Used for Treating Jet Fuel

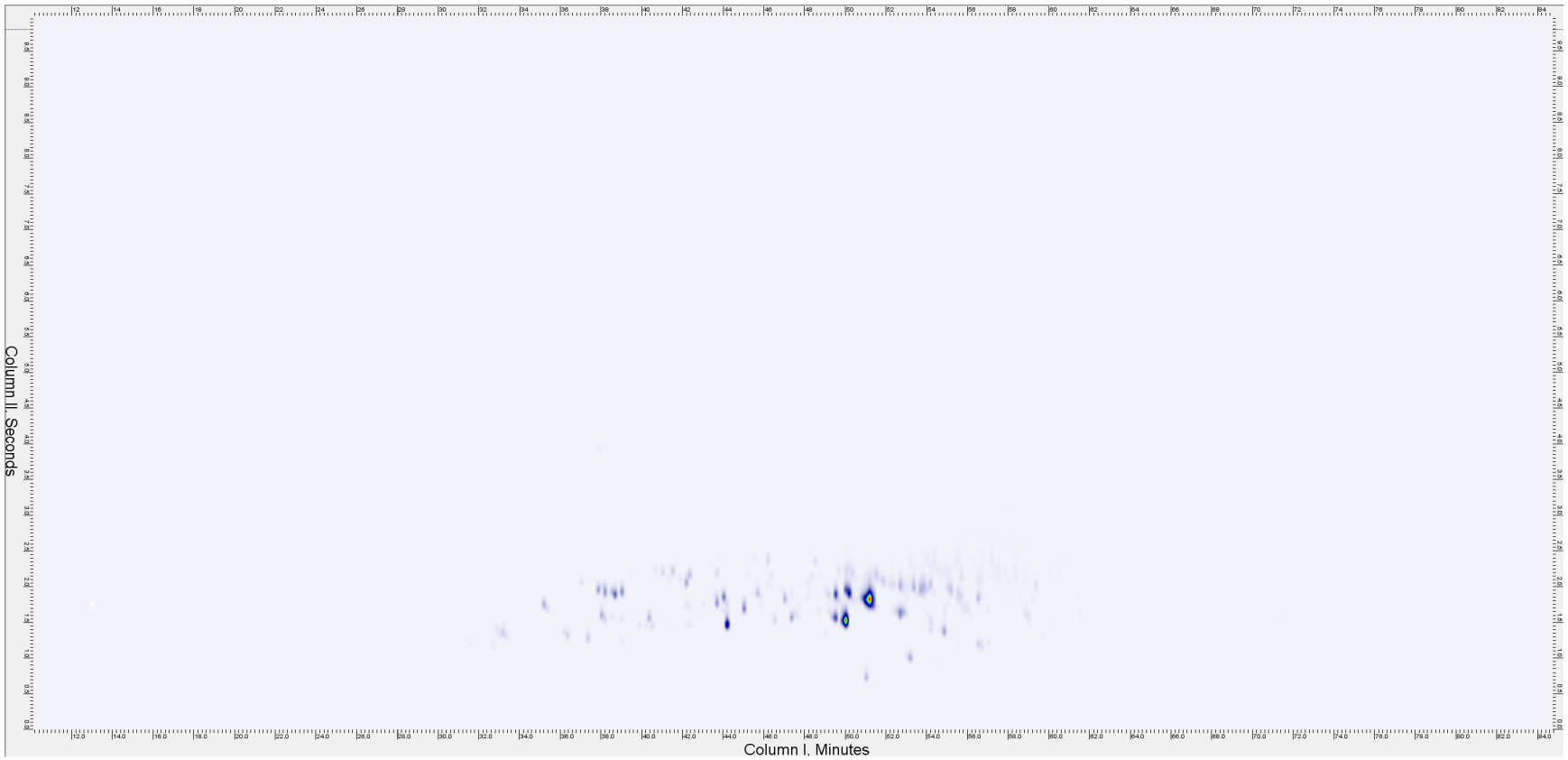

Supplemental Figure 6.9 GCxGC/MS Electron ionization EIC for $C_nH_{2n-7}N$ (consistent with alkyl tetrahydroquinolines/tetrahydroisoquinolines) for the DCM/MeOH Extracted Fraction of Attapulgus Clay Used for Treating Jet Fuel

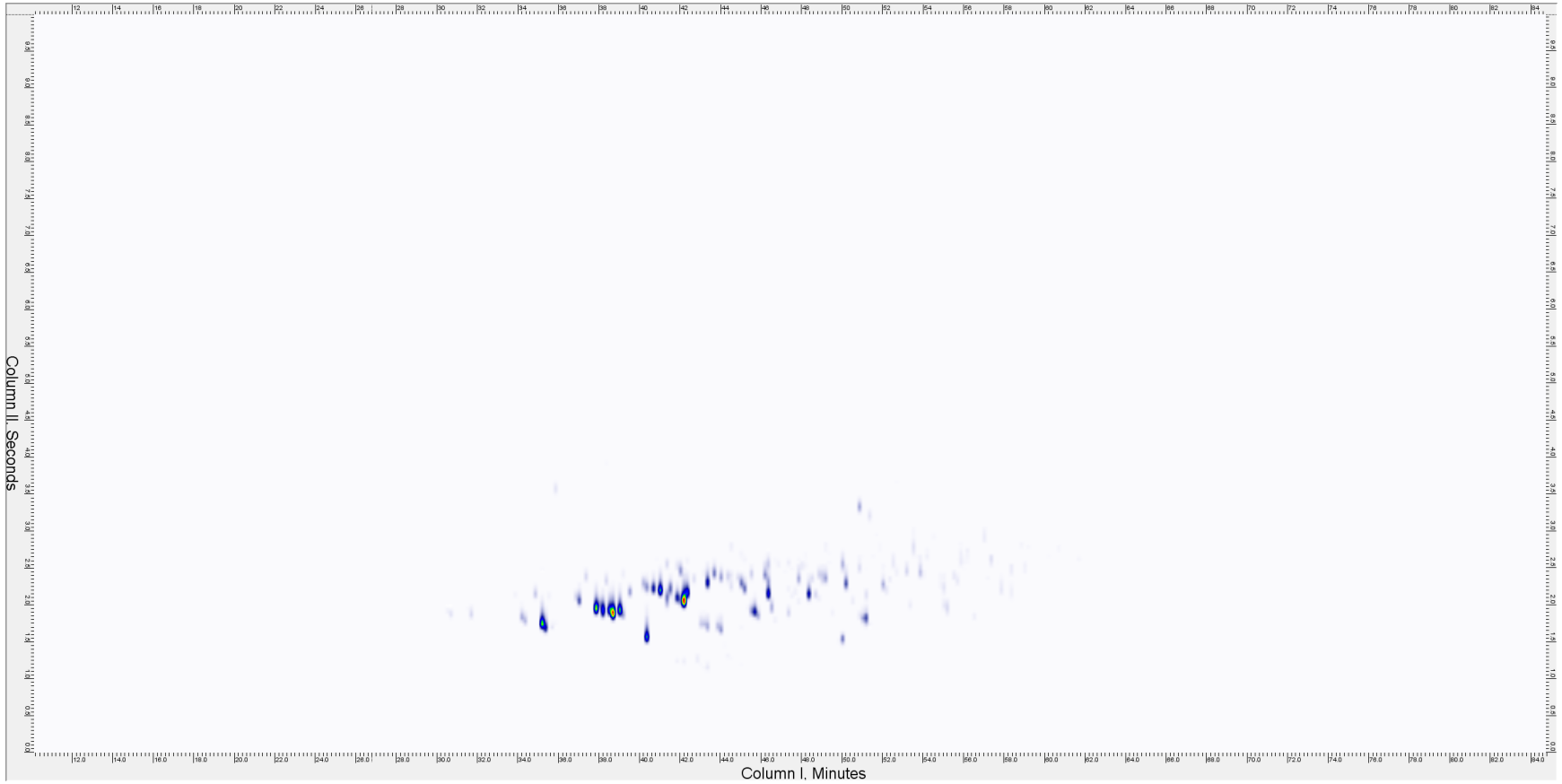

Supplemental Figure 6.10 GCxGC/MS Electron ionization EIC for $C_nH_{2n-5}N$ (consistent with alkyl anilines/pyridines) for the DCM/MeOH Extracted Fraction of Attapulgus Clay Used for Treating Jet Fuel

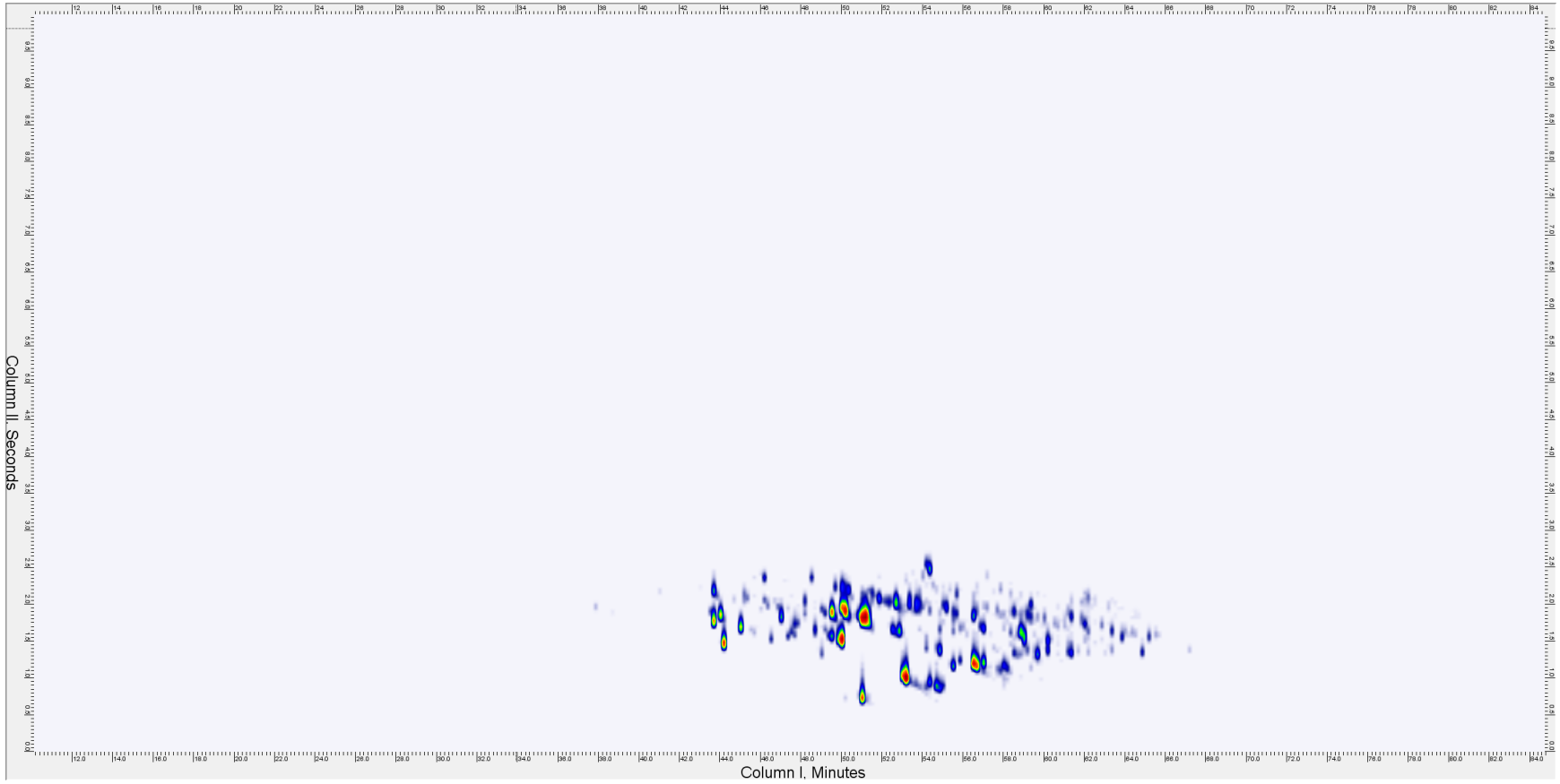

Supplemental Figure 6.11 GCxGC/MS Electron ionization EIC for $C_nH_{2n-9}N$ (consistent with alkyl indoles) for the DCM/MeOH Extracted Fraction of Attapulgus Clay Used for Treating Jet Fuel. The lower series is the alkyl indoles. Some isotope and fragment peaks from the tetrahydroquinoline series get extracted in the EIC which show in the upper series.

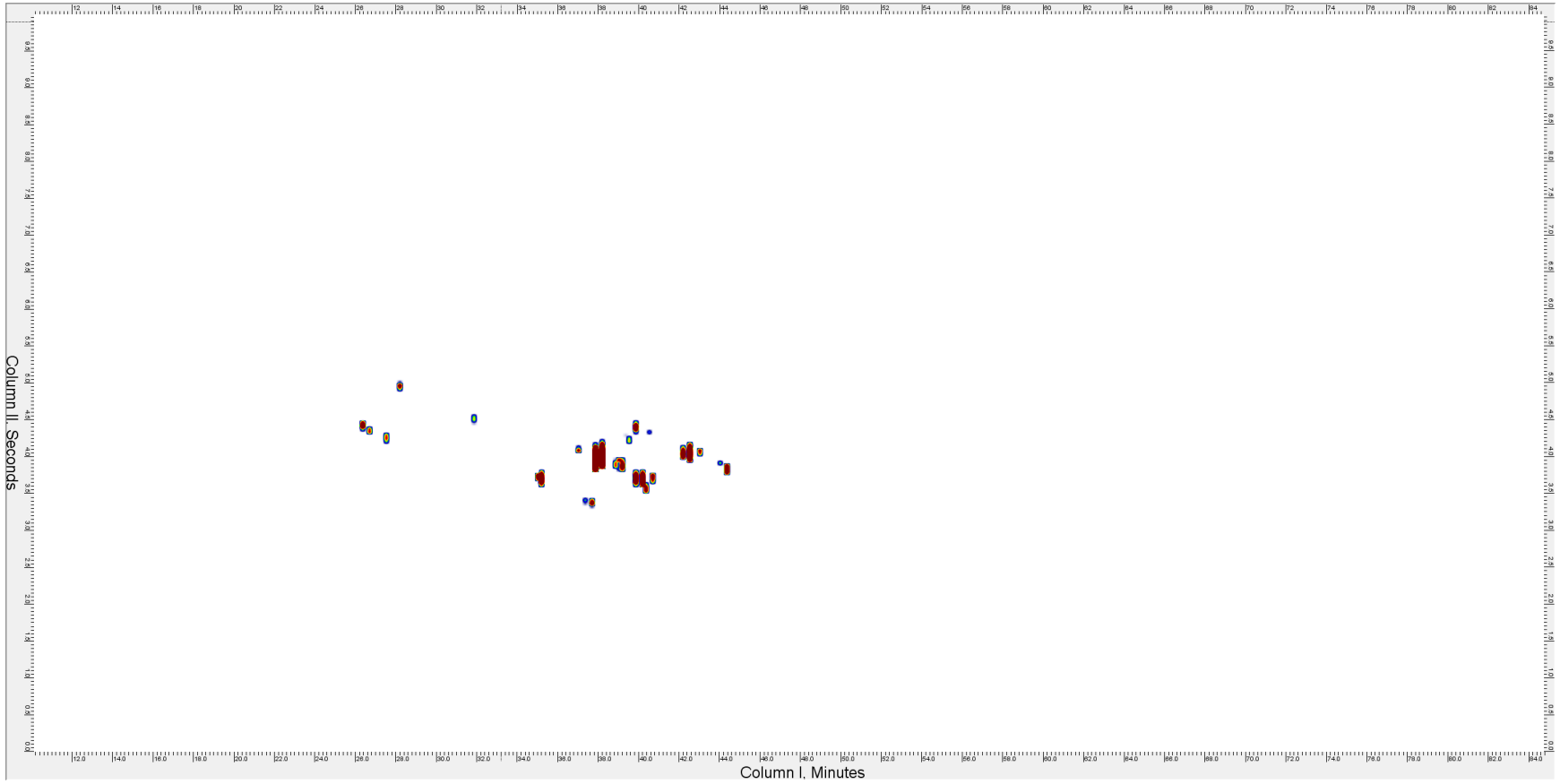

Supplemental Figure 6.12 GCxGC/MS Electron ionization EIC for $C_nH_{2n-1}N$ (consistent with alkyl indolizidines) for the DCM/MeOH Extracted Fraction of Attapulgus Clay Used for Treating Jet Fuel. The lower series is the alkyl indoles. Some isotope and fragment peaks from the tetrahydroquinoline series get extracted in the EIC which show in the upper series.

APPENDIX C: Study of the Electron Ionization Fragmentation Patterns of 1-Alkoxycyclohexenes

The following paper is the first project that was completed. The following manuscript will be submitted for publication after some additional work. It does not fit with the main dissertation research but represents a significant amount of effort and therefore is included in the appendix.

Introduction

The use of electron ionization (EI) fragmentation patterns obtained with gas chromatography/mass spectrometry (GC/MS) for the identification of unknowns has become ubiquitous in analytical and research laboratories. This is due, in large part, to the availability of large EI mass spectral libraries. Although the libraries contain tens of thousands of spectra, they are still not comprehensive. For example, the National Institute of Standards and Technology (NIST) Database (NIST 14) has spectra of 242,466 compounds in the mainlib.[1] However, NIST 14 also includes a Retention Index (RI) Database with 82,868 compounds of which only 56,216 have EI mass spectra in the mainlib.[1] Therefore, there are at least 26,652 known compounds of sufficient volatility to be analyzed by gas chromatography that do not have mass spectra in this particular library. The newest version of the NIST RI Database, NIST 17, has 27,039 compounds that do not have mass spectra in the accompanying EI Library.[2]

Naturally, as a result of this, there are times when an unknown cannot be identified by searching mass spectral libraries. During the course of research, it was

discovered that a homologous series of 1-alkoxycyclohexenes were not in the NIST 14 Database. Additionally, the majority of this class of compounds is not available commercially. 1-Alkoxycyclohexenes are cyclic enol ethers (Figure 1). This compound class, like enamines, are considered activated alkenes because of electron donation into the β-carbon of the double bound through resonance with the oxonium ion.[3] This creates enhanced reactivity of the double bond. Enol ethers generally participate in 3 types of reactions; Lewis acid catalyzed cationic polymerization, H-X addition across the double bond, and A-X (A ≠ H) addition across the double bond.[3] This led to the hypothesis that such compounds might be encountered in the analysis of various industrial products. In addition, there might be some interesting fragmentation mechanisms in the EI mass spectra of these compounds, which could be used to facilitate the identification of unknowns.

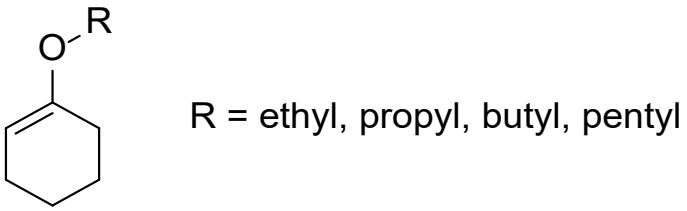

Figure 1. General Structure of 1-alkoxycyclohexenes.

In order to generate and study their EI mass spectra and submit them to NIST for inclusion in the NIST 17 EI mass spectral Library, a subset of the homologous series of 1-alkoxycyclohexenes was synthesized; 1-ethoxycyclohexene, 1-propoxycyclohexene, 1-butoxycyclohexene, and 1-pentyloxycyclohexene. Tandem quadrupole mass spectrometers offer a method of studying EI fragmentation through precursor and product ion analyses. By combining accurate mass measurements of the EI mass spectra with precursor and product ion spectra it was possible to derive insights into the fragmentation mechanisms for 1-alkoxycyclohexenes.

Experimental

Synthesis of 1-alkoxycyclohexenes was carried out according to a modification of a published methodology that describes the synthesis of 1-methoxycyclohexene (Figure 2).[4] The cyclohexanone (1 mol eq.) was reacted with the appropriate trialkylorthoformate (1.1 mol eq.) in the presence of catalytic amounts of p-toluenesulfonic acid (0.005 mol eq.). In cases where the solution darkened upon addition of the trialkylorthoformate, the alcohol that corresponded to the alkoxy chain in

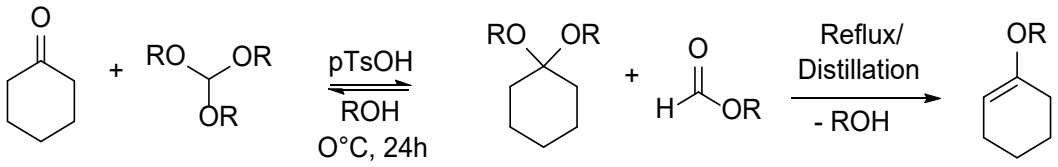

Figure 2. Reaction to form 1-alkoxycyclohexene from cyclohexanone.

the product was used as a solvent. Initially, the reaction was stirred at 0°C in an ice bath and then allowed to come to room temperature.

After a minimum of 24 hours, a two-step distillation was performed. First, the reaction mixture was fractionally distilled at atmospheric pressure to remove the formate ester and the alcohol that formed during the reaction. This also helped to drive the formation of more product from the acetal intermediate. Next, a fractional vacuum distillation was performed to isolate the product from any remaining intermediate. This yielded product that was sufficiently pure for NMR analysis.

The progress of the reaction and purification were monitored by a Direct Analysis in Real Time (DART) ionization/sample introduction method coupled with a JEOL AccuTOF API TOF mass spectrometer. This allowed for simultaneous determination of the monoisotopic mass of the products by acquiring accurate mass spectra of the protonated molecules along with determination if any of the precursors or side products were still present. Once it was determined that the compounds were sufficiently pure, 1H NMR spectra were acquired to confirm the structure of the products (spectra available in the supplemental information) on a JEOL ECA 600 NMR spectrometer (600 MHz).

EI mass spectra of the synthetic products were measured by two different instruments. First, they were generated by GC/MS using an Agilent 7890A GC coupled with an Agilent 5975C MSD using Standard-spectrum Tune for submission to NIST for inclusion in the NIST 17 Database. Next, the accurate EI mass spectra were generated by GC/MS using an Agilent 7890B GC coupled with a JEOL GCv 4G AccuTOF time-of-

flight mass spectrometer. This allowed for generation of elemental compositions for each of the peaks in the mass spectra which was helpful in understanding the fragmentation mechanisms. All spectra were submitted to the NIST MS Search 2.2 program and as expected no acceptable hits were returned for any of the spectra.

Precursor and product ion spectra were generated for 5 ions (*m/z* 98, *m/z* 83, *m/z* 70, *m/z* 55, and *m/z* 41) in the EI mass spectra of the 1-alkoxycyclohexene synthetic products using two different instruments; a Thermo Scientific Trace 1310 GC coupled to a Thermo Scientific TSQ 8000 Tandem Quadrupole mass spectrometer and an Agilent 7890B GC coupled to an Agilent 7000 Tandem Quadrupole mass spectrometer. This helped with interpreting the fragmentation pathways in the EI mass spectrum.

Detailed descriptions of the acquisition parameters can be found in the supplemental information.

Results and Discussion

The EI mass spectra for the four 1-alkoxycyclohexene compounds (Figure 3) all share distinct similarities. They exhibit relatively strong molecular ion peaks and, in all spectra, the next significant peak is an odd electron ion at *m/z* 98.

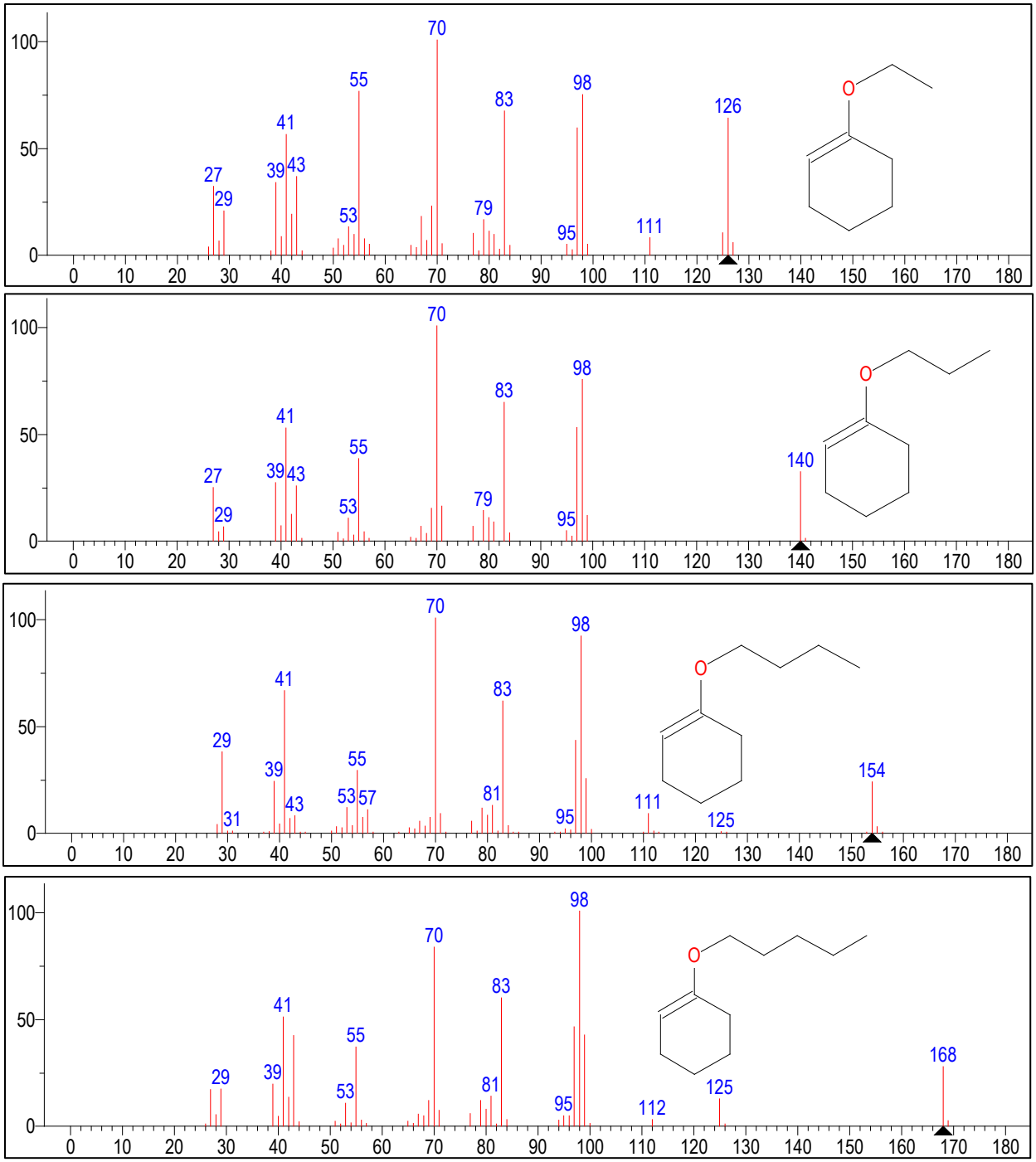

Figure 3. EI mass spectra for the four 1-alkoxycyclohexene compounds. Spectra plotted in MS Search v.2.3

The likely fragmentation mechanism to form the ion in the mass spectra at *m/z* 98 is a γ-hydrogen shift β-cleavage relative to the double-bond (Figure 4).

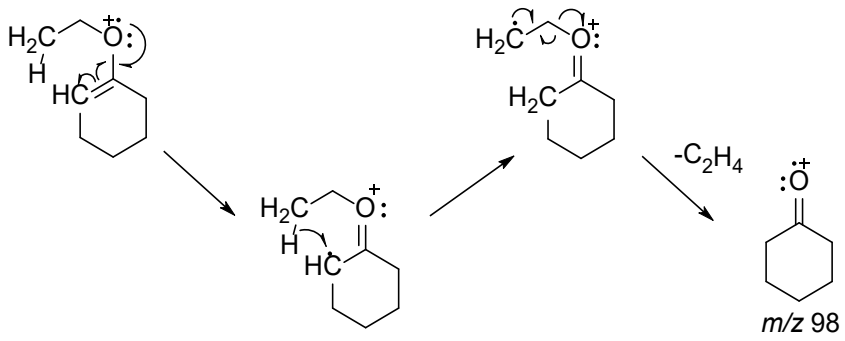

Figure 4. Fragmentation pathway to form odd-electron ion at *m/z* 98.

This is further evidenced by the mass spectrum of 1-methoxycyclohexane from the NIST 14 EI Library which does not exhibit a significant peak at *m/z* 98, representing an odd-electron ion, but instead has a peak at *m/z* 97, representing an even-electron ion from the loss of a methyl radical (Figure 5).[5] For 1-methoxycyclohexene, the γ-hydrogen shift would have to go through a five-membered ring transition instead of a six-membered ring transition, which likely contributes to the preferential loss of the methyl radical.

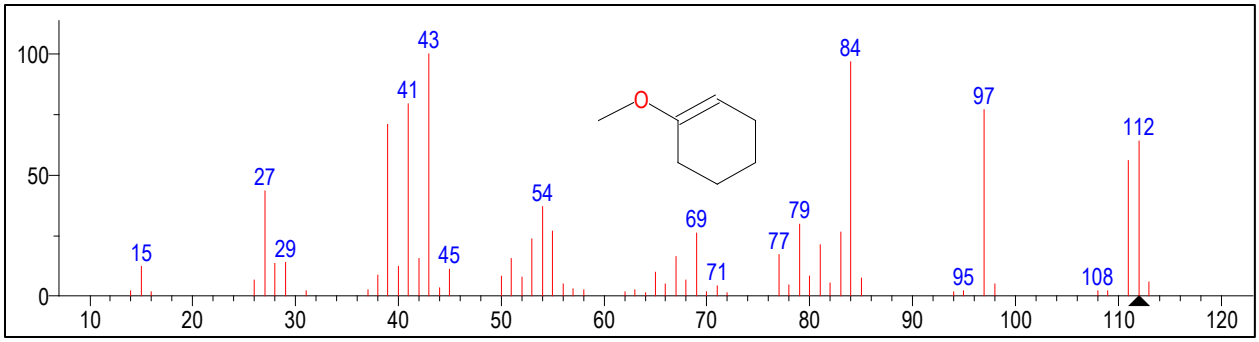

Figure 5. EI Mass Spectrum of 1-methoxycyclohexene (NIST#113215). Spectrum plotted in MS Search v.2.3

Even though it is less abundant than the ion with *m/z* 98, all of the spectra for the 1-alkoxycyclohexene compounds with alkyl chains larger than a methyl group also have an even-electron ion with *m/z* 97 due to the loss of an alkyl radical. As the alkyl chain gets longer, the relative intensity of the peak at *m/z* 98 increases and the relative intensity of the peak at *m/z* 97 decreases. The odd-electron ion with *m/z* 98 is isobaric with

Table 1. Accurate masses and elemental compositions for selected fragment

the molecular ion for cyclohexanone. Based on the proposed fragmentation mechanism it is apparent this fragment ion likely has the same structure as the molecular ion of cyclohexanone. Comparison of the EI mass spectrum for cyclohexanone from the NIST 14 Library[6] with the mass spectrum of 1-ethoxycyclohexene shows that they share many ions of the same *m/z* value (Figure 6).

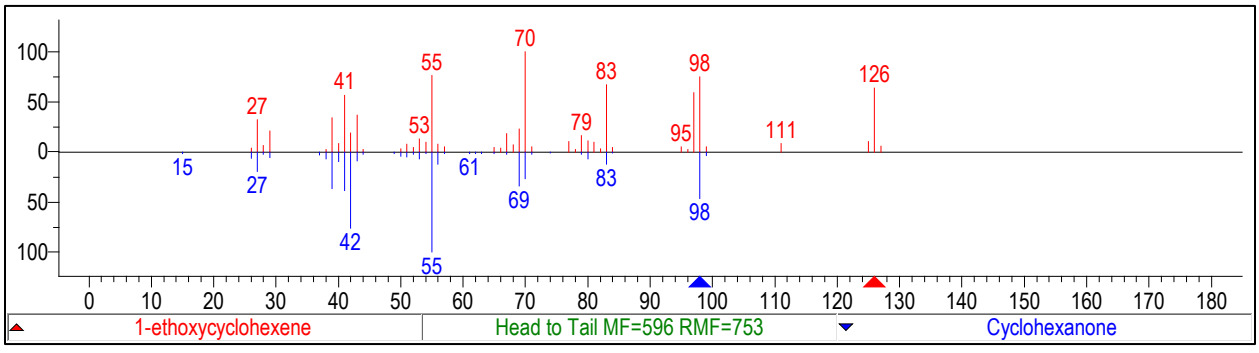

Figure 6. Comparison of EI Mass Spectra of 1-ethoxycyclohexene and cyclohexanone (NIST#114118). Spectrum plotted in MS Search v.2.3

GC/MS accurate *m/z*-value measurements allow for the generation of elemental compositions for the ions represented in the spectra. The elemental composition for ions in the spectrum of 1-ethoxycyclohexene are shown in Table 1.

***m/z*, measured**	***m/z*, theoretical**	**Elemental Composition**
98.0715	98.0732	$C_6H_{10}O^{\bullet+}$
83.0490	83.0497	$C_5H_7O^+$
70.0410	70.0419	$C_4H_6O^{\bullet+}$
55.0534	55.0548	$C_4H_7^+$
55.0159	55.0184	$C_3H_3O^+$
41.0376	41.0391	$C_3H_5^+$

Table 1. Accurate masses and elemental compositions for selected fragment ions.

The results are comparable for the other spectra. These ions were also selected for precursor and product ion studies by GC/MS/MS. One of the interesting features of the accurate *m/z*-value, high resolution EI mass spectra is that there is a doublet for the ion with integer *m/z* 55. The ion with *m/z* 55.0159, which has an elemental composition of $C_3H_3O^+$, is about 10 times more abundant than the ion with *m/z* 55.0534, which has an elemental composition of $C_4H_7^+$.

The product ion spectrum of 1-pentyloxycyclohexene for *m/z* 98 (Figure 7) shows that the ions with *m/z* 83, *m/z* 70, and *m/z* 55 are all secondary fragment ions from this primary fragment ion although the relative intensity of the peak at *m/z* 70 is much lower in the MS/MS spectrum than in the EI mass spectrum. Interestingly, depending on the

instrument used to generate the product ion spectra, the relative intensity of the peaks at *m/z* 70 and *m/z* 69 are different. In the spectrum acquired on the Agilent 7000 the peak at *m/z* 69 is larger than the peak at *m/z* 70. The opposite is true for the spectrum acquired on the Thermo TSQ 8000 instrument. This highlights that reproducibility of MS/MS spectra between different instruments is poor, even if they have the same general settings, which has been shown previously.[7]

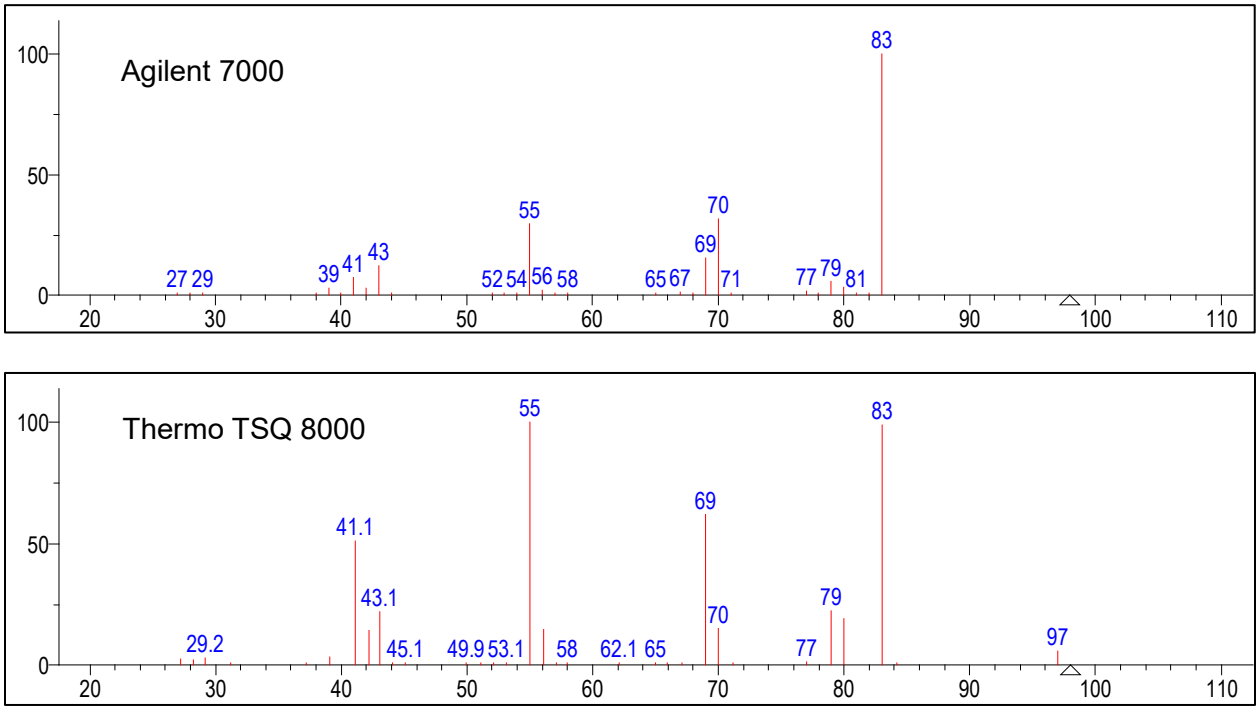

Figure 7. Product ion spectra for *m/z* 98 of 1-pentyloxycylohexene. Both spectra were acquired with the same collision energy (CE = 10). Spectra plotted in MS Search v.2.3

The ions with *m/z* 83, *m/z* 69, and the most abundant fragment ion with integer *m/z* 55 can be explained by fragmentation mechanisms that have been previously reported for cyclohexanone (Figure 8).[8] The two main differences between the spectrum for cyclohexanone and the 1-alkoxycyclohexene spectra are the intensity of the peaks representing the odd electron ions with *m/z* 70 and *m/z* 42. The fragmentation

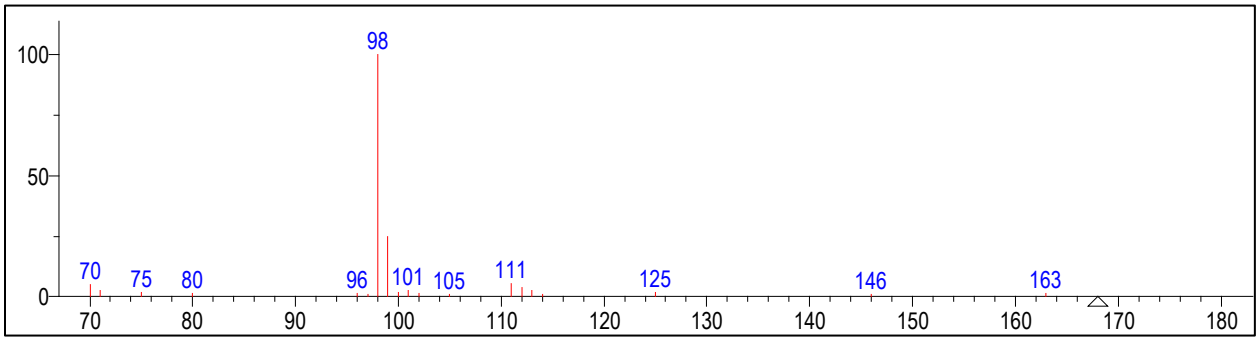

Figure 8. Precursor ion spectrum for *m/z* 70 of 1-pentyloxycylohexene. Spectrum plotted in MS Search v.2.3

mechanism to form the ion with *m/z* 42 has also been previously reported for cyclohexanone (Figure 9).[8] The precursor ion spectrum of 1-pentyloxycyclohexene for the ion with *m/z* 70 shows that it is a secondary fragment ion that comes from the ion with *m/z* 98 and does not involve the ion with *m/z* 83 (Figure 10). The precursor ion spectrum of 1-pentyloxycyclohexene for *m/z* 41 shows that it is an even-electron ion that can likely be formed by different pathways (Figure 11). It can likely be formed by the loss of a hydrogen radical from the ion with *m/z* 42. It can also likely be formed from the loss of CO from the ion with *m/z* 69. The precursor and product ion spectra that are

not shown for the other 1-alkoxycyclohexene compounds are virtually indistinguishable from the shown spectra.

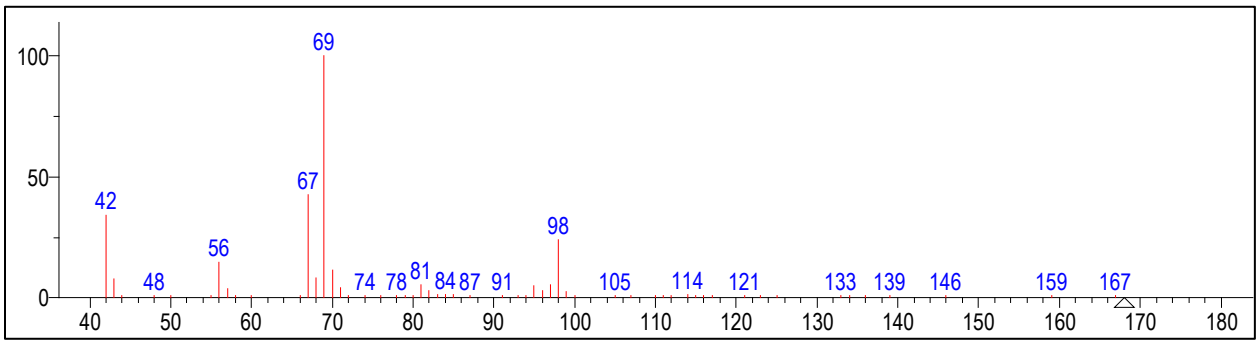

Figure 9. Precursor ion spectrum for *m/z* 41 of 1-pentyloxycylohexene. Spectrum plotted in MS Search v.2.3

Submitting the spectra for 1-propoxycyclohexene and cyclohexanone to MS Interpreter* (Version 3.2.7 build 6/18/2018) give some insight into the fragmentation pathway that forms the odd electron ion with *m/z* 70. In both instances, MS Interpreter suggests the odd electron ions with *m/z* 70 have elemental compositions of $C4H6O^{\bullet+}$ which matches the elemental composition of this fragment ion determined from its accurate *m/z*-value. For cyclohexanone, MS Interpreter suggests that the ion is formed through 1,2-dissociation (Figure 10). This pathway also explains the odd-electron ion with *m/z* 70 in the 1-alkoxycyclohexene molecules as being secondary fragments of the odd-electron ion with *m/z* 98 which is structurally identical to the molecular ion of cyclohexanone.

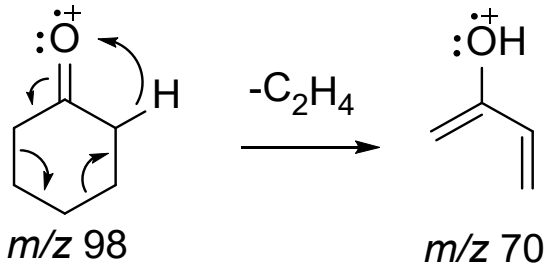

Figure 10. Fragmentation pathway to form odd-electron ion with *m/z* 70.

* MS Interpreter is a software package that is included with the NIST MS Search program. It aids in the interpretation of fragmentation patterns by offering logical fragmentation explanations based on the structure of the molecule and the peaks in the spectrum.

Summary

There are still opportunities to improve mass spectral libraries by finding compounds that are absent from their databases and adding them. This was the case with the homologous series of 1-alkoxycyclohexenes. In order to do so, it was necessary to synthesize the molecules because they are not readily available from a commercial supplier. Once the molecules were synthesized it was possible to study their EI mass spectra through accurate *m/z*-value measurements and GC/MS/MS studies.

The 1-alkoxycyclohexene molecules, where the alkyl chain was longer than a methyl group, all share similar features. The only truly unique feature of their spectra is the peak representing the molecular ion. They all fragment to form an odd-electron ion with *m/z* 98 which is isobaric with a cyclohexanone molecular ion. The likely fragmentation mechanism suggests that this ion is also structurally the same as the molecular ion of cyclohexanone. The spectra also share similarities with the EI mass spectrum for cyclohexanone starting at *m/z* 98 and below. GC/MS/MS studies of a number of prominent peaks in the spectra confirmed that all of the peaks below *m/z* 98 are secondary or tertiary fragment of the odd-electron ion with *m/z* 98.

References

1. National Institute of Standards and Technology, README.TXT. NIST 14 ed.; 2014.

2. Sparkman, O. D., Introduction of NIST 17—A Major Update of Mass Spectral Libraries and Software—at the 65th ASMS Conference on Mass Spectrometry and Allied Topics. American Laboratory 2017.

3. Effenberger, F., Chemistry of enol ethers. Angew. Chem., Int. Ed. Engl. 1969, 8 (5), 295-312.

4. WOHL, R. A., A CONVENIENT ONE-STEP PROCEDURE FOR THE SYNTHESIS OF CYCLIC ENOL ETHERS, THE PREPARATION OF 1-METHOXY-1-CYCLOALKENES. ChemInform 1974, 5 (16).

5. National Institute of Standards and Technology., NIST# 113215 NIST 17 ed. 2017.

6. National Institute of Standards and Technology, NIST# 114118 NIST 14 ed. 2014.

7. Jansen, R.; Lachatre, G.; Marquet, P., LC-MS/MS systematic toxicological analysis: Comparison of MS/MS spectra obtained with different instruments and settings. Clin. Biochem. 2005, 38 (4), 362-372.

8. Budzikiewicz, H.; Djerassi, C.; Williams, D. H., Mass spectrometry of organic compounds. 1964.